DESIGN OF FLIGHT CONTROL LAWS FOR AIRCRAFT WITH FLEXIBLE WINGS USING QUANTITATIVE FEEDBACK THEORY

THESIS

Christina L. Osmon
Second Lieutenant, USAF

AFIT/GE/ENG/95D-20

DISTRIBUTION STATEMENT A
Approved for public release;
Distribution Unlimited

DEPARTMENT OF THE AIR FORCE
AIR UNIVERSITY
AIR FORCE INSTITUTE OF TECHNOLOGY

Wright-Patterson Air Force Base, Ohio

DTIC QUALITY INSPECTED 1

AFIT/GE/ENG/95D-20

DESIGN OF FLIGHT CONTROL LAWS FOR AIRCRAFT WITH FLEXIBLE WINGS USING QUANTITATIVE FEEDBACK THEORY

THESIS

Christina L. Osmon
Second Lieutenant, USAF

AFIT/GE/ENG/95D-20

19960617 008

Approved for public release; distribution unlimited

The views expressed in this thesis are those of the author and do not reflect the official policy or position of the Department of Defense or the U. S. Government.

AFIT/GE/ENG/95D-20

DESIGN OF FLIGHT CONTROL LAWS FOR AIRCRAFT WITH FLEXIBLE WINGS USING QUANTITATIVE FEEDBACK THEORY

THESIS

Presented to the Faculty of the Graduate School of Engineering
of the Air Force Institute of Technology
Air University
In Partial Fulfillment of the
Requirements for the Degree of
Master of Science in Electrical Engineering

Christina L. Osmon, B.S.E.E.
Second Lieutenant, USAF

December, 1995

Approved for public release; distribution unlimited

Acknowledgements

I would like to thank Dr. Pachter and Dr. Houpis for their continual support in this thesis effort. Without their guidance and vast knowledge, this work would not have been possible.

I would also like to thank all of my classmates who kept me on track and provided hours of entertainment and stimulating conversation. Most of all I would like to thank my husband, John, for his incredible support throughout these long months.

Christina L. Osmon

Table of Contents

Page

Acknowledgements ii

List of Figures vi

List of Tables x

Abstract xi

I. Introduction 1-1

1.1 Problem Statement 1-2

1.2 Literature Review 1-3

1.2.1 History of the F-18 1-4

1.2.2 Flexible Wing Research 1-5

1.3 Assumptions 1-8

1.4 Scope 1-8

1.5 Approach and Methodology 1-9

1.5.1 Controller Design 1-9

1.5.2 Simulation 1-11

1.6 Organization of Thesis 1-11

II. QFT Theory 2-1

2.1 Effective Plant 2-2

2.2 Tracking and Stability Specifications 2-3

2.3 Effective MISO Equivalent Plants 2-4

2.4 Frequency Templates 2-7

2.5 Bounds on the Nichols Chart 2-8

Page

2.6 Compensator Design 2-11

2.7 Pre-Filter Design 2-13

2.8 Frequency Domain Validation 2-13

III. The F-18 HARV 3-1

3.1 The Aircraft 3-1

3.2 Linear Plant Models 3-2

3.3 Control Surface Descriptions 3-4

3.4 Actuator Models 3-5

3.5 Flight Conditions 3-5

IV. Flight Control System Design 4-1

4.1 System Specifications 4-1

4.1.1 Tracking Specifications 4-1

4.1.2 Stability Specifications 4-3

4.1.3 Cross-Coupling Effect Rejection Specifications 4-3

4.2 Effective Plants 4-4

4.3 Design 1 4-7

4.3.1 Weighting Matrix 4-7

4.3.2 QFT FCS Design 4-7

4.3.3 Design Validation 4-17

4.4 Design 2 4-21

4.4.1 Weighting Matrix 4-21

4.4.2 QFT FCS Design 4-22

4.4.3 Design Validation 4-26

4.5 Design 3 4-30

4.5.1 Weighting Matrix 4-30

4.5.2 QFT FCS Design 4-33

Page

4.5.3 Design Validation 4-37

4.6 Chapter Summary 4-40

V. Time Domain Simulation 5-1

5.1 Setup 5-1

5.2 Design 1 5-3

5.3 Design 2 5-8

5.4 Design 3 5-13

5.5 Comparison of Designs 5-19

5.6 Design Summary 5-22

VI. Conclusions and Recommendations 6-1

6.1 Summary 6-1

6.2 Conclusions 6-2

6.3 Recommendations 6-3

Appendix A. Plant Transfer Functions A-1

Bibliography BIB-1

Vita VITA-1

List of Figures

Figure		Page
1.1.	Flight Control System Block Diagram	1-9
2.1.	Effective Plant	2-3
2.2.	MISO Equivalent Plants	2-5
2.3.	Diagonal Dominance Condition	2-7
2.4.	Example of Frequency Templates	2-8
2.5.	Stability Bounds on the Nichols Chart	2-9
2.6.	Tracking Bounds on the Nichols Chart	2-10
2.7.	Cross-Coupling Bounds on the Nichols Chart	2-11
2.8.	Loop Transmission Example	2-12
2.9.	Stability Validation Example	2-14
3.1.	The F-18 Aircraft	3-1
3.2.	Control Effector Sign Conventions for the F-18 HARV	3-4
3.3.	Flight Envelope of F-18 HARV	3-6
4.1.	P-channel Tracking Bounds in Time and Frequency Domains	4-2
4.2.	Tracking and Cross-Coupling Bounds - Both Channels	4-4
4.3.	Dutch Roll Damping Block Diagram	4-5
4.4.	Verification of Diagonal Dominance	4-6
4.5.	p Channel Templates - Design 1	4-8
4.6.	β Channel Templates - Design 1	4-8
4.7.	Nominal Plant Selection - Design 1	4-9
4.8.	Stability Bounds for p Channel - Design 1	4-10
4.9.	Stability Bounds for β Channel - Design 1	4-10
4.10.	Tracking Bounds for p Channel - Design 1	4-11

Figure Page

4.11. Tracking Bounds for β Channel - Design 1 4-12

4.12. Cross-Coupling Effect Bounds for p Channel - Design 1 4-13

4.13. Cross-Coupling Effect Bounds for β Channel - Design 1 4-13

4.14. Composite Bounds for p Channel - Design 1 4-14

4.15. Composite Bounds for β Channel - Design 1 4-15

4.16. Nominal Loop Transmission for p Channel - Design 1 4-16

4.17. Nominal Loop Transmission for β Channel - Design 1 4-16

4.18. Stability Validation for p Channel - Design 1 4-18

4.19. Stability Validation for β Channel - Design 1 4-18

4.20. Tracking Validation for Design 1 4-20

4.21. p Channel Templates - Design 2 4-22

4.22. β Channel Templates - Design 2 4-23

4.23. Composite Bounds for p Channel - Design 2 4-24

4.24. Composite Bounds for β Channel - Design 2 4-24

4.25. Nominal Loop Transmission for p Channel - Design 2 4-25

4.26. Nominal Loop Transmission for β Channel - Design 2 4-26

4.27. Stability Validation for p Channel - Design 2 4-27

4.28. Stability Validation for β Channel - Design 2 4-27

4.29. Tracking Validation for Design 2 4-29

4.30. Example of Optimal Weighting Matrix Calculation 4-32

4.31. p Channel Templates - Design 3 4-33

4.32. β Channel Templates - Design 3 4-34

4.33. Composite Bounds for p Channel - Design 3 4-35

4.34. Composite Bounds for β Channel - Design 3 4-35

4.35. Nominal Loop Transmission for p Channel - Design 3 4-36

4.36. Nominal Loop Transmission for β Channel - Design 3 4-37

4.37. Stability Validation for p Channel - Design 3 4-38

Figure Page

4.38. Stability Validation for β Channel - Design 3 4-38

4.39. Tracking Validation for Design 3 4-39

5.1. Block Diagram used for Time Domain Simulation 5-2

5.2. Block Diagram for the Effective Plant 5-2

5.3. Example of Block Diagram for the Actuators 5-2

5.4. Time Response to Unit Step Input p Channel - Design 1 (1 of 2) 5-3

5.5. Time Response to Unit Step Input p Channel - Design 1 (2 of 2) 5-4

5.6. Time Response to Unit Step Input β Channel - Design 1 (1 of 2) 5-5

5.7. Time Response to Unit Step Input β Channel - Design 1 (2 of 2) 5-6

5.8. Time to Bank 90° - Design 1 (1 of 2) 5-7

5.9. Time to Bank 90° - Design 1 (2 of 2) 5-7

5.10. Time Response to Unit Step Input p Channel - Design 2 (1 of 2) 5-9

5.11. Time Response to Unit Step Input p Channel - Design 2 (2 of 2) 5-9

5.12. Time Response to Unit Step Input β Channel - Design 2 (1 of 2) 5-10

5.13. Time Response to Unit Step Input β Channel - Design 2 (2 of 2) 5-11

5.14. Time to Bank 90° - Design 2 (1 of 2) 5-12

5.15. Time to Bank 90° - Design 2 (2 of 2) 5-12

5.16. Time Response to Unit Step Input p Channel - Design 3 (1 of 2) 5-14

5.17. Time Response to Unit Step Input p Channel - Design 3 (2 of 2) 5-14

5.18. Time Response to Unit Step Input β Channel - Design 3 (1 of 2) 5-15

5.19. Time Response to Unit Step Input β Channel - Design 3 (2 of 2) 5-16

5.20. Time to Bank 90° - Design 3 (1 of 2) 5-17

5.21. Time to Bank 90° - Design 3 (2 of 2) 5-17

5.22. Time to Bank 90° - Design 3 with no Rate Limits (1 of 2) 5-18

5.23. Time to Bank 90° - Design 3 with no Rate Limits (2 of 2) 5-19

5.24. Comparison of the Three Designs (1 of 2) 5-20

5.25. Comparison of the Three Designs (2 of 2) 5-21

Figure Page

5.26. Final Lateral/Directional Flight Control System Block Diagram 5-22

List of Tables

Table		Page
3.1.	F-18 HARV Control Surface Position and Rate Limits	3-4
3.2.	F-18 HARV Control Surface Actuator Models	3-5
3.3.	Flight Conditions for All Plants	3-7
5.1.	Maximum Surface Deflection Due to a Unit Step Roll Rate Command	5-19
5.2.	Comparison of Wing Torsion and Bending Moment Loads	5-20
5.3.	Comparison of Compensator Designs	5-22

Abstract

Aircraft composed of lightweight composite materials are extremely enticing since their structural weight is greatly reduced. However, the control of these aircraft is complicated by the resultant flexibility of the wings. Two avenues of approach are possible; stiffen the wings thus losing some of the weight reduction benefits, or design the lateral/directional flight control system cognizant of the wing's flexibility. In this thesis the second approach is taken. The design of three lateral/directional flight control systems for the sub-sonic flight envelope of the F-18 is presented. The Quantitative Feedback Theory (QFT) robust control design technique is used. These designs incorporate weighting matrices to distribute generalized aileron and rudder commands to the five control surfaces available on the F-18. The degree of freedom afforded by the use of all control surfaces allows for the reduction of the load on the wings, while at the same time meeting military specifications for roll maneuvers. A baseline flight control system is designed and then improved upon; the final design incorporates load alleviation concepts to reduce the load on the wings thus avoiding wing twisting. All flight control systems designed in this thesis are shown to meet military specifications, as verified with nonlinear time simulations.

DESIGN OF FLIGHT CONTROL LAWS FOR AIRCRAFT WITH FLEXIBLE WINGS USING QUANTITATIVE FEEDBACK THEORY

I. Introduction

Conventional lateral/directional flight control methods envisage a rigid wing with movable control surfaces. The deflection of the control surface is used to generate aerodynamic forces and moments for flight control. Wing flexibility is a negative property in this approach; as it reduces control effectiveness, resulting in poor rolling performance at high dynamic pressures ($\bar{q}$). Thus, when the ailerons of the aircraft are deflected at high $\bar{q}$ to generate a commanded rolling moment, the finite wing stiffness allows the wing to twist and bend creating an opposing moment, counter-acting the desired effects of the commanded rolling moment. When this occurs, it becomes necessary to use other available control surfaces or increase wing stiffness in order to improve the rolling performance. Thus, stiffness considerations are more often than not the driving design factor in aircraft design. This calls for stiff wings, which, in turn, calls for less aerodynamically efficient, low aspect ratio wing planform designs, or an undesired increase in structural weight.

The Active Flexible Wing (AFW) technology strives to gainfully employ the wing's aeroelastic flexibility. Control surfaces on the wing are used as aeroelastic "tabs" that induce wing twist in the proper direction instead of trying to fight it. The wing's total twist creates the control forces and moments used in the AFW technology. In this research the focus is exclusively on twisting the wing to provide maneuver control power for rolling the aircraft; thus, only lateral/directional flight control is considered. The AFW technology seeks the use of a wing with reduced

torsional stiffness and multiple trailing and leading edge control surfaces which aeroelastically twist the wing into an optimal shape at all flight conditions, i.e., low and high dynamic pressures $\bar{q}$. Optimality here refers to achieving the required control power while at the same time minimizing the aerodynamic loads imposed on the twisting wing's structure.

The benefits of the AFW technology include:

1. Reduced structural and takeoff weight allowing for greater payload and/or increased fuel capacity and greater range,
2. Reduced drag resulting in increased range,
3. The length of hinge lines is reduced and the control surface deflections are relatively small, which in turn reduces the aircraft's radar cross section during maneuvering and enhances stealth.

The aircraft under consideration in this research is the F-18 High Angle of attack Research Vehicle which provides an excellent test bed for AFW flight control system design. The F-18 HARV has five control surfaces available for use in the lateral/directional channel; leading edge flaps, trailing edge flaps, ailerons, differential horizontal tail, and rudders. The lateral/directional channel is the focus of this research due to the fact that the majority of the flexibility related problems occur during rolling maneuvers. A full non-linear simulation program, designed by NASA, is available for generating the linearized plants and for testing of final control designs.

1.1 Problem Statement

The objective of this thesis research is to develop a full subsonic flight envelope lateral/directional flight control system for the F-18 using the robust Quantitative Feedback Theory (QFT) control design method to effectively blend the available control surfaces in order to improve roll performance. For this research, the subsonic flight envelope is defined as speeds from 0.22 to 0.9 Mach, and altitudes between

5,000 and 40,000 ft. These limits are imposed by the capabilities of the simulation program as well as limits of the aircraft itself.

1.2 Literature Review

With recent advances in composite material technology, fighter aircraft have been constructed with lighter-weight materials. Obviously, the use of lightweight materials provides advantages including improved range, speed, and serviceability; however, under the conventional flight control design paradigm there are also disadvantages such as increased flexibility. Flexibility, caused by decreased stiffness in the wings results in poor rolling performance at high dynamic pressures ($\bar{q}$). An example of a fighter aircraft with flexible wings is the F-18. Furthermore, the current control law in the F-18 accomplishes the blending of control surface commands using gain scheduling, a costly, and computationally intensive method of control.

In recent years several different design methods for high performance control system synthesis have been proposed, including H_2 - H_∞ [1], Dynamic Inversion [4], and Quantitative Feedback Theory (QFT) [7]. Wright Laboratory has sponsored a series of AFIT theses using the QFT robust control design method to design control systems for several aircraft, e.g. the VISTA F-16 [12] and the Unmanned Research Vehicle (URV) [15]. In the continuing effort to explore the benefits of QFT, Wright Laboratory has sponsored a thesis to design a flight control system (FCS) for the lateral/directional channel of the F-18. Using QFT, an FCS design can be accomplished to robustly blend the control surface commands, eliminating the need for gain scheduling and improving rolling performance.

This literature review covers two major areas: background information on the F-18 and its flight control system problems, and current research in the area of flexible wings.

1.2.1 History of the F-18. In 1976, the U.S. Navy signed a formal contract with McDonnell Aircraft Company to develop and build the F-18. The F-18 was unique in that it incorporated several untested technological advances. One of the design advancements was the use of composite materials in the aircraft main structure/frame. As opposed to traditional materials, the composite material was lightweight, resulting in a lighter aircraft with superior maneuverability characteristics.

Unfortunately, during flight tests, the achieved roll performance fell below military specifications [2]. The lightweight materials in the wing provided less stiffness, allowing the wings to twist under high stress. This twisting was one of the causes of poor roll performance. Initially, the stiffness of the wings was increased as well as increasing the size of the aileron control surface. However, the results of flight testing still showed unacceptable roll performance. As opposed to increasing the stiffness of the wings a second time, engineers decided to create a flight control system, scheduled with dynamic pressure, to compensate for the decreased performance from the ailerons. This controller incorporated numerous point designs, blending the use of the available control surfaces, i.e. ailerons and trailing edge flaps, at different flight conditions. The F-18 naturally lends itself to this type of roll control concept because of the five available control surfaces that affect roll performance: leading edge flaps, trailing edge flaps, stabilators, and rudders. Although the final flight control system was designed to avoid wing twisting, some designers have since then seen potential for using the twist in a positive manner.

In the past five years, several paper designs using "modern" control techniques have been performed on the F-18. However, there were several problems with these designs and they lacked relevancy to the control of wing twisting. In the thesis by Hartley [6], the control system design was based on only one point in the heart of the flight envelope. A complete and practical design would need to account for the entire flight envelope, including high angle of attack and high $\bar{q}$ regions, in order

to ensure the controller would be adequate for the aircraft. The paper by Sparks et. al. [14] described a full envelope controller design; however, their test methods were questionable in that their FCS was tested on a computer simulation created by the same engineers who designed the control system. This computer simulation was based on the non-linear equations of motion, but it lacked the aeroelastic effects, such as bending modes, responsible for wing twist. The papers by Enns et al. [4] and Buffington et al. [1] designed controllers for only the longitudinal axis (pitch). While some wing twist may occur in longitudinal motion, the majority of wing twist results from aileron deflections used to generate rolling moments; therefore, to truly address the problems caused by wing twisting only controllers for the lateral/directional axis are considered in this thesis.

1.2.2 Flexible Wing Research. More recently, the Active Flexible Wing (AFW) project has been exploring the benefits and controllability of flexible wing aircraft. In its initial phase, this project was conducted jointly by NASA, Rockwell International, and the U.S. Air Force. Initially the project was tasked with demonstrating the concept of flexible wings. After the successful completion of the first phase, a second phase conducted by NASA and Rockwell strove to accomplish two major goals. The first goal of the AFW project was to demonstrate effective suppression of flutter during high $\bar{q}$ conditions. The second goal was to successfully design a controller capable of efficiently blending the use of the available control surfaces to alleviate the load on the wings during rolling maneuvers, and thereby improve the roll performance of the aircraft [11]. Only the second goal of rolling maneuver load alleviation (RMLA) is discussed here since it is most applicable to the work performed in this research.

The AFW wind-tunnel model, created by Rockwell International, was a full aeroelastically scaled fighter aircraft with a wing span of 8.67ft. Each wing had four available control surfaces (two leading edge flaps, and two trailing edge flaps) for use in flight control. The AFW wind-tunnel model was sting mounted, allowing the

model to roll freely about the body x-axis. In addition, the angle of the sting could be remotely adjusted to provide angles of attack between $-1.5°$ and $13.5°$ [11].

In the area of RMLA, two different designs were tested. The first control design was based on LQG/LTR modern control methods to control roll rate and wing loads [16]. The FCS controlled five surfaces (trailing edge inboard surfaces collectively, trailing edge outboard left, trailing edge outboard right, leading edge outboard left, and leading edge outboard right) using five feedback signals (roll rate and wing torsion at four different locations). The total load on the wing had two components, aerodynamic and inertial loads. Aerodynamic loads were a function of the angle of attack (α), roll rate (p), surface deflection (δ), and dynamic pressure ($\bar{q}$) while inertial loads were dependent on the roll acceleration ($\dot{p}$). These loads created wing root bending moments, and torsion torques at the wing root and outboard wing panels. The magnitude of the bending moment and torsion torques was also dependent on the wing area and wing span. Equations relating the wing root bending moment (f_{BM}) and torsion torques (f_{TM}) to the roll rate and effector deflection can be expressed as follows:

$$f_{BM} = C_{BM_p} p + C_{BM_\delta} \delta \tag{1.1}$$

$$f_{TM} = C_{TM_p} p + C_{TM_\delta} \delta \tag{1.2}$$

where C_{BM_p}, C_{BM_δ}, C_{TM_p}, C_{TM_δ} are influence coefficients relating the bending moment and torque created by roll rate and surface deflections.

Through experimentation, it was determined that the trailing edge inboard control surfaces (typically ailerons) had the greatest effect on rolling moment while the leading edge outboard and trailing edge outboard control surfaces were capable of controlling the wing loads without adversely effecting the rolling moment. For load alleviation, the outboard surfaces had to be operated in the opposite direction of the inboard surface and the slight decrease in rolling moment was compensated for by increasing the aileron deflection. The control scheme involved feeding back

roll rate to the inboard and outboard surfaces along with a command signal to the leading edge inboard surface. Two designs were tested, one using the leading edge outboard flaps along with the trailing edge inboard flaps, and the other utilized the trailing edge outboard flaps in conjunction with the trailing edge inboard flaps. Both designs used a simple gain in the feedback control law to obtain the desired results.

The designs were tested on the AFW wind tunnel model at the NASA Langley Transonic Dynamics Tunnel. Results for both designs were favorable with respect to alleviating torsional torques at both inboard and outboard stations. However, mixed results were obtained for the alleviation of bending moments. Overall, it was judged that the best control combination was using the trailing edge inboard control surfaces for generating the required rolling moment, and the leading edge outboard control surfaces for load alleviation. This design was successful in reducing the torsional loads on the wing by 40% without adversely affecting roll performance [16]. One thing this research lacked was an attempt to use both leading and trailing edge outboard control surfaces for load alleviation in a single design to determine if the peak loads could be reduced even further than the values found in the use of a single control surface for load alleviation.

A second group used feed-forward nonlinear optimal control techniques to design a compensator [10]. For the feed-forward design the only inputs were the commanded roll rate and the actual (measured) roll rate. Optimization techniques were used to develop look-up tables based on experimental data. These look-up tables were used in a feed-forward configuration to command outboard surface deflections in order to reduce loads on the wing. This method of control worked to alleviate loads only when they reached a specified threshold, allowing full control power to be available for control designs when load levels were low.

This design was also tested on the AFW wind tunnel and was successful in limiting the wing loads to levels below the maximum threshold. The roll performance achieved when the load alleviation controller was active was nearly identical

to the baseline controller. Overall, both of these design methods were successful at demonstrating the feasibility of load alleviation control concepts.

1.3 Assumptions

As in most flight control design work the following assumptions are made:

1. The aircraft mass is constant with time.
2. Aircraft mass distribution is constant with time (no fuel sloshing).
3. The earth is an inertial reference frame and the gravitational acceleration is constant with altitude.
4. The atmosphere is fixed with respect to the earth (no gust effects are considered.)
5. The aircraft is symmetric about the xz– and xy–planes.
6. The lateral/directional and longitudinal channels can be decoupled.

The first six assumptions are valid due to the short time span the controller will be active (between pilot inputs.) The last assumption is valid for small perturbations about a nominal condition. This assumption isn't always valid; however the assumption, commonly used in flight control design, greatly simplifies the problem and the resulting control design is tested to ensure adequate performance during large perturbations.

1.4 Scope

In this thesis, the robust flight control system design that exploits the wing's flexibility is limited to the lateral/directional channel of the F-18. The flight envelope of the F-18 is restricted to subsonic regions above 5,000 ft in altitude (a limit established by the HARV simulation). The controller is constrained to a second order diagonal prefilter and a third order diagonal compensator. A linear simulation is used to test the final flight control system design.

1.5 *Approach and Methodology*

This thesis is composed of two major sections; controller design and simulation. Controller design is accomplished using the method of Quantitative Feedback Theory (QFT) [8]. The structure of a generic MIMO QFT controller is shown in Fig. 1.1. The resulting design is tested on a linear simulation using Matlab.

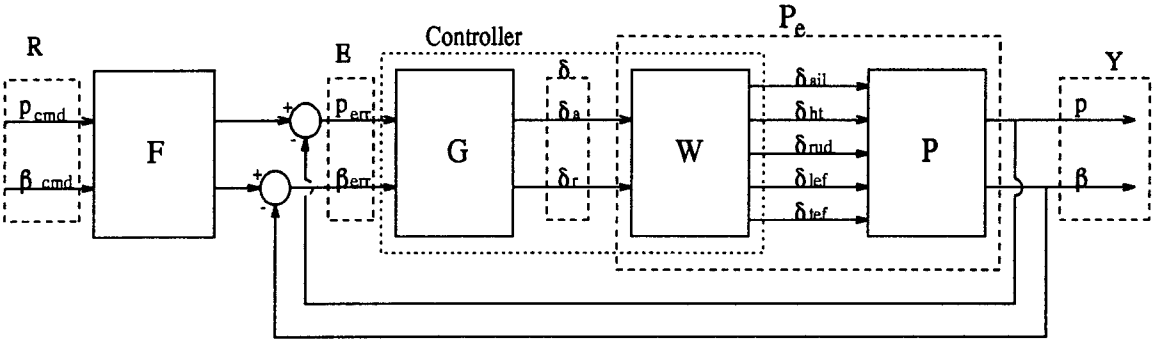

Figure 1.1 Flight Control System Block Diagram

1.5.1 *Controller Design.*

1.5.1.1 Plant Models. Using the QFT design approach, the plant uncertainty set $\mathcal{P}$ is defined as the subsonic flight envelope. Over 30 flight conditions are chosen to cover this region of uncertainty. The linear aircraft model (P), a non-square plant with five inputs and two outputs, is extracted from the HARV F-18 simulation for each flight condition. Once the models are determined, the lateral/directional channel is isolated from the full model. These models are then entered into a QFT CAD package developed by Sating [9].

1.5.1.2 Weighting Matrix. The weighting matrix allows one generic control input to be distributed among several control surfaces. The weighting matrix is designed based on the effectiveness of the control surface at each dynamic pressure ($\bar{q}$). In addition, the weighting matrix, when combined with the plant matrices, defines the effective square plant matrix (P_e) required in the design process. However,

in practice, the weighting matrix forms part of the designed compensator, as shown in Fig. 1.1.

1.5.1.3 Tracking and Cross-Coupling Effect Rejection Bounds. Frequency domain bounds representing the desired time domain responses are calculated. The upper and lower bounds of time domain responses are determined based on specifications in MIL-STD 1797A *Flying Qualities of Piloted Aircraft* [5]. These bounds create a region in which the closed-loop frequency response must lie for all flight conditions.

1.5.1.4 Template Generation. Templates are generated for frequencies one octave apart over the frequency range of interest. The high frequency cutoff is controlled by the bending modes of the aircraft. For the F-18 this frequency cutoff is 15 rps.

1.5.1.5 Compensator Design. Once the bounds and templates have been generated, the compensators ($\mathbf{G}$) are designed interactively using the QFT CAD package. Loop shape satisfaction on the Nichols chart of the stability and composite bounds (a worst case combination of tracking and cross-coupling effect rejection bounds) is the ending criteria. In addition, the compensator is chosen to be constrained to a third order design in order to decrease time delays.

1.5.1.6 Pre-Filter Design. After the compensator design is complete, a pre-filter is designed to ensure the closed loop frequency response lies within the tracking bounds previously specified. The pre-filter design is accomplished with the aid of the QFT CAD package.

1.5.1.7 Validation. The QFT CAD package provides a method for verification of specifications in the frequency domain. This is the final step of the

compensator design. If all specifications are met by the design the next step is linear time simulation.

1.5.2 Simulation. As an initial check to determine the performance of the controller, a time simulation of the FCS using Matlab is completed. This simulation tests the thirty-one points originally chosen to cover the flight envelope. As a first test, a unit step command is used to independently check each channel for stability and cross-coupling effects. Following this, a step input of roll rate is commanded to determine the time to 90° bank angle. Meeting all standards from MIL-STD 1797A is the ending criteria for linear time simulation.

1.6 Organization of Thesis

Chapter 2 presents some basics of MIMO QFT theory. A description of the F-18 HARV is detailed in Chapter 3. Chapter 4 describes the flight control system design followed by the time simulations of the lateral-directional flight control systems in Chapter 5. Finally, conclusions and recommendations for further research are discussed in Chapter 6.

II. QFT Theory

Quantitative Feedback Theory is different from other methods of controller design in the transparency of its techniques. This transparency allows the engineer to determine if a control solution is possible early in, and during, the design process. If no solution exists, changes must be made to ease the design specifications. In most modern control techniques, the designer would realize that specifications could not be met only after repeated trial and error.

The QFT design is performed in the frequency domain instead of the time domain. By using the frequency domain, the mathematics of the problem are greatly simplified (algebraic multiplication in the frequency domain versus convolution in the time domain.) In the frequency range of interest i.e., in the pilot's bandwidth of 0.1 to 3.5 rps, a good correlation between the time domain and frequency domain exists. This correlation justifies the transformation into the frequency domain.

Another advantage of QFT is its ability to account for system modeling errors ("structured plant uncertainty") relatively easily. In flight control, plant uncertainty is caused by changes in aerodynamic performance as flight condition varies. To account for these changes, most design techniques choose several points throughout the flight envelope and perform flight control system designs for each point. These individual point designs are then combined through gain scheduling to create a controller for all flight conditions. These designs have large costs associated with computer time and validation, and in the end, there is no guarantee that the designs will work successfully for all flight conditions. As opposed to doing numerous point designs, QFT techniques lead to a single design covering the entire flight envelope. The boundary of the flight envelope is used to define the plant uncertainty, thus the resulting controller is guaranteed to work for all flight conditions. The QFT design yields a "wide coverage controller", not the gain scheduled point designs of other methods.

The remainder of this chapter discusses the different steps involved in the QFT design process with respect to flight control system design, giving some of the theory behind the steps. However, it is assumed that the reader has some general knowledge of QFT and for the most part results are given without proof. For more detail, refer to Chapter 18 of the D'Azzo and Houpis modern control textbook [3] and the Wright Laboratory Technical Report on QFT [8]. In addition, terminology is used in accordance with Sating's QFT CAD package [13].

2.1 Effective Plant

Typically, the behavior of an aircraft is modeled by the state space system

$$\dot{\mathbf{x}} = \mathbf{A}\mathbf{x} + \mathbf{B}\mathbf{u}$$

$$\mathbf{y} = \mathbf{C}\mathbf{x} + \mathbf{D}\mathbf{u} \tag{2.1}$$

where for the F-18 lateral/directional case $\mathbf{x} = [p \quad r \quad \beta \quad \phi]^T$, $\mathbf{y} = [p \quad \beta]^T$ and $\mathbf{u} = [\delta_{ail} \quad \delta_{ht} \quad \delta_{rud} \quad \delta_{lef} \quad \delta_{tef}]^T$ where δ represents the surface deflection of the ailerons, stabilators, rudders, leading edge flaps and trailing edge flaps respectively. The plant $\mathcal{P}$ is determined through Eq. (2.2) for the linear time-invariant case.

$$\mathbf{P} = \mathbf{C}[s\mathbf{I} - \mathbf{A}]^{-1}\mathbf{B} \tag{2.2}$$

The values for the **A** and **B** matrices are dependent on the flight condition, thus in this case the plant uncertainty is the flight envelope of the aircraft. Based on the flight scenario, $\iota = 1, 2, \ldots, \mathcal{J}$, LTI plants $\mathbf{P}_\iota$ are determined that satisfactorily describe the region of plant uncertainty. In QFT the effective plant ($\mathbf{P_e}$) must be a square matrix for design purposes. A non-square system (as in this case with five inputs and two outputs) is squared down through the use of a weighting matrix. This weighting matrix takes a generalized command signal (aileron and rudder) and converts it into the five different control surface signals. A more detailed explanation

of the development of the weighting matrix is found in Chapter IV. Since the inputs to the effective plants are generalized signals, the control surface actuator dynamics must also be included in the effective plant, following the weighting matrix. A block diagram representation of the m x m (where in this case $m = 2$) effective plant is shown in Fig. 2.1.

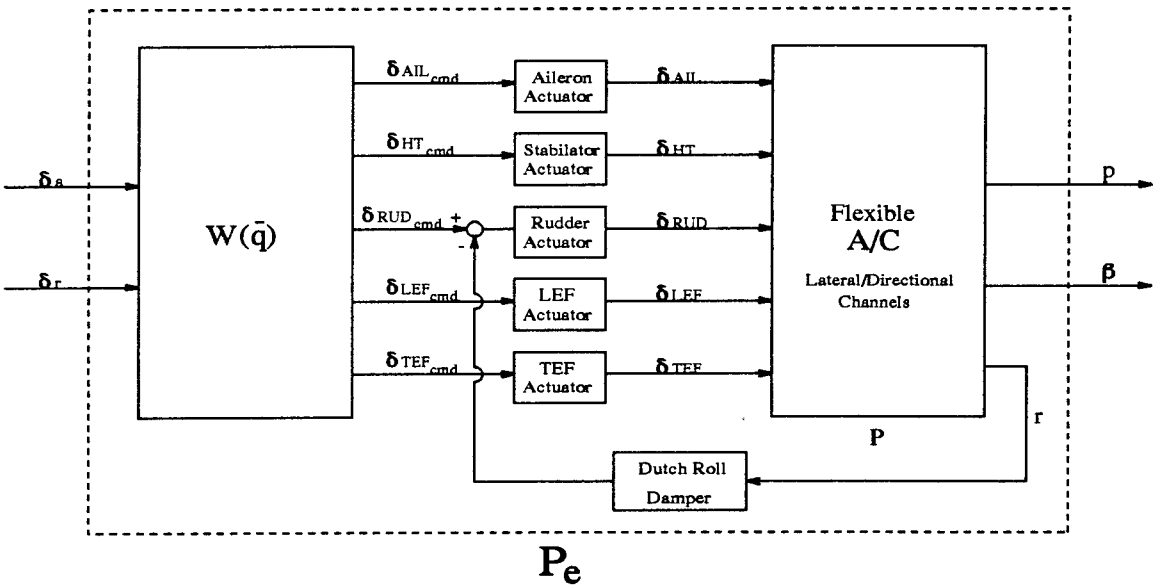

Figure 2.1 Effective Plant

For the purposes of the QFT design process, the effective plant is treated as the plant to be controlled. However, during implementation, the weighting matrix is considered part of the controller and not part of the plant.

2.2 Tracking and Stability Specifications

From the block diagram of Fig. 1.1, the ratio of input to output signals is determined as follows:

$$\mathbf{E}(s) = \mathbf{F}(s)\mathbf{R}(s) - \mathbf{Y}(s) \tag{2.3}$$

$$\mathbf{Y}(s) = \mathbf{P_e}(s)\mathbf{G}(s)\mathbf{E}(s) \tag{2.4}$$

$$\mathbf{T}(s) = \frac{\mathbf{Y}(s)}{\mathbf{R}(s)} = [\mathbf{I} + \mathbf{P_e}(s)\mathbf{G}(s)]^{-1}\mathbf{P_e}(s)\mathbf{G}(s)\mathbf{F}(s) \tag{2.5}$$

$$\mathbf{T}(s) = \begin{bmatrix} \frac{p(s)}{p_{cmd}(s)} & \frac{p(s)}{\beta_{cmd}(s)} \\ \frac{\beta(s)}{p_{cmd}(s)} & \frac{\beta(s)}{\beta_{cmd}(s)} \end{bmatrix} = \begin{bmatrix} t_{11}(s) & t_{12}(s) \\ t_{21}(s) & t_{22}(s) \end{bmatrix} \tag{2.6}$$

Performance specifications for the system set limits on the values of the t_{ij} control ratios. For this research, the performance specifications are defined by MIL-STD 1797A. In the ideal situation only the diagonal terms have bounds with the off-diagonal terms being equal to zero. However, in the real world, some cross-coupling between the channels exists; and cross-coupling effect rejection bounds must be determined for the system. For the most part, performance specifications are stated in the time domain. For use in QFT design, these specifications must be translated into the frequency domain. Although this is not an exact transformation, reasonable results are produced for the frequency range of interest, and the final results are tested against the original time domain specifications.

In addition to tracking specifications, QFT uses stability specifications in its design procedures. Stability specifications can be stated in terms of gain margin (g_m), phase margin angle (γ), or the corresponding critical M_L contour on the Nichols chart. For aircraft design, the phase margin angle is typically specified to be $\gamma = 30°$ which equates to $M_L = 6.02dB$

2.3 Effective MISO Equivalent Plants

In order to simplify the MIMO design problem, QFT maps the m x m MIMO plant into m^2 MISO equivalent plants. Thus, with a diagonal compensator matrix, the design problem is decomposed into m MISO equivalent plants with two inputs (a desired signal (commanded input) and an undesired signal (cross-coupling)) and one output. This greatly facilitates the design procedure without losing information due to the simplification process.

The MISO equivalent plants are based on elements in the Q matrix where the q_{ij} terms are the element by element inverse of the matrix inverse of the effective

plant $\mathbf{P_e}$. For this research,

$$\mathbf{Q} = \begin{bmatrix} q_{11} & q_{12} \\ q_{21} & q_{22} \end{bmatrix} = \begin{bmatrix} 1/p_{11}^* & 1/p_{12}^* \\ 1/p_{21}^* & 1/p_{22}^* \end{bmatrix} \tag{2.7}$$

where

$$\mathbf{P^{-1}} = \begin{bmatrix} p_{11}^* & p_{12}^* \\ p_{21}^* & p_{22}^* \end{bmatrix} \tag{2.8}$$

Thus the transmission functions can be written from the signal flow graphs of Fig. 2.2. The off-diagonal MISO loops only have a cross-coupling input (no tracking signal, thus $f_{ij} = 0$ for $i \neq j$) while the diagonal MISO loops have both a cross-coupling and a tracking input.

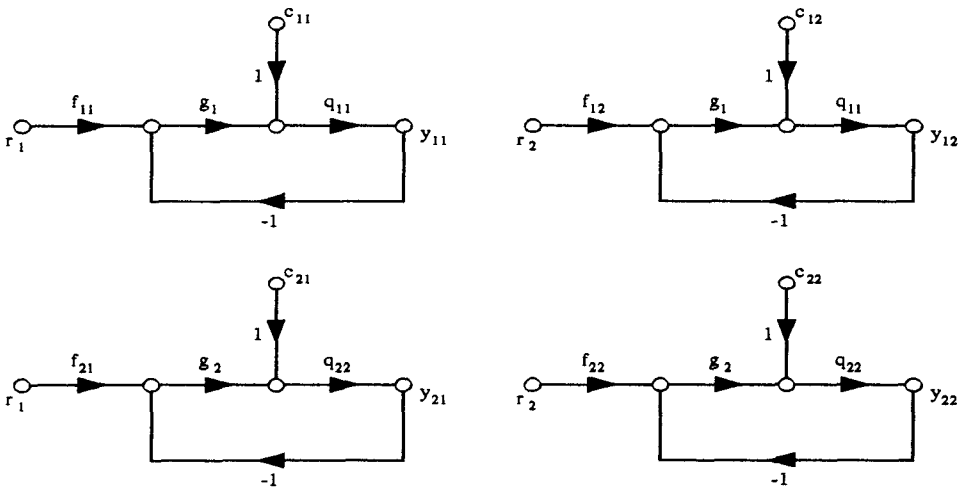

Figure 2.2 MISO Equivalent Plants

$$t_{ij} = t_{r_i} + t_{c_{ij}} \quad \text{for } i = j \tag{2.9}$$

and

$$t_{ij} = t_{c_{ij}} \quad \text{for } i \neq j \tag{2.10}$$

The closed-loop transfer functions is:

$$t_{r_i} = \frac{y_{ii}}{r_i} = \frac{f_{ii} g_i q_{ii}}{1 + g_i q_{ii}} = \frac{f_{ii} L_i}{1 + L_i} \tag{2.11}$$

and

$$t_{c_{ij}} = \frac{y_{ij}}{c_{ij}} = \frac{g_i q_{ii}}{1 + g_i q_{ii}} = \frac{L_i}{1 + L_i} \tag{2.12}$$

where

$$L_i = g_i q_{ii} \tag{2.13}$$

For the diagonal terms both an upper and lower bound must be specified as follows:

$$a_{ii} \leq t_{ii} \leq b_{ii} \qquad \text{for } i = 1, 2, \ldots m \tag{2.14}$$

For off-diagonal terms, only an upper bound is necessary and is defined as:

$$t_{ij} \leq b_{ij} \qquad \text{for } i, j = 1, 2, \ldots m \quad i \neq j \tag{2.15}$$

In addition, the stability margin for each row is defined as:

$$\left| \frac{L_i}{1 + L_i} \right| \leq M_L \qquad \text{for } i = 1, 2, \ldots m \tag{2.16}$$

Two conditions on the plants must exist in order to apply Method 1 of QFT. First the inverse of the effective plant ($\mathbf{P_e^{-1}}$) must exist. This is an obvious condition easily seen by examining the previous equations. A second condition is that *diagonal dominance* must exist as $\omega \rightarrow \infty$. The equation for determining diagonal dominance is given in Eq. (2.17).

$$|p_{11}(j\omega) p_{22}(j\omega)| > |p_{12}(j\omega) p_{21}(j\omega)| \quad \forall \; p \in \mathcal{P} \tag{2.17}$$

Diagonal dominance is a necessary condition derived from the cross-coupling analysis of the MISO equivalent loops. If this condition is not satisfied, it is possible to try to re-order the plant inputs and outputs. The diagonal dominance condition can be evaluated by Sating's QFT CAD package for all plants. An example plot of the diagonal dominance analysis is shown in Fig. 2.3 where dominance exists if the normalized plot is greater than zero as $\omega \rightarrow \infty$.

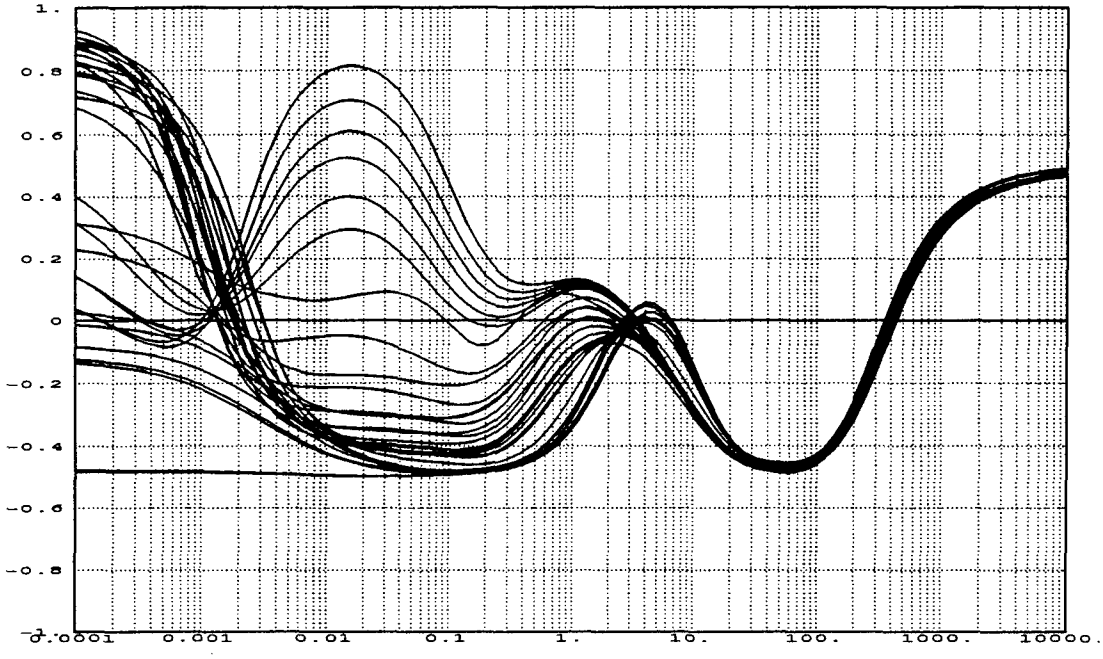

Figure 2.3 Diagonal Dominance Condition

2.4 Frequency Templates

Once the MISO equivalent plants have been determined, they are used to map the plant uncertainty into the frequency domain. A template is created by plotting the phase and magnitude of each plant for a given frequency. Thus, one template is created for each frequency. The template graphically shows the amount of uncertainty in the plant. An example of a frequency template is shown in Fig. 2.4. The size of the template determines how difficult it will be to accomplish a successful design [Chapter 7 [8]]. If the template has a large dB range, then it is known a priori

that a single controller design is not achievable. As a solution, the plant uncertainty can be divided and multiple control designs performed on the smaller uncertainty sets; eventually, the various controllers then need to be gain scheduled.

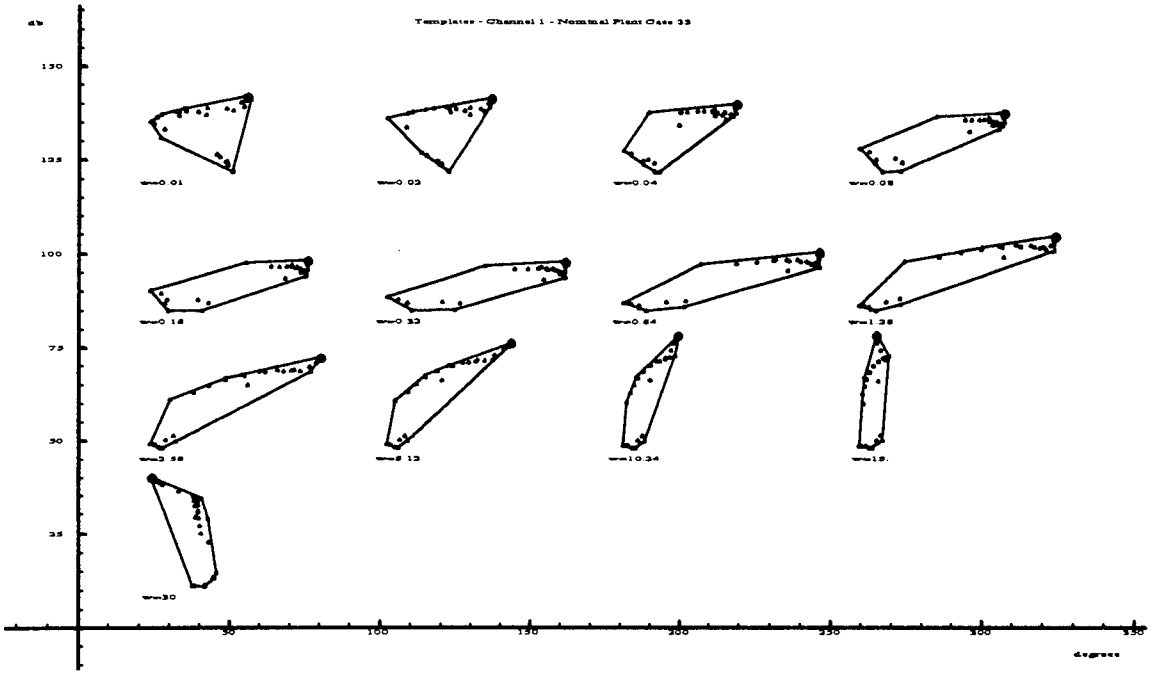

Figure 2.4 Example of Frequency Templates

After the templates are constructed, it is necessary to chose a nominal plant. This nominal plant is used as a marker on the frequency template. With foresight, it is wise to chose the uppermost plant on the frequency template that corresponds to the bending modes of the aircraft. Doing this ensures that if the nominal plant has the desired phase margin frequency ω_ϕ then all of the other plants will also have the desired phase margin frequency.

2.5 Bounds on the Nichols Chart

The frequency templates are then used to create bounds on the Nichols chart. Typically in the QFT design process there are four types of bounds: stability, tracking, cross-coupling effect rejection, and outside disturbance rejection. These bounds are determined using the frequency templates, thus incorporating the plant uncer-

tainty into the bounds. QFT has a certain amount of inherent over design in the establishment of bounds. Based on these bounds, a worst-case composite bound is generated. If the loop transmission function lies above the composite bound for a give frequency, then the system is guaranteed to meet specifications. However the system may still meet specifications even if the bounds are not satisfied. Thus it is possible that a slight violation of bounds may still yield acceptable final results.

Stability bounds are determined for each frequency by plotting the nominal plant as the template traverses the edge of the M_L contour. This ensures that if the nominal plant doesn't cross the stability bounds then none of the plants violate the M_L contour and thus the stability specifications are satisfied. Since the templates are different for each frequency, the stability bound vary with frequency. An example of the stability bounds for the F-18's β channel is shown in Fig. 2.5.

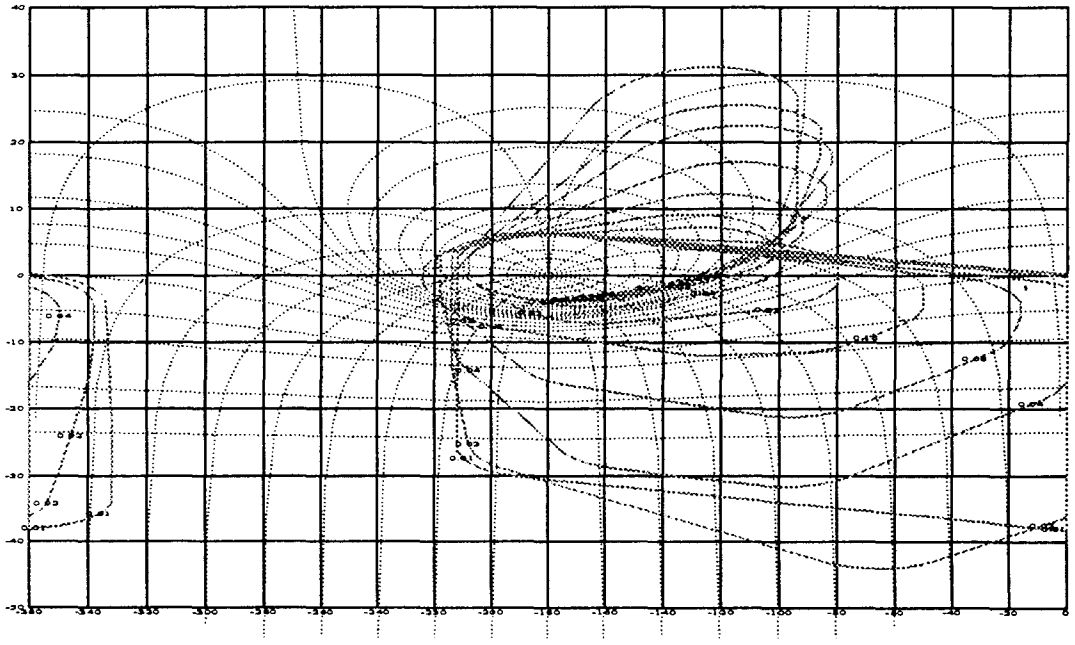

Figure 2.5 Stability Bounds on the Nichols Chart

As previously stated, the diagonal plants must lie within a prescribed region, called δ_R, determined by the upper and lower tracking bounds. Mathematically this

is described by:

$$\delta_R = 20\log\left(\frac{b_{ii}}{a_{ii}}\right) = 20\log(b_{ii}) - 20\log(a_{ii}) \tag{2.18}$$

Once again, δ_R is dependent on frequency and thus the tracking bounds vary with frequency. An example of the tracking bounds for the F-18 is shown in Fig. 2.6. A more detailed description of the calculation of tracking bounds can be found in [8].

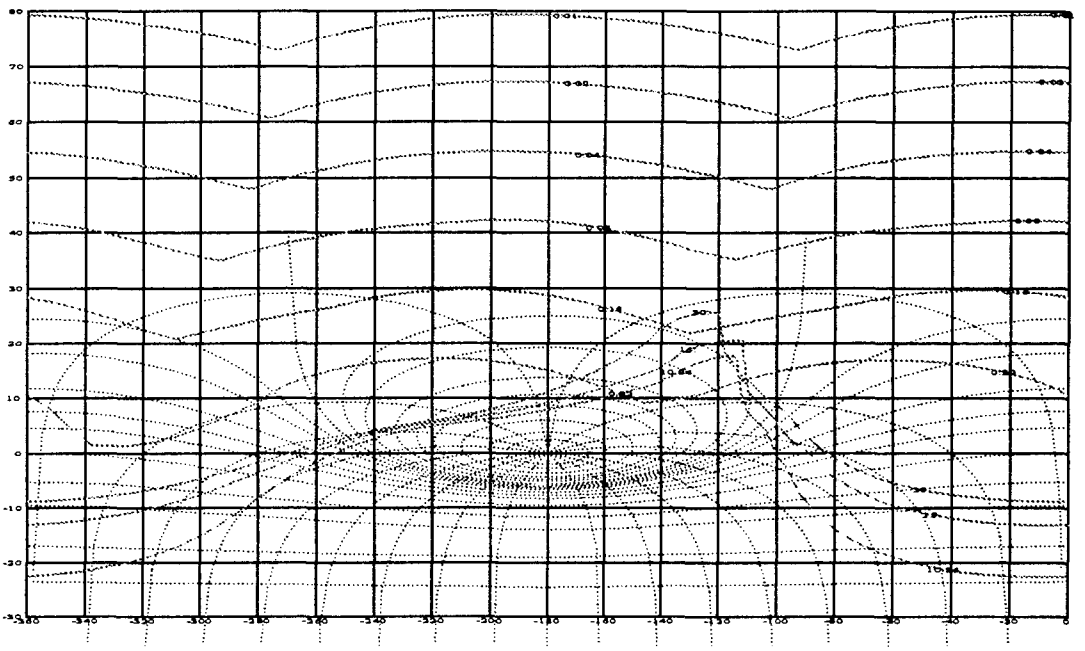

Figure 2.6 Tracking Bounds on the Nichols Chart

The cross-coupling effects are a function of the system dynamics and are generally undesired. In the case of a flight control design, differential aileron deflection causes adverse and proverse yaw. Thus a commanded input of roll rate (p) results in an undesired response in the side slip (β) channel. According to the specifications, cross-coupling effects must be kept below an established maximum $t_{ij} \leq b_{ij}$ for $i \neq j$. An example of the cross-coupling bounds generated by the QFT CAD package is shown in Fig. 2.7.

For the purpose of the design problem, the loop transmission function for each frequency must be on or above the highest bound on the Nichols chart. Thus the

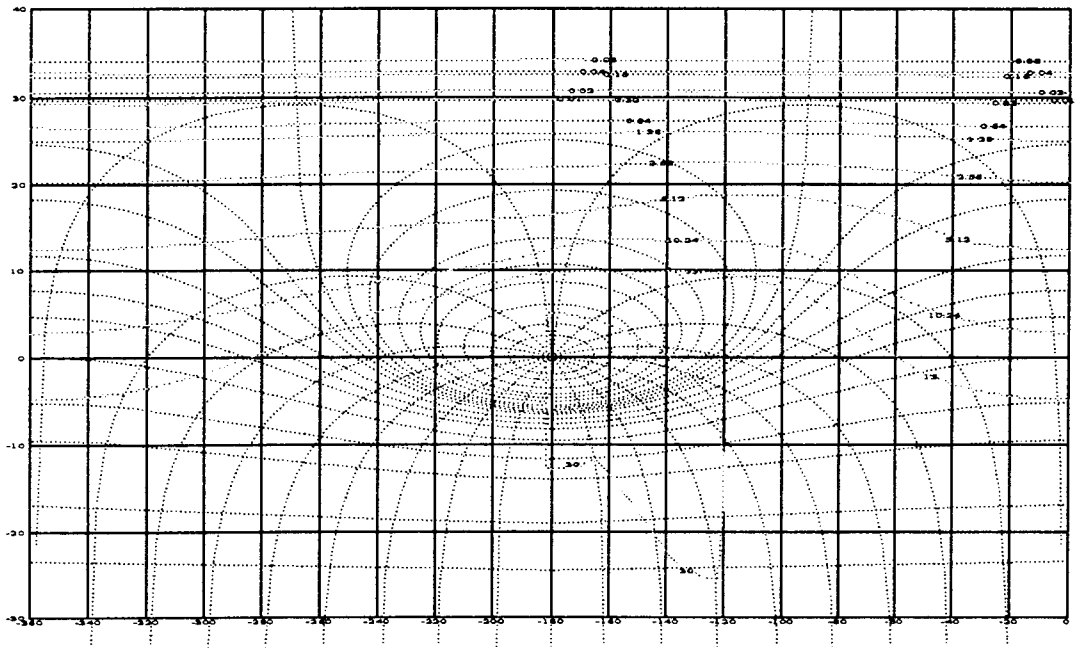

Figure 2.7 Cross-Coupling Bounds on the Nichols Chart

QFT CAD package computes the composite bound at each frequency for use in loop shaping by taking the largest magnitude at each phase angle.

2.6 Compensator Design

Once the composite bounds have been determined, the compensator design can begin. The loop transmission $L_{io} = g_i q_{iio}$ of the nominal plant is initially plotted for $g_i = 1$. Poles and zeros, as well as gain, are added until the bounds are met and the desired phase margin frequency is achieved. An example of the loop transmission plot is shown in Fig. 2.8. The loop shaping is another of the features of QFT that reduces the number of iterations required for a successful controller. By design, if the nominal loop transmission function satisfies all of the bounds, then all other plants are guaranteed to meet the bounds. In addition, due to the graphical interface, it is easy to see the effects of pole/zero placement. Another benefit of the QFT design method: the engineer can quickly and easily determine if all specifications can be met. If the bounds cannot be satisfied for all frequencies, then the engineer can

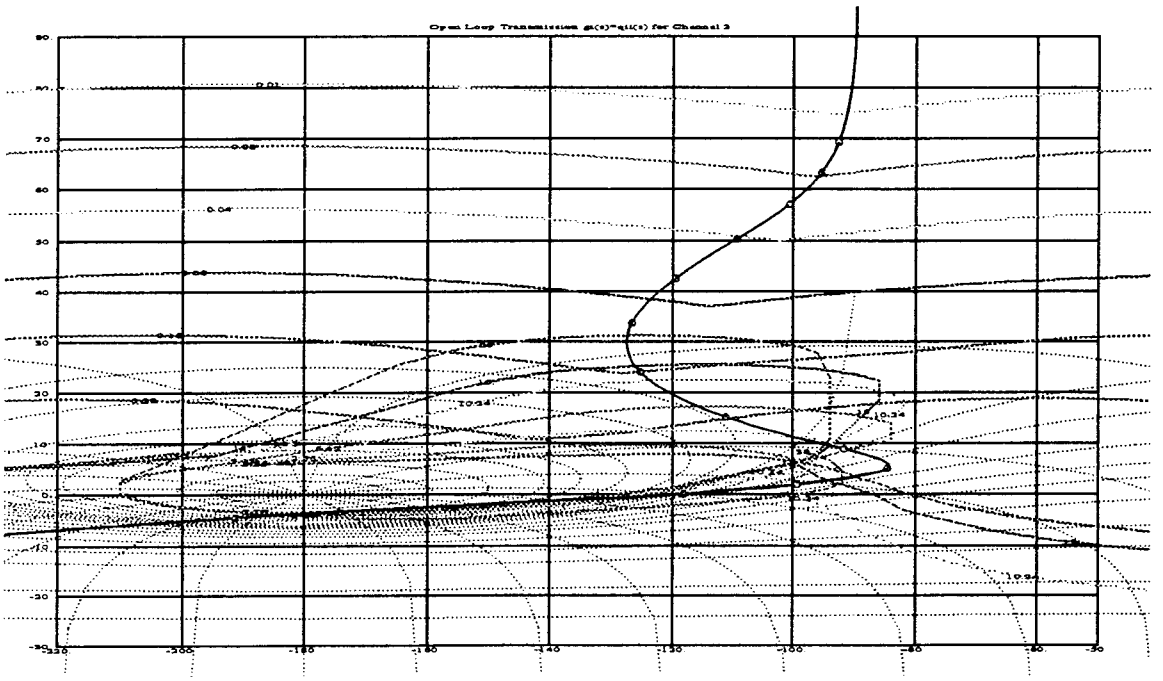

Figure 2.8 Loop Transmission Example

decide what range of frequencies are truly important. For example, in the flight control system design, since the pilot's bandwidth is approximately 0.1 to 3.5 rps, then it is only essential that tracking bounds are met in this range. Above and below this frequency range, only stability bounds are of importance.

Another factor in the compensator design is the order of the compensator. In order to reduce the delay in the system, a low order compensator is desired. By starting with a unity gain compensator, the order can be limited. For this design, the goal is to create a compensator of third order or less. In addition, although this is not a digital design, the poles and zeros are placed only at frequencies below 60 rps. This ensures an easy transition into the digital $\mathcal{Z}$-domain (where a 50 Hz sampling rate is used) in future research.

2.7 Pre-Filter Design

Once the compensator has been designed there is one final step in the design process. Although the compensator satisfies the bounds on the Nichols chart, this only guarantees that the response has a desired range of variation. It is therefore necessary to design a pre-filter to ensure that this range of variation lies within the previously established frequency domain tracking bounds. This step is also done interactively in the QFT CAD package starting with a unity gain pre-filter. As in the compensator, poles and zeros are added to achieve the desired shape. For the pre-filter, it is necessary to maintain a DC gain of one to ensure zero tracking error. Note that the pre-filter matrix is diagonal since there are no tracking specifications and no input signal for the off diagonal terms.

2.8 Frequency Domain Validation

After completion of the design, it must be checked in the frequency domain to verify that the specifications have been met. The QFT CAD package can be used to validate that stability, tracking and cross-coupling effects specifications have been met for all plants in the frequency domain. All that is then left is to check time responses using any available simulation programs to validate that time specifications have been met. An example of the stability validation performed by the QFT CAD package is shown in Fig. 2.9. As seen in the figure, all $\mathcal{J}$ loop transmission functions do not penetrate the stability (M_L) contour (represented by the thick line) on the Nichols chart.

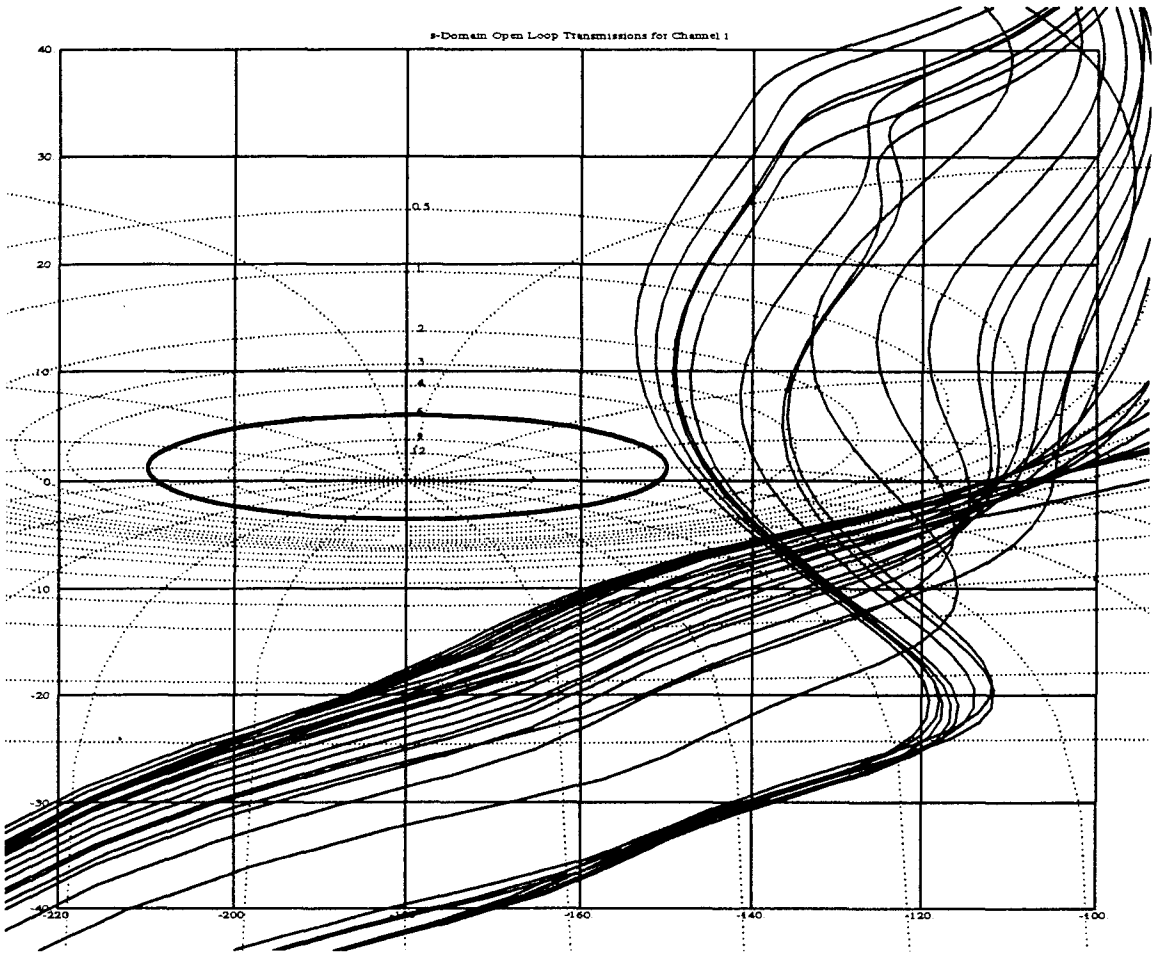

Figure 2.9 Stability Validation Example

III. The F-18 HARV

This chapter provides a description of the F-18 High Angle of attack Research Vehicle (HARV) with emphasis on the aspects important to this research. A non-linear simulation of the F-18 HARV, developed by NASA is available through Wright Laboratory's Flight Dynamics Directorate for use in this research.

3.1 The Aircraft

The F-18 HARV is a pre-production F/A-18, Fig. 3.1, on loan to NASA from

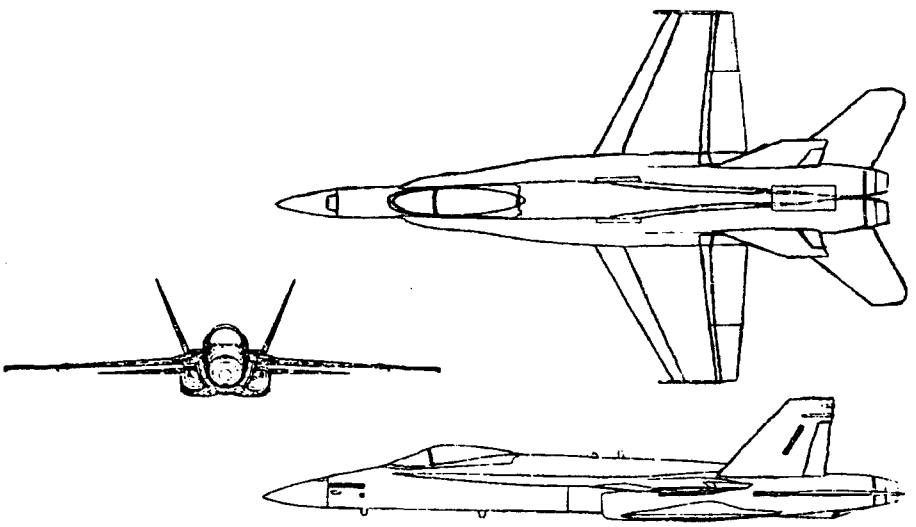

Figure 3.1 The F-18 Aircraft

the U.S. Navy. The major difference between the HARV and the production F/A-18's is the incorporation of thrust vectoring nozzles in both of the engines. These nozzles can be adjusted to give additional pitch and yaw control in low $\bar{q}$ flight conditions where conventional control surfaces are incapable of generating adequate control forces. Another difference is the HARV has been specially equipped to allow for testing of different control laws. To aid in the development of these control laws, NASA has generated a non-linear simulation of the F-18 HARV. This simulation

combined with the numerous available control surfaces and the F-18's previously established problems with wing twist make this aircraft an excellent candidate in the study of control designs for aircraft with flexible wings.

3.2 Linear Plant Models

The F-18 HARV simulation program is capable of providing a linearized model of the full non-linear system about a specified trim condition. The complete linear model is an eleven state, twelve input system. Since, for this research, it has been determined that the lateral/directional dynamics are of greatest importance, this full linear model is paired down to a four state, six input model. In doing this, it is assumed that the longitudinal and lateral/directional dynamics can be decoupled. As previously stated this assumption is valid for small perturbations about a trim condition. To further reduce the size of the problem, the thrust vectoring capability has been eliminated. This is done to reduce the differences between the HARV and the current production of the F/A-18 aircraft. Thus, the linear plant models use in this research can be represented by:

$$\dot{\mathbf{x}} = \mathbf{A}\mathbf{x} + \mathbf{B}\mathbf{u}$$

$$\mathbf{y} = \mathbf{C}\mathbf{x} + \mathbf{D}\mathbf{u} \tag{3.1}$$

where $\mathbf{x}$ are the states of the system, i.e.,

$$x = \begin{bmatrix} p \\ r \\ \beta \\ \phi \end{bmatrix} \begin{array}{l} \text{roll rate (deg/sec)} \\ \text{yaw rate (deg/sec)} \\ \text{side slip (deg)} \\ \text{bank angle (deg)} \end{array} \tag{3.2}$$

and **u** represents the system inputs, i.e.,

$$u = \begin{bmatrix} \delta_{ail} \\ \delta_{ht} \\ \delta_{rud} \\ \delta_{lef} \\ \delta_{tef} \end{bmatrix} \begin{array}{l} \text{ailerons (deg)} \\ \text{stabilators (deg)} \\ \text{rudders (deg)} \\ \text{leading edge flaps (deg)} \\ \text{trailing edge flaps (deg)} \end{array} \tag{3.3}$$

A and **B** are the system dynamics given by the following matrices, respectively:

$$\mathbf{A} = \begin{bmatrix} L_p & L_r & L_\beta & 0 \\ N_p & N_r & N_\beta & 0 \\ Y_p & Y_r & Y_\beta & 0 \\ 0 & 0 & 0 & 1 \end{bmatrix} \tag{3.4}$$

$$\mathbf{B} = \begin{bmatrix} L_{\delta_{ail}} & L_{\delta_{ht}} & L_{\delta_{rud}} & L_{\delta_{lef}} & L_{\delta_{tef}} \\ N_{\delta_{ail}} & N_{\delta_{ht}} & N_{\delta_{rud}} & N_{\delta_{lef}} & N_{\delta_{tef}} \\ Y_{\delta_{ail}} & Y_{\delta_{ht}} & Y_{\delta_{rud}} & Y_{\delta_{lef}} & Y_{\delta_{tef}} \\ 0 & 0 & 0 & 0 & 0 \end{bmatrix} \tag{3.5}$$

A listing of all of the **A** and **B** matrices used in this research can be found in Appendix A. Since only the roll rate (p) and sideslip (β) are controlled by the pilot, the **C** and **D** matrices are defined respectively as:

$$\mathbf{C} = \begin{bmatrix} 1 & 0 & 0 & 0 \\ 0 & 0 & 0 & 0 \\ 0 & 0 & 1 & 0 \\ 0 & 0 & 0 & 0 \end{bmatrix} \quad \mathbf{D} = \begin{bmatrix} 0 & 0 & 0 & 0 & 0 \\ 0 & 0 & 0 & 0 & 0 \\ 0 & 0 & 0 & 0 & 0 \\ 0 & 0 & 0 & 0 & 0 \end{bmatrix} \tag{3.6}$$

After being entered into the QFT CAD package, the state space representation of the plant is transformed into a transfer function realization for use in the QFT design method.

3.3 Control Surface Descriptions

Once the plant model is determined, it is necessary to analyze the **B** matrix to determine the correct signs for surface deflections. Based on this analysis, the control surface sign conventions are shown in Fig. 3.2

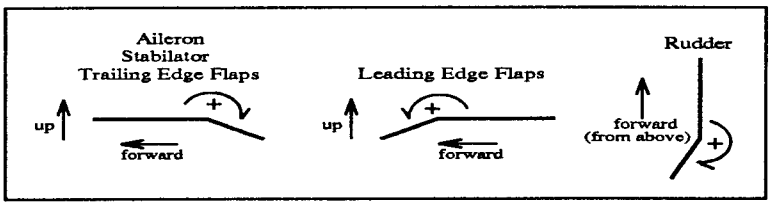

Figure 3.2 Control Effector Sign Conventions for the F-18 HARV

In this research, both position and rate limits of the control surfaces, Table 3.1, are incorporated into the time domain simulation. The control surface groups are

Surface	Position Limits (deg)	Rate Limits (deg/sec)
Leading Edge Flap	+33, −3	15
Trailing Edge Flap	+45, −8	18
Aileron	+45, −25	100
Stabilator	+10.5, −24	40
Rudder	±30	82

Table 3.1 F-18 HARV Control Surface Position and Rate Limits

internally scaled by the HARV simulation so that the maximum positive and negative deflections are reached at the same time. In other words, given a maximum positive roll aileron command, the left aileron is driven to +45° while the right aileron goes to −25° at the same time. This internal scaling simplifies the simulation process. The position and rate limits are the only non-linearities included in the time domain simulation due to the drastic effects they can have on aircraft stability.

3.4 Actuator Models

One thing that the linear plant models don't take into account is the dynamics of the actuators. This information is very important in forming the effective plant (P_e) for use in QFT and in robust control in general. The actuators have the effect of delaying the input signal and can have drastic effects on the output. A listing of the transfer functions for each control surface actuator is shown in Table 3.2. These transfer functions are determined directly from data in the HARV simulation program.

Control Surface	Transfer Function
Leading Edge Flap	$\frac{2230}{s^2 + 109.8s + 2230}$
Trailing Edge Flap	$\frac{1225}{s^2 + 49.7s + 1225}$
Aileron	$\frac{5625}{s^2 + 88.5s + 5625}$
Stabilator	$\frac{945}{s^2 + 31.29s + 945}$
Rudder	$\frac{5198}{s^2 + 99.5s + 5189}$

Table 3.2 F-18 HARV Control Surface Actuator Models

3.5 Flight Conditions

As previously stated, the HARV simulation program takes in a user specified flight condition and returns the corresponding linearized system dynamics. The user specifies two out of the following three variables: altitude, speed and angle of attack. The simulation then determines the trim condition and the value of the third variable for the specified flight condition. For this research the altitude and Mach number are chosen as the specified variables. Thirty-one flight conditions are chosen to represent the sub-sonic flight envelope. To determine values for the high angle of attack region, flight conditions are chosen to ensure the dynamic pressure $\bar{q}$ is greater than 50 slugs/ft s^2. The upper limit for Mach is set at 0.9 Mach to stay

out of trans-sonic and super-sonic flight conditions. The lower bound on altitude is set at 5,000 ft by the simulation program, and the upper bound of 40,000 ft is determined by typical maximum flying altitudes. A figure showing the thirty-one chosen flight conditions can be seen in Fig. 3.3, followed by a listing of the flight conditions in Table 3.3.

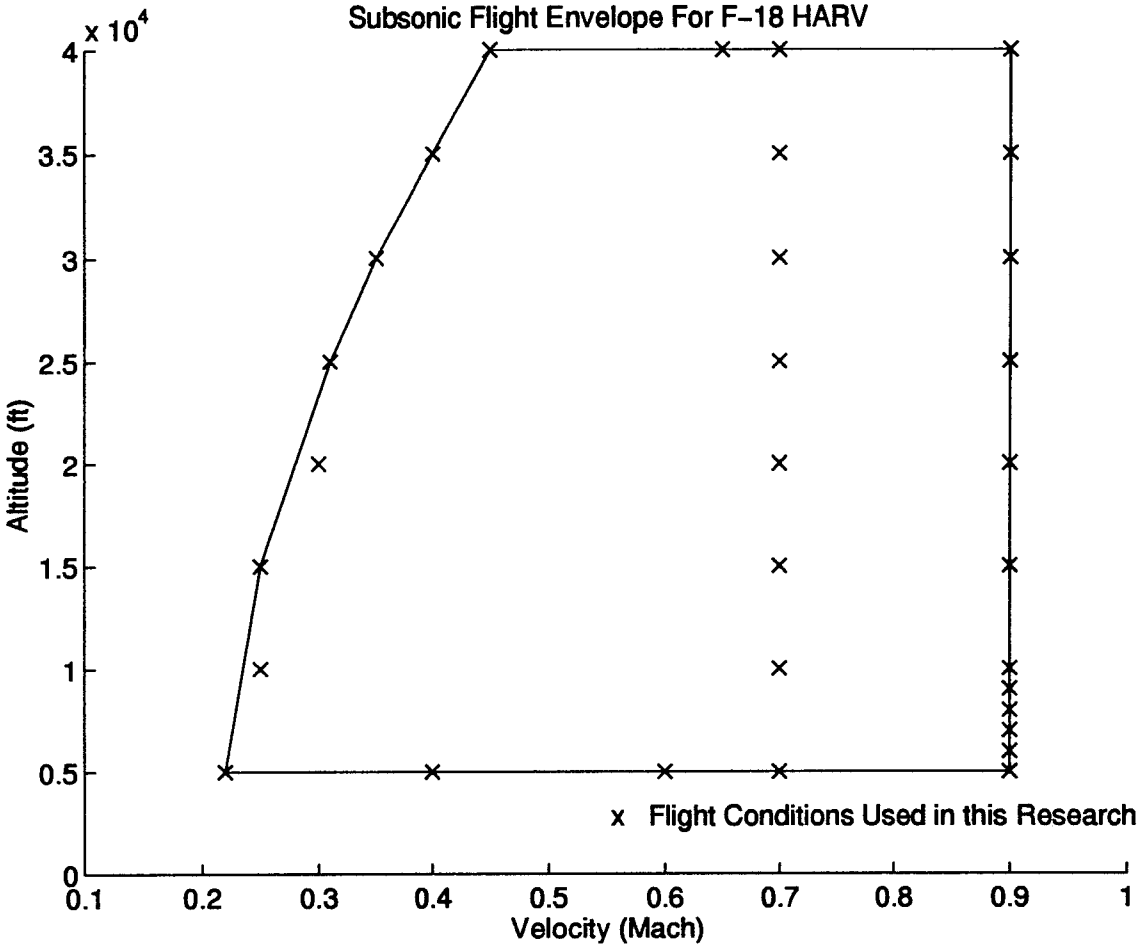

Figure 3.3 Flight Envelope of F-18 HARV

Flight Condition	Velocity (Mach)	Altitude (ft)	Angle of Attack (deg)	Dynamic Pressure ($slug/ft * sec^2$)
1	.22	5000	22.9	59.7
2	.25	15000	23.6	52.0
3	.35	30000	25.8	54.0
4	.45	40000	24.3	55.8
5	.65	40000	16.0	116.5
6	.9	40000	3.50	223.0
7	.9	30000	2.36	357.3
8	.9	15000	1.50	678.2
9	.9	10000	1.36	825.5
10	.9	5000	1.21	999.4
11	.6	5000	2.53	444.2
12	.4	5000	5.24	197.4
13	.25	10000	18.1	63.7
14	.9	9000	1.34	858.5
15	.3	20000	19.6	61.3
16	.31	25000	22.79	53.0
17	.4	35000	23.5	56.0
18	.9	35000	3.68	283.4
19	.9	25000	2.01	446.3
20	.9	20000	1.75	552.1
21	.9	8000	1.30	892.2
22	.9	7000	1.29	926.4
23	.9	6000	1.27	962.2
24	.7	40000	9.00	135.1
25	.7	35000	5.22	171.4
26	.7	30000	4.26	216.1
27	.7	25000	3.51	270.0
28	.7	20000	2.93	334.0
29	.7	15000	2.49	410.2
30	.7	10000	2.12	499.4
31	.7	5000	1.84	604.6

Table 3.3 Flight Conditions for All Plants

IV. Flight Control System Design

This chapter details the steps taken in creating the flight control system in this research. Three different designs are accomplished and tested, each having a different weighting matrix. This chapter is organized in three major parts. The first two sections cover general conditions that apply to all of the designs. They are presented once in the hope of reducing the amount of repetition involved. The following three sections describe the step taken in each of the three designs. The chapter ends with a comparison of the designs.

4.1 System Specifications

Where possible the system specifications are generated from MIL-STD 1797A. However, QFT requires specifications on more variables than are found in the military specifications. When specifications are not given, an attempt is made to generate reasonable values. These values are then used in all three designs.

4.1.1 Tracking Specifications. According to MIL-STD 1797A, a Class IV aircraft in Category A and C flight must have a maximum roll mode time constant τ_R of 1 sec. In order to use this information in QFT, the specification must be changed into a form that can be translated into the frequency domain. Putting this in terms of a transfer function yields:

$$\frac{1}{s+\tau_R} = \frac{1}{s+1} \tag{4.1}$$

From this transfer function it is determined that the 2% settling time (t_s) is approximately 4 sec. Thus, for use in QFT, the upper and lower bounds for the roll channel are specified to have a settling time of 4 sec. The lower bound chosen in this research is the over-damped response determined by the transfer function in Eq. (4.1) along with a second pole at -10 to ensure that the upper and lower bounds continue to

separate as the frequency increases. Thus, the lower bound a_{11} is described by:

$$a_{11} = \frac{1}{(s+1)(s+10)} \tag{4.2}$$

For the upper bound (b_{11}), a transfer function is generated so that $\zeta \approx 0.7$ in addition to the required settling time. A transfer function that satisfies these two conditions is listed in Eq. (4.3). Note that an additional zero has been added to again ensure that the frequency responses diverge.

$$b_{11} = \frac{\omega_n^2(s+z_1)}{s^2+2\zeta\omega_n s+\omega_n^2} = \frac{4.277(s+0.65)}{s^2+2.4s+2.78} \tag{4.3}$$

where $\zeta = 0.72$ and $\omega_n = 1.667$. A plot of the time and frequency domain responses for a_{11} and b_{11} are shown in Fig. 4.1

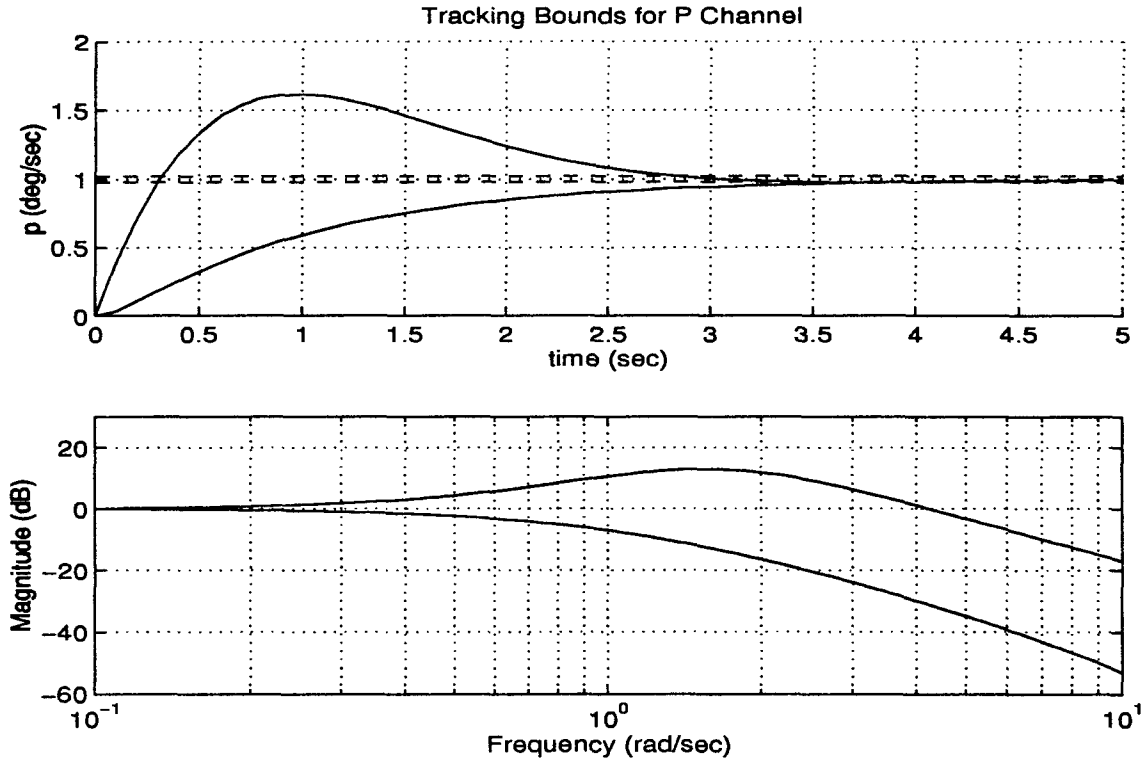

Figure 4.1 P-channel Tracking Bounds in Time and Frequency Domains

In addition, the aircraft must be capable of reaching a 90° bank angle in 1 sec with a maximal roll rate command. Although this specification cannot be used in the QFT design process, it is checked in the time domain to ensure that it has been met.

Since no specifications are given on the β channel, the same upper and lower bounds as in the p channel are used as the tracking bounds for the β channel.

4.1.2 Stability Specifications. As stated in Chapter 2, the lateral/directional channel must have a phase margin angle of at least 30°. This corresponds to the 6dB M_L contour on the Nichols Chart.

4.1.3 Cross-Coupling Effect Rejection Specifications. Since, for this research, there are no external disturbance signals, only cross-coupling effect rejection specifications need to be set. As specified in MIL-STD 1797A, the β response to a unit step p command can be no more than 0.067° for low speeds (low $\bar{q}$) conditions and no greater than 0.022° for middle and high speeds. In this research, these regions are $\bar{q} \leq 200$ for low speeds and $\bar{q} > 200$ for middle and high speeds. Using the more lenient specification, the QFT design results in a cross-coupling effect rejection specification of $T_{D_{12}} = -23$ dB. In addition, by specification, the total sideslip can be no greater than 6° for a maximum roll rate command. Since this specification cannot easily be converted into a form useful in the QFT design, verifying that it is satisfied is done in the time domain simulation.

MIL-STD 1797A does not list any specifications for a p response to a unit step input in the β channel. This is due to the fact that pilot's rarely have the need to command a change in β thus, there are few specifications listed for β. Once again, the bounds determined for the β response to a unit step p command are used for the p response to a unit step β command specifications.

The complete tracking and cross-coupling effect rejection specifications for all channels is shown in Fig. 4.2.

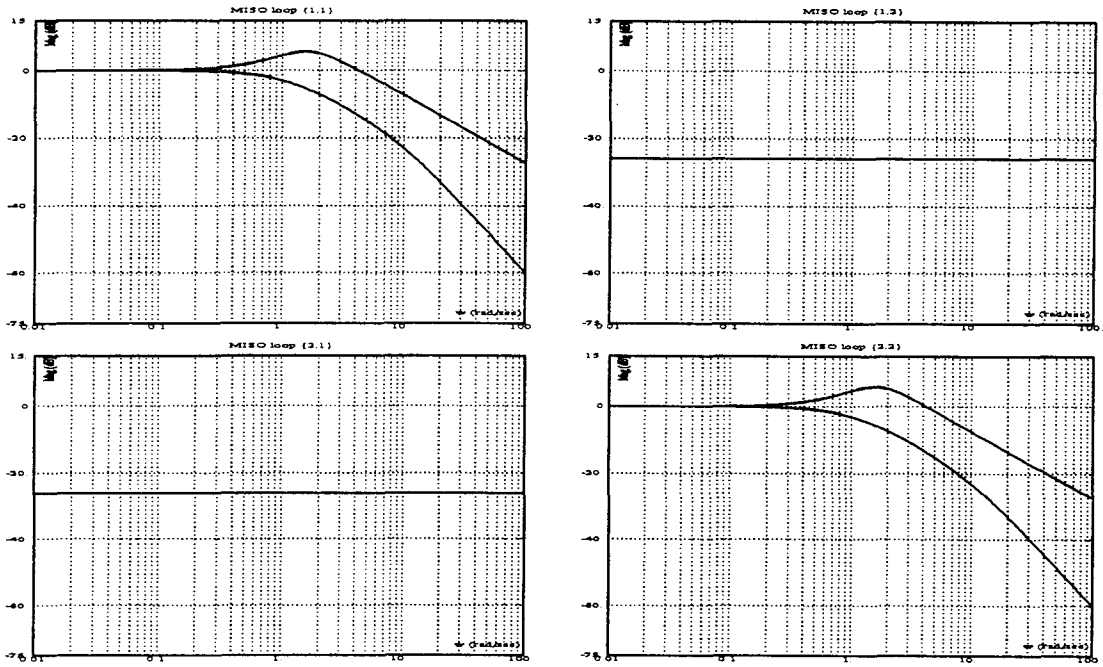

Figure 4.2 Tracking and Cross-Coupling Bounds - Both Channels

4.2 Effective Plants

As discussed in Chapter II the effective plant is composed of the lateral/directional aircraft plant, actuator models, and a weighting matrix. In addition, a dutch roll damper is designed to increase the damping ratio of the dutch roll mode. The structure of this circuit which is placed after the weighting matrix is shown in Fig. 4.3. The washout circuit chosen is a single pole/zero (high pass filter) configuration which is utilized to reduce the size of the templates. The pole placement and gain are determined through trial and error since there is no easy way of doing this mathematically. The trial and error consists of choosing a pole and gain and then looking at the β channel templates. Reducing the size of the β channel templates allows greater freedom in the design of the compensator and achieve a low order compensator with a lower value of gain. There is no change in the p channel templates due

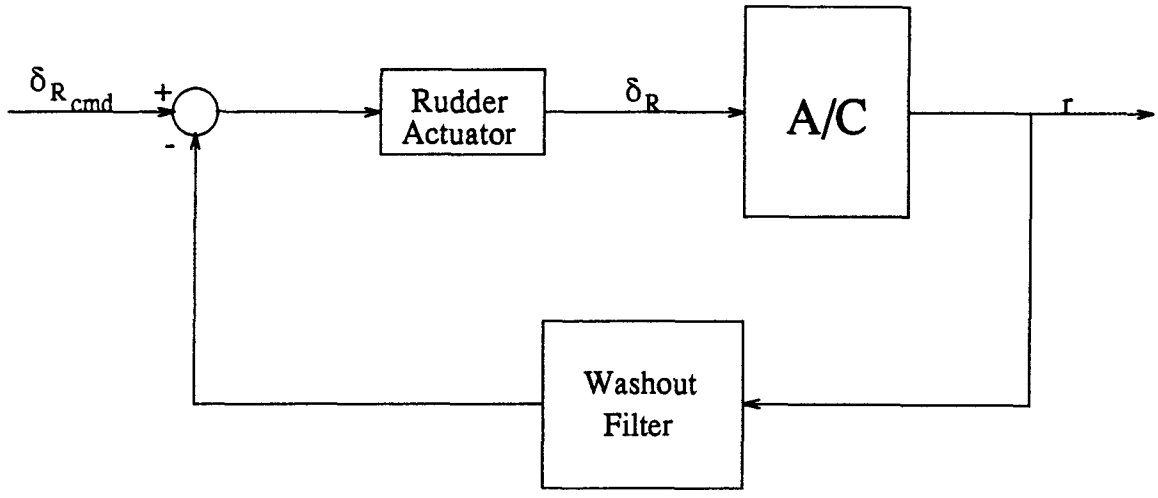

Figure 4.3 Dutch Roll Damping Block Diagram

to the dutch roll damper only acting on yaw rate and thus sideslip. The final design is mathematically described by Eq. (4.4).

$$\text{washout circuit} = \frac{9s}{s+0.2} \tag{4.4}$$

One aspect of the weighting matrix design is important to mention here as it is used in all three of the designs. The weighting matrix design has been broken down into two portions. The first portion is a rudder-aileron interconnect and the second portion is design specific. Thus the complete weighting matrix is described as follows:

$$W = W_{rud-ail} * W_2 \tag{4.5}$$

where $W_{rud-ail}$ is the rudder-aileron interconnect portion. $W_{rud-ail}$ is a 5 x 5 matrix relating the effect of the different control surfaces on yaw rate to the effect of rudders

on yaw rate. Thus,

$$W_{rud-ail} = \begin{bmatrix} 1 & 0 & 0 & 0 & 0 \\ 0 & 1 & 0 & 0 & 0 \\ \frac{C_{n_{\delta_{ail}}}}{C_{n_{\delta_r}}} & 0 & 1 & \frac{C_{n_{\delta_{lef}}}}{C_{n_{\delta_r}}} & \frac{C_{n_{\delta_{tef}}}}{C_{n_{\delta_r}}} \\ 0 & 0 & 0 & 1 & 0 \\ 0 & 0 & 0 & 0 & 1 \end{bmatrix} \tag{4.6}$$

Once the effective plant has been determined, it is necessary to analyze diagonal dominance. Although the effective plant is slightly different for each design iteration, the results are similar and are only presented once. From Fig. 4.4, it is seen that the normalized value is greater than one as $\omega \rightarrow \infty$ for all plants. Thus the diagonal dominance condition is satisfied, therefore, QFT Method One is chosen as the design tool for this research.

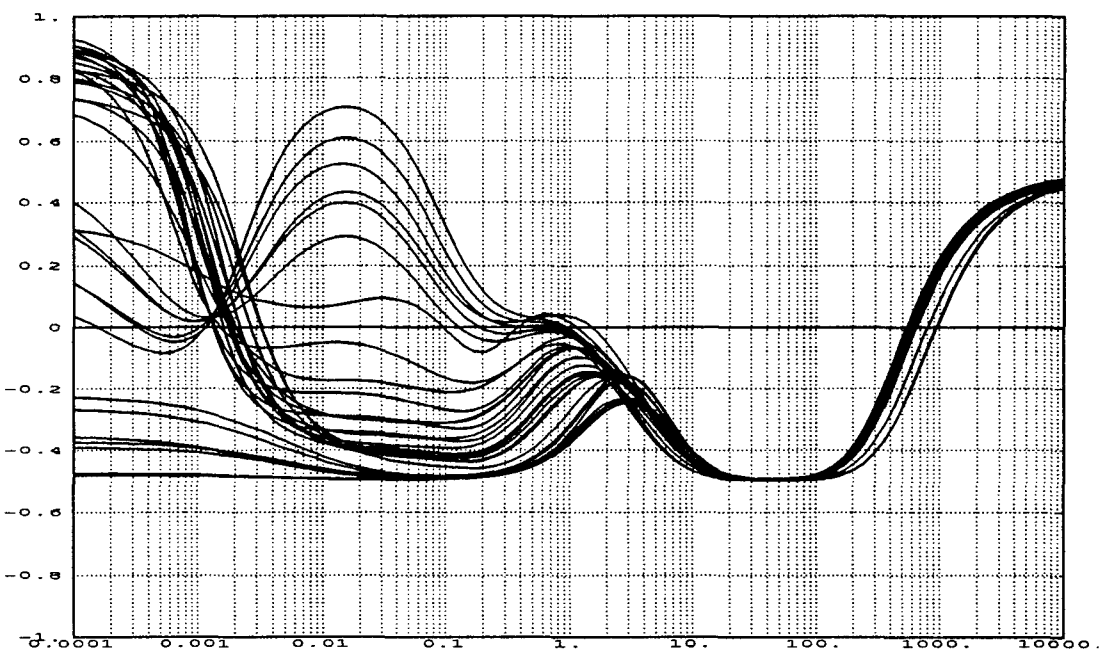

Figure 4.4 Verification of Diagonal Dominance

4.3 Design 1

The following sections give the details involved in the first design.

4.3.1 Weighting Matrix. For the first design, the weighting matrix is chosen so that all of the surfaces on the wing reach their maximum position limit at the same time. This is accomplished by taking the ratio of the maximum positive surface deflection to the maximum positive surface deflection of the surface with the greatest possible deflection (ailerons). The weighting on the stabilator is chosen to be 0.3333 since most of the stabilator's control authority needs to be available for the longitudinal channel. Mathematically this is expressed as

$$W_2 = \begin{bmatrix} \frac{\delta_{ail}^{max}}{\delta_{ail}^{max}} & 0 \\ \frac{1}{3} & 0 \\ 0 & 1 \\ \frac{\delta_{lef}^{max}}{\delta_{ail}^{max}} & 0 \\ \frac{\delta_{tef}^{max}}{\delta_{ail}^{max}} & 0 \end{bmatrix} = \begin{bmatrix} 1 & 0 \\ 0.3333 & 0 \\ 0 & 1 \\ 0.7333 & 0 \\ 1 & 0 \end{bmatrix} \tag{4.7}$$

4.3.2 QFT FCS Design. Once the weighting matrix is determined, the templates are generated by the QFT CAD package. The template frequencies are picked based on the pilot's bandwidth and the bending modes of the F-18. The pilot's bandwidth lies between 0.1 and 3.5 rps while the bending modes lie above 15 rps [17]. Thus the template frequencies are ω = [0.01, 0.02, 0.04, 0.08, 0.16, 0.32, 0.64, 1.28, 2.56, 5.12, 10.24, 15, 30]. The templates for the p channel are shown in Fig. 4.5 followed by the templates for the β channel in Fig. 4.6.

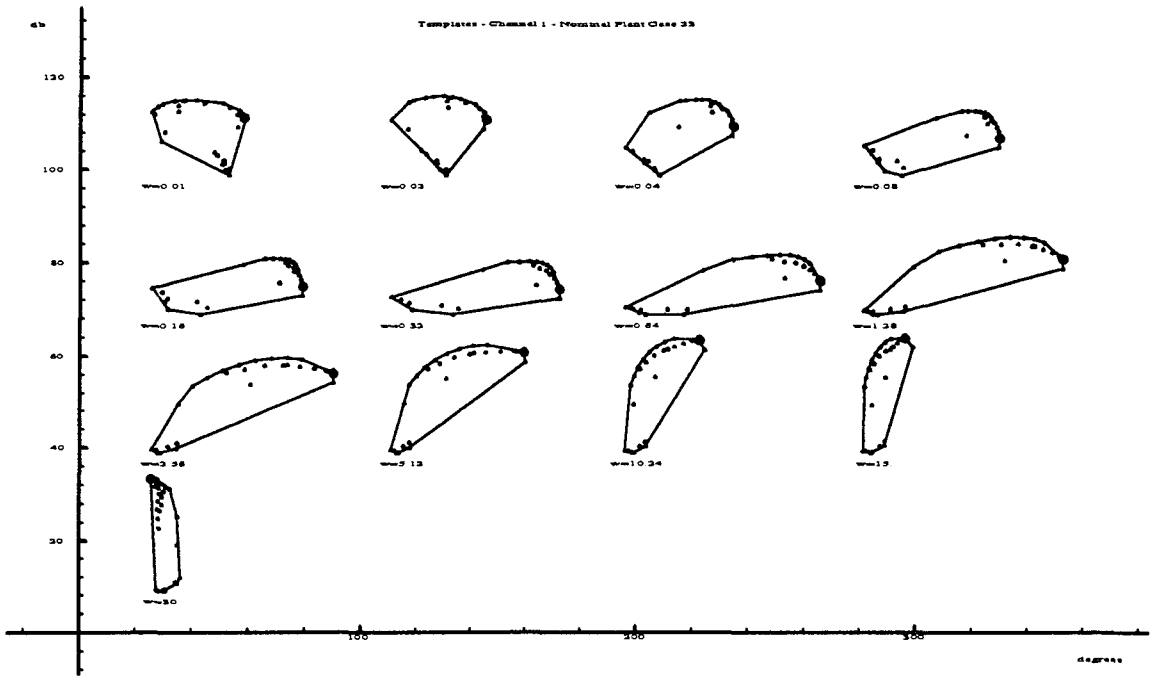

Figure 4.5 p Channel Templates - Design 1

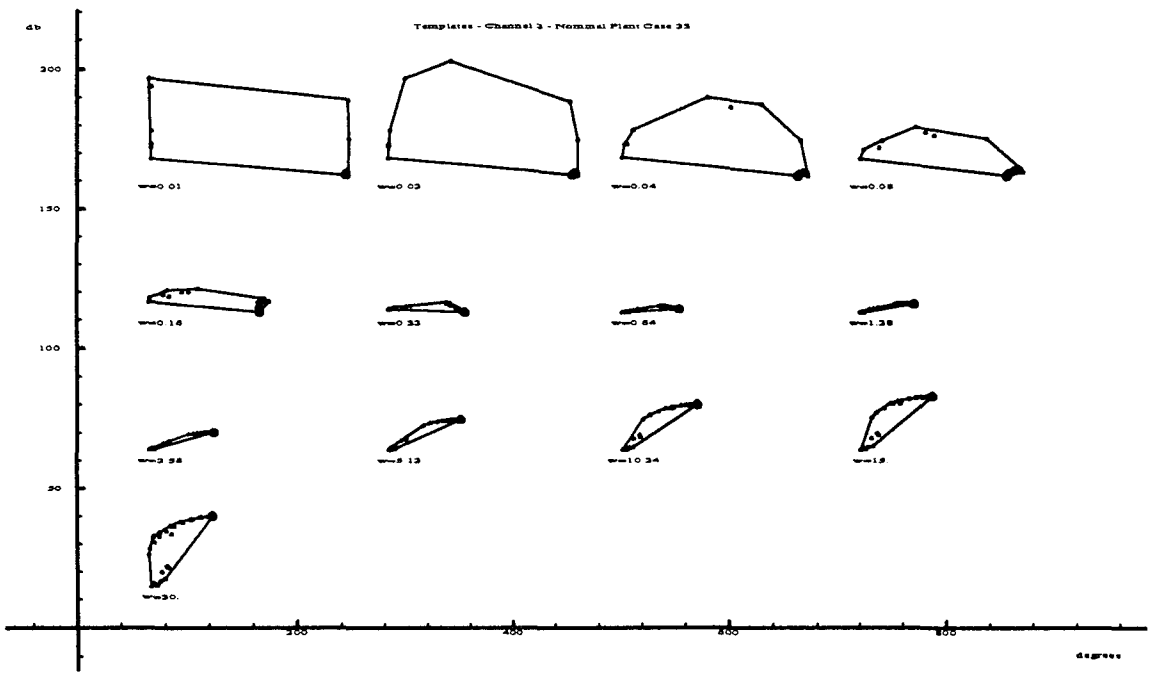

Figure 4.6 β Channel Templates - Design 1

The size of the templates show that the β channel has the least freedom for design. Fortunately the greatest variance in phase angle is at the lower frequency where the tracking bounds must be satisfied. If a large variance in phase angle existed at higher frequencies it would have been impossible to meet the stability bounds and more than one compensator would have been needed. The nominal plant is chosen to be plant #23 (altitude = 6,000ft Mach = 0.9) since it lies at the top of the 15 rps frequency template (Fig. 4.7). The 15 rps template is used since it represents the bending modes, and it is important that the phase margin frequency (ω_ϕ) for all plants be less than 15 rps so that none of the bending modes are excited.

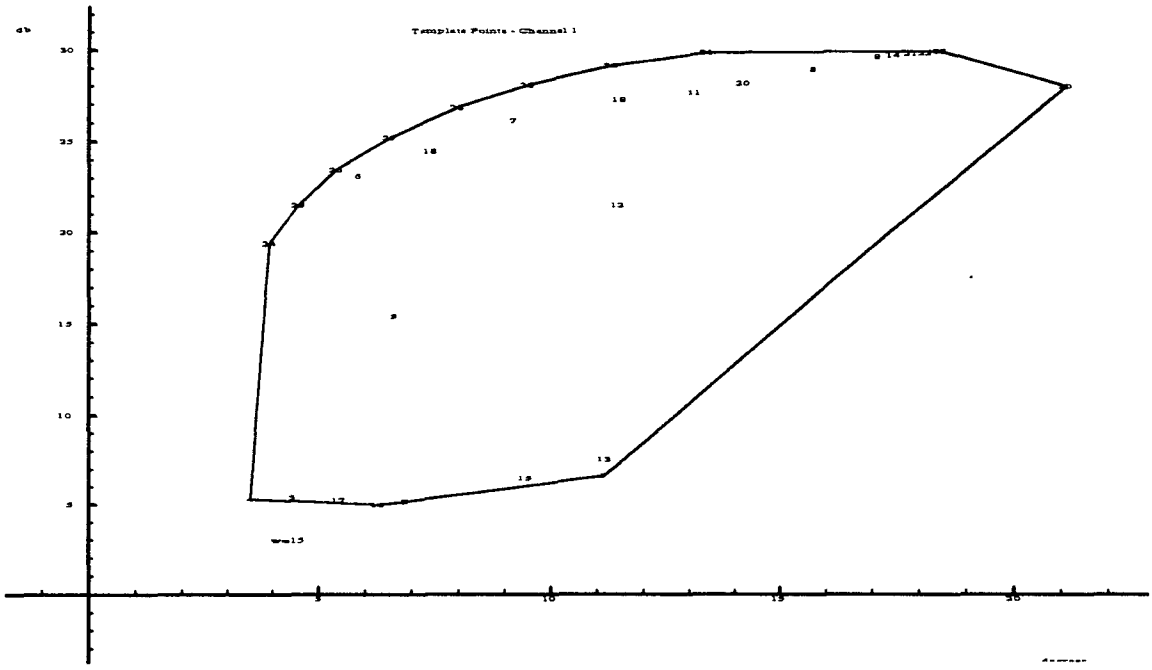

Figure 4.7 Nominal Plant Selection - Design 1

Using the templates, the bounds are generated via the QFT CAD package and plotted on the Nichols chart. The stability bounds are shown in Fig. 4.8 for the p channel and in Fig. 4.9 for the β channel.

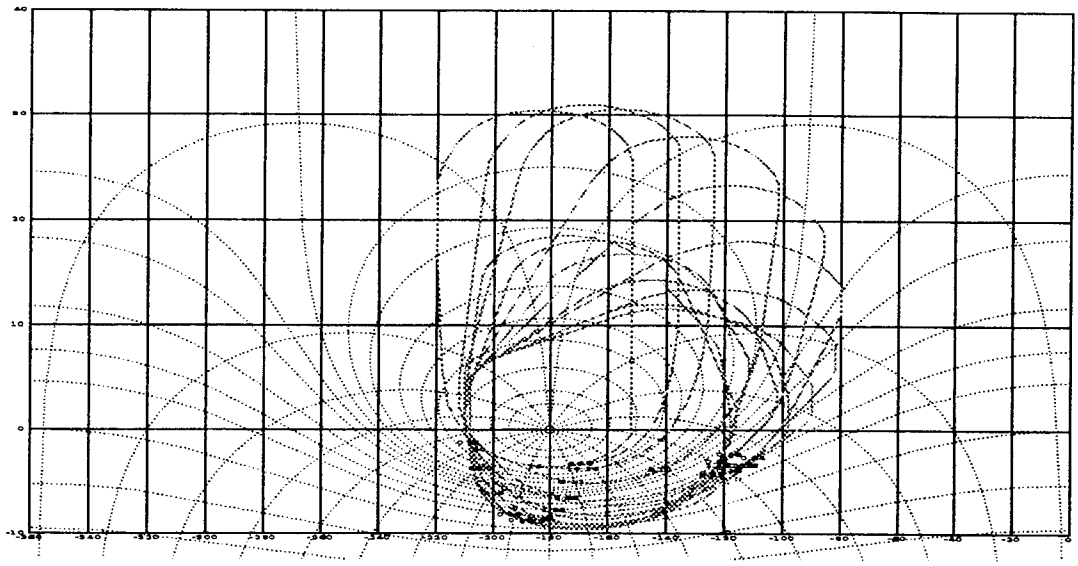

Figure 4.8 Stability Bounds for p Channel - Design 1

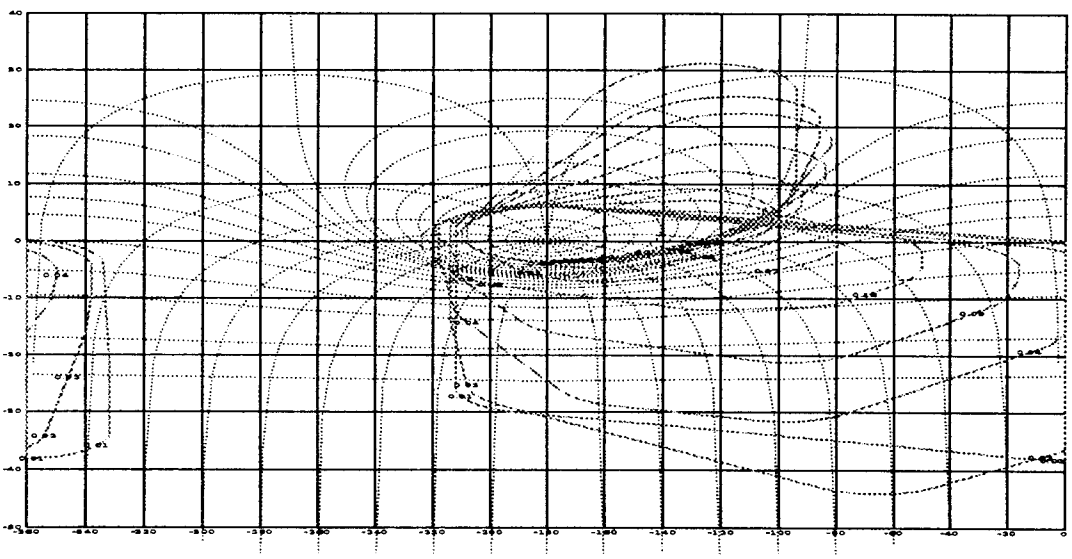

Figure 4.9 Stability Bounds for β Channel - Design 1

The stability bounds of the β channel verify the effects of the large phase angle variation at the lower frequencies. Judging from the stability bounds, a single design is capable of at least stabilizing the aircraft over the frequencies of interest.

The tracking bounds based on the tracking specifications are shown in Fig. 4.10 for the p channel and in Fig. 4.11 for the β channel.

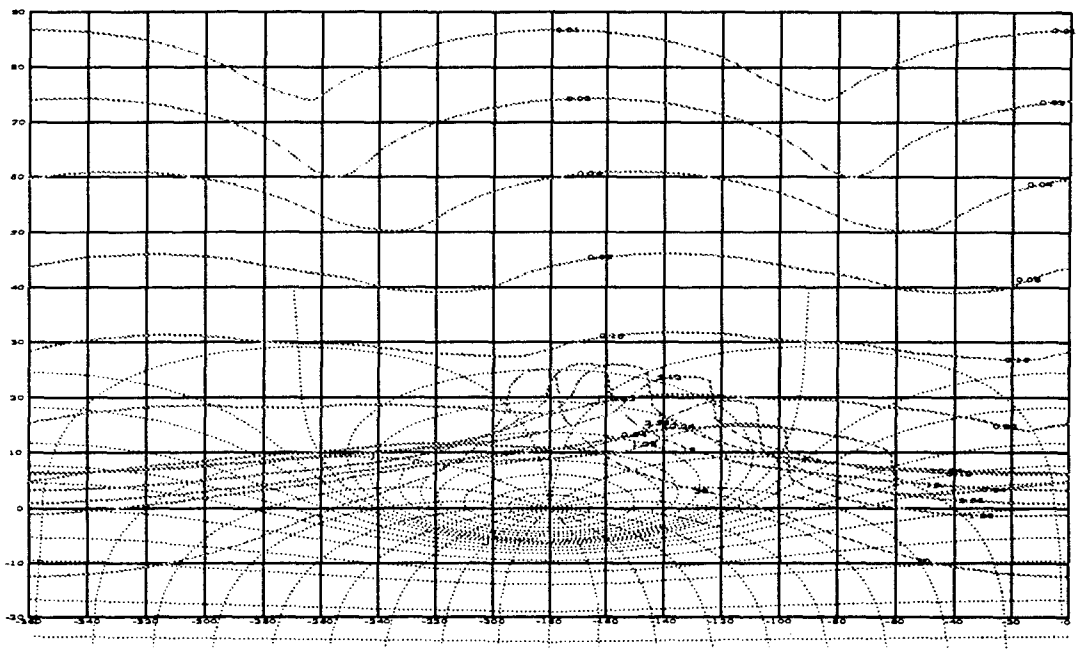

Figure 4.10 Tracking Bounds for p Channel - Design 1

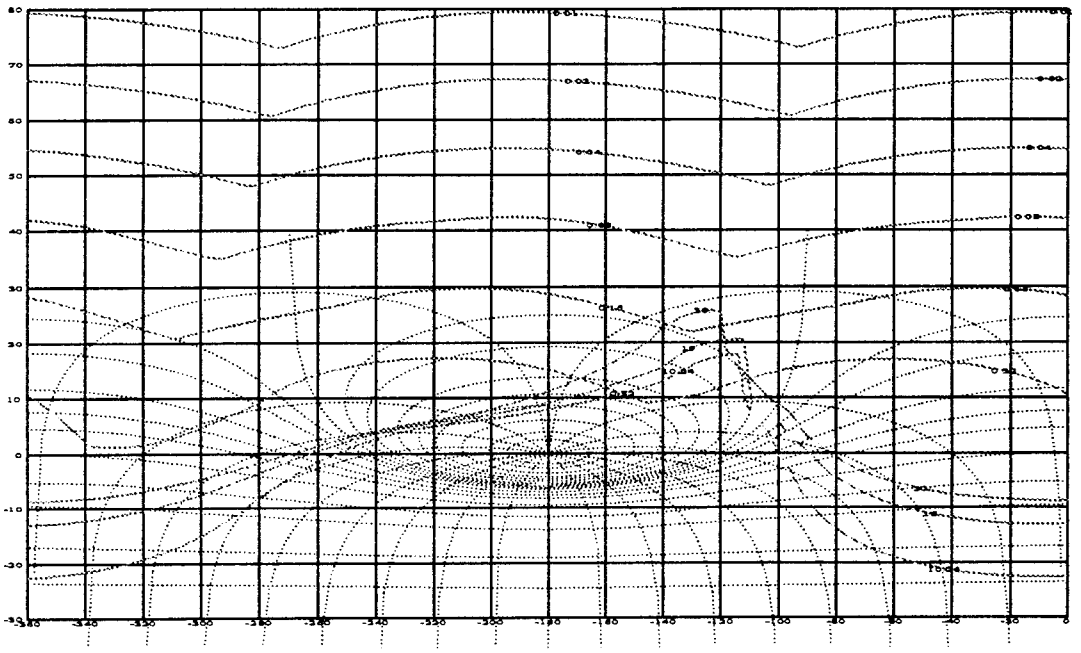

Figure 4.11 Tracking Bounds for β Channel - Design 1

From these bounds it is already evident that the lower frequency tracking bounds are very difficult to meet. Fortunately, these frequencies are below the pilot's bandwidth and are not extremely important to satisfy.

A plot of the cross-coupling effect bounds is shown in Fig. 4.12 for the p channel and in Fig. 4.13 for the β channel. This plot shows that the cross-coupling effect bounds are nearly impossible to meet for all frequencies, and if they are used as a part of the composite bounds, they will mask the tracking bounds making the design meaningless. Therefore, the composite bounds are only based on tracking and stability bounds. The time domain simulations are used to verify that the cross-coupling effects meet military specifications.

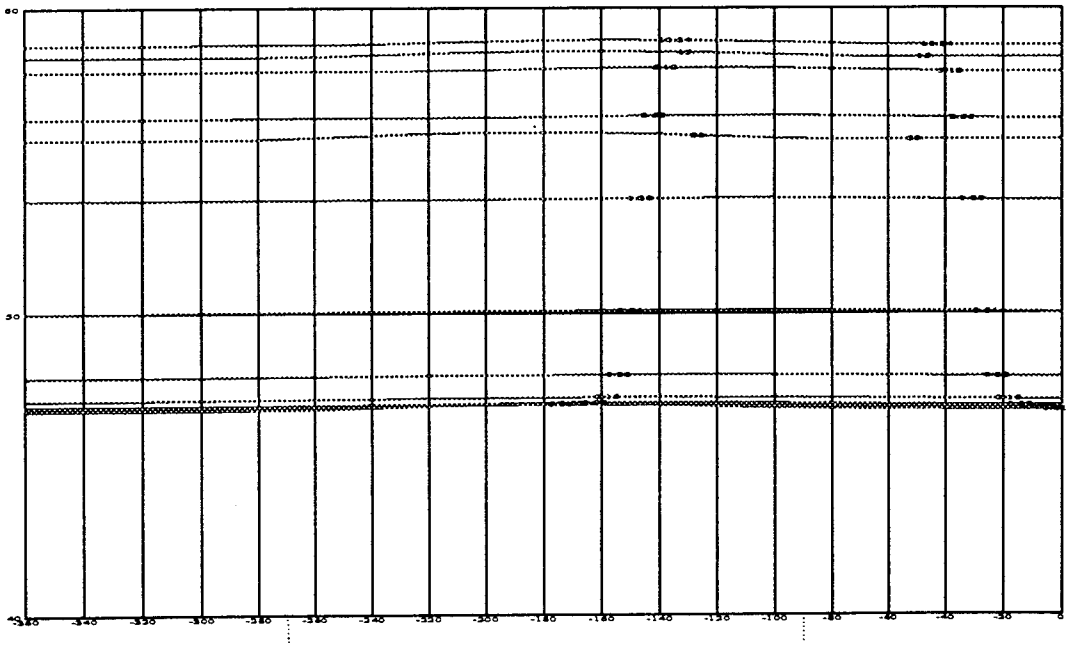

Figure 4.12 Cross-Coupling Effect Bounds for p Channel - Design 1

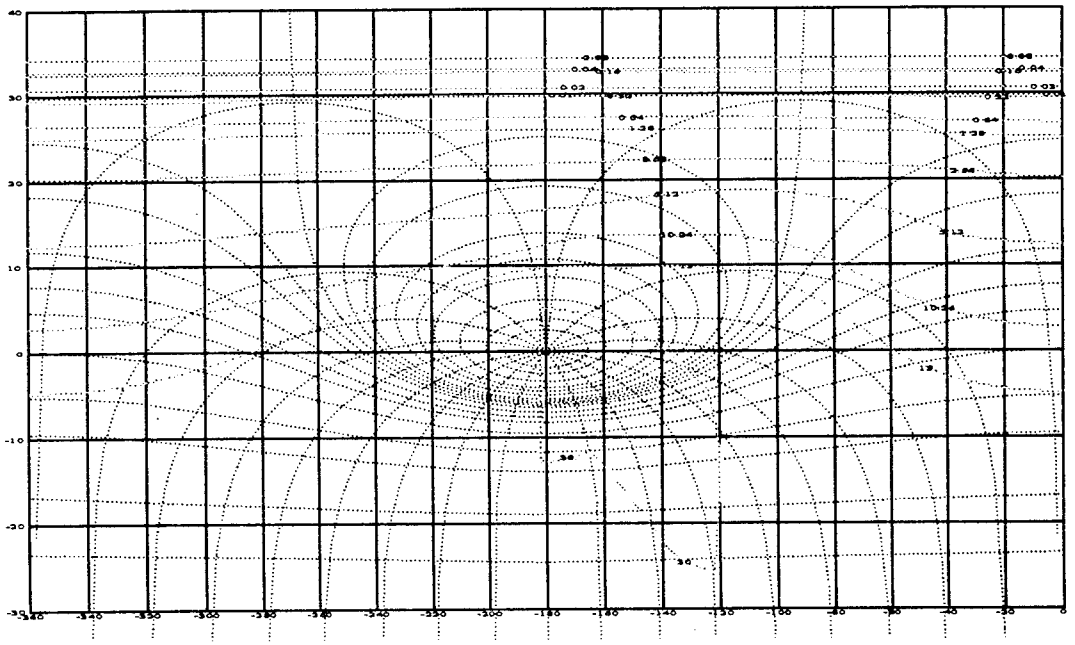

Figure 4.13 Cross-Coupling Effect Bounds for β Channel - Design 1

The composite bounds are shown in Fig. 4.14 for the p channel and in Fig. 4.15 for the β channel. These bounds show that at low frequencies the tracking bounds are dominant while at higher frequencies the stability specifications play a greater roll. In addition, both the p channel and β channel have a dip in the composite bounds at lower frequencies. These dips of $\approx$ 5dB allow the gain to be reduced by this amount. Although 5dB doesn't sound like much, it translates into reducing the gain by a factor of 1.8, a significant reduction indeed. If it is possible, the loop transmission functions will go through these dips, allowing the gain of the compensator to be reduced.

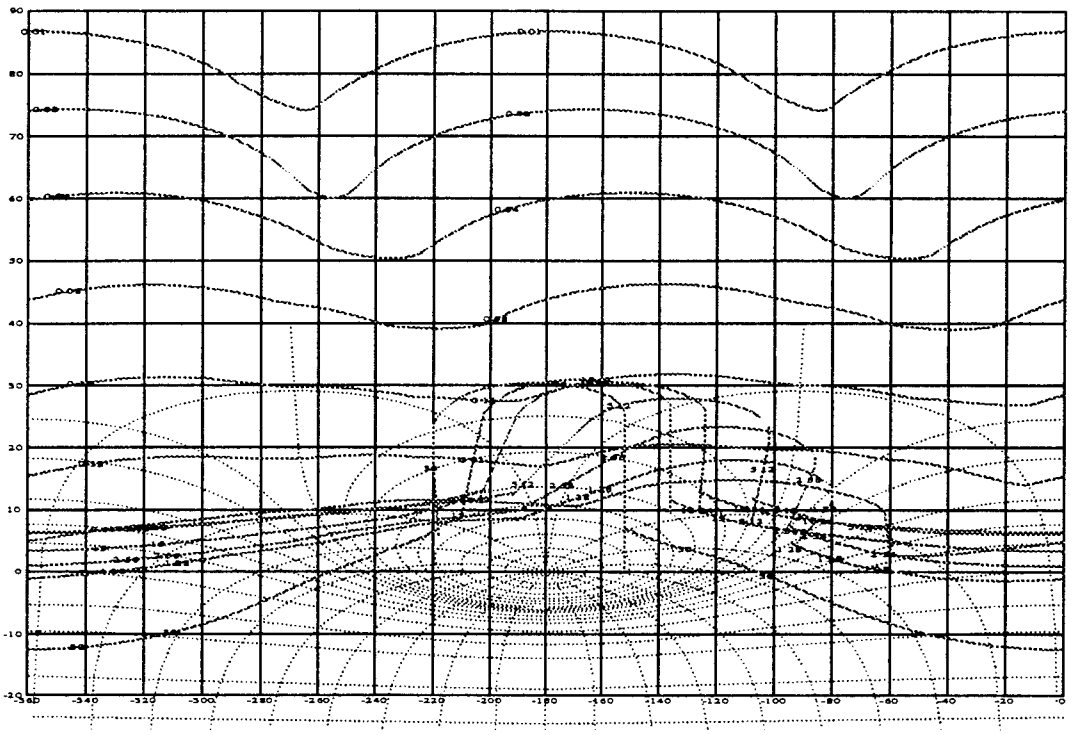

Figure 4.14 Composite Bounds for p Channel - Design 1

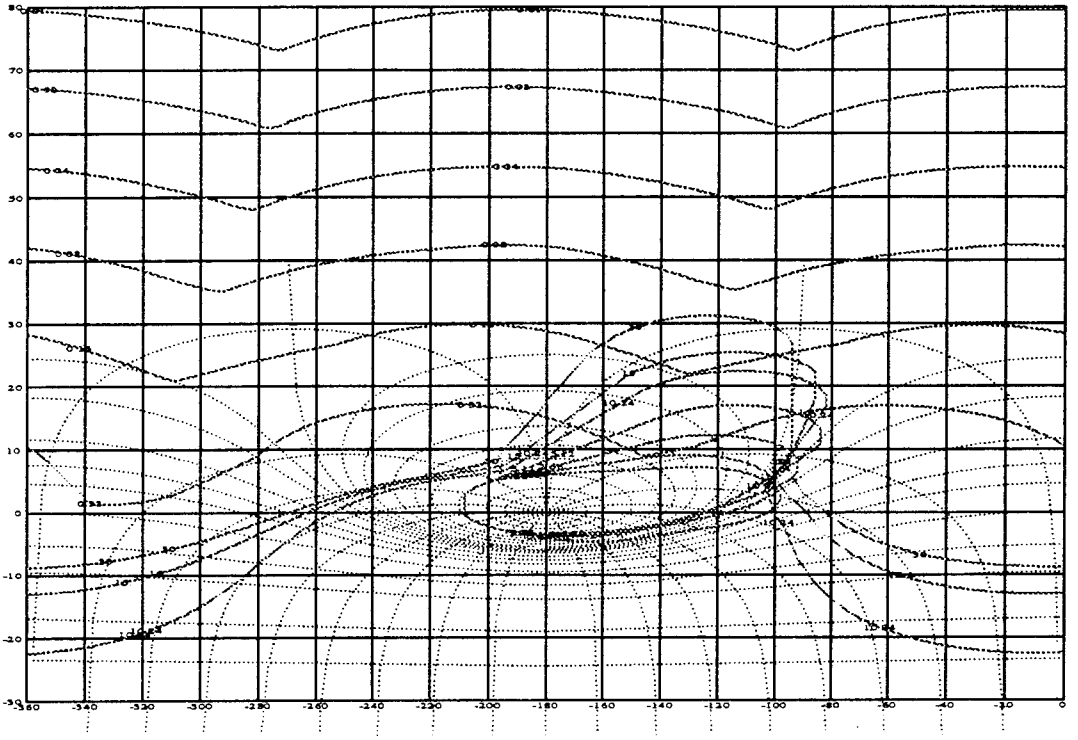

Figure 4.15 Composite Bounds for β Channel - Design 1

With the determination of the composite bounds complete, the loop shaping is done with the aid of the QFT CAD package in order to determine the transfer functions of the compensators. The loop transmission functions for the final compensator designs are shown in Fig. 4.16 for the p channel and Fig. 4.17 for the β channel. These plots show that the composite bounds are not met for all frequencies. However, over the important pilot bandwidth of 0.1 rps to 3.5 rps the bounds are indeed met. In addition, the phase margin frequency (frequency where the loop transmission function crosses the zero dB line) for the nominal plant is 15 rps as desired for this design. Based on these observations, the compensator designs are deemed satisfactory.

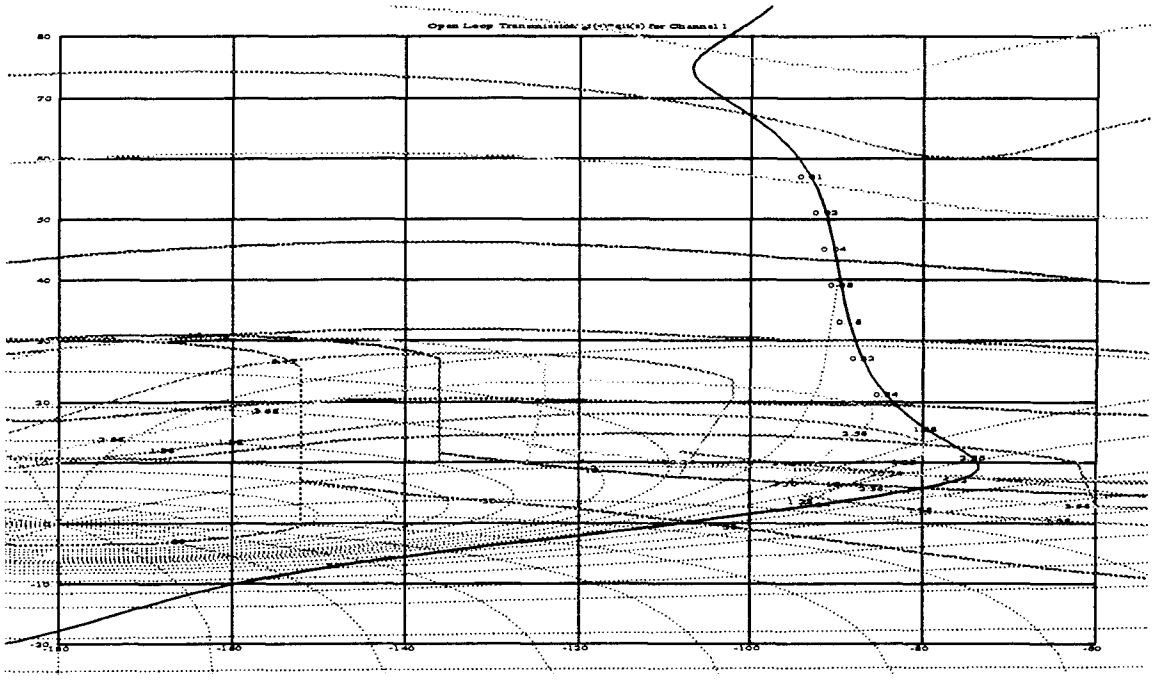

Figure 4.16 Nominal Loop Transmission for p Channel - Design 1

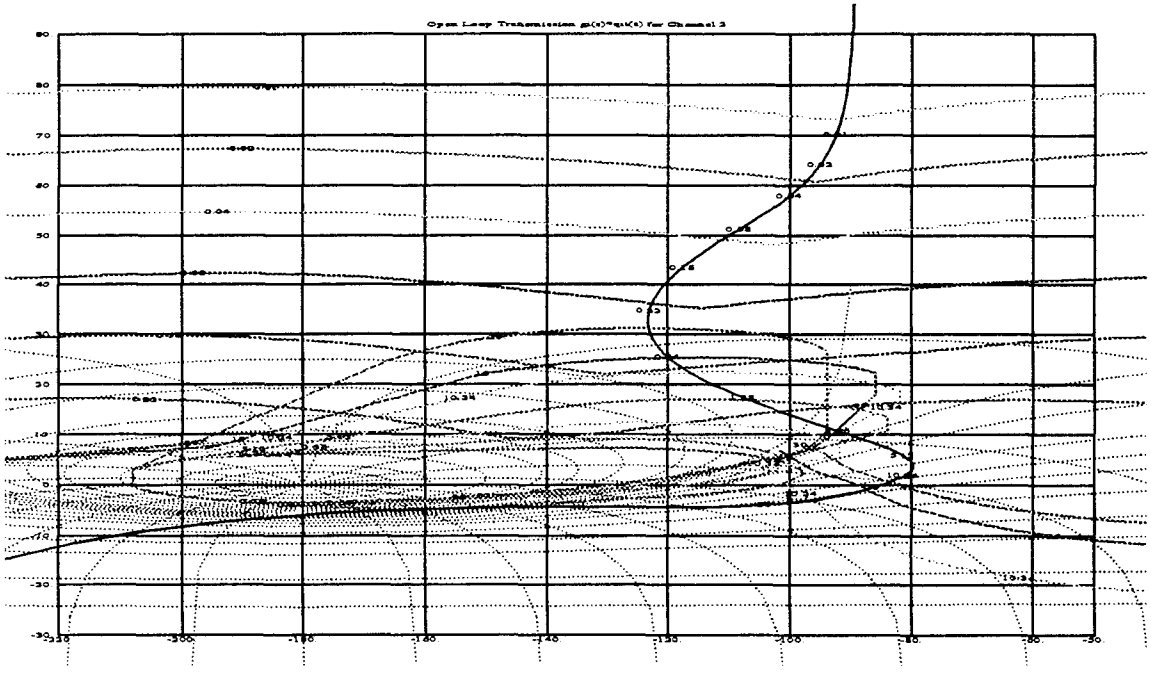

Figure 4.17 Nominal Loop Transmission for β Channel - Design 1

The transfer functions of the designed compensators are given by:

$$G_p = \frac{0.4(s+3)}{s} \tag{4.8}$$

$$G_\beta = \frac{145(s+0.8)(s+5)}{s(s+10)} \tag{4.9}$$

which are of low order.

In designing a pre-filter, it is important that the pilot's tracking commands are not attenuated. Thus, the p channel pre-filter's bandwidth must be greater than 3.5 rps. Since the pilot doesn't typically attempt β tracking, the β channel pre-filter doesn't have these restrictions. The final pre-filter designs are given in Eq. (4.10) and Eq. (4.11).

$$F_p = \frac{5}{(s+5)} \tag{4.10}$$

$$F_\beta = \frac{0.5}{(s+0.5)} \tag{4.11}$$

4.3.3 Design Validation. Having designed a compensator and pre-filter, the complete flight control system must be tested in the frequency domain to ensure stability and that tracking and cross-coupling effect rejection specifications are met over the bandwidth of concern. The stability validation generated by the QFT CAD package is shown in Fig. 4.18 and Fig. 4.19. Since none of the $\mathcal{J}$ loop transmission functions violate the stability bound, the aircraft is stable over the entire flight envelope.

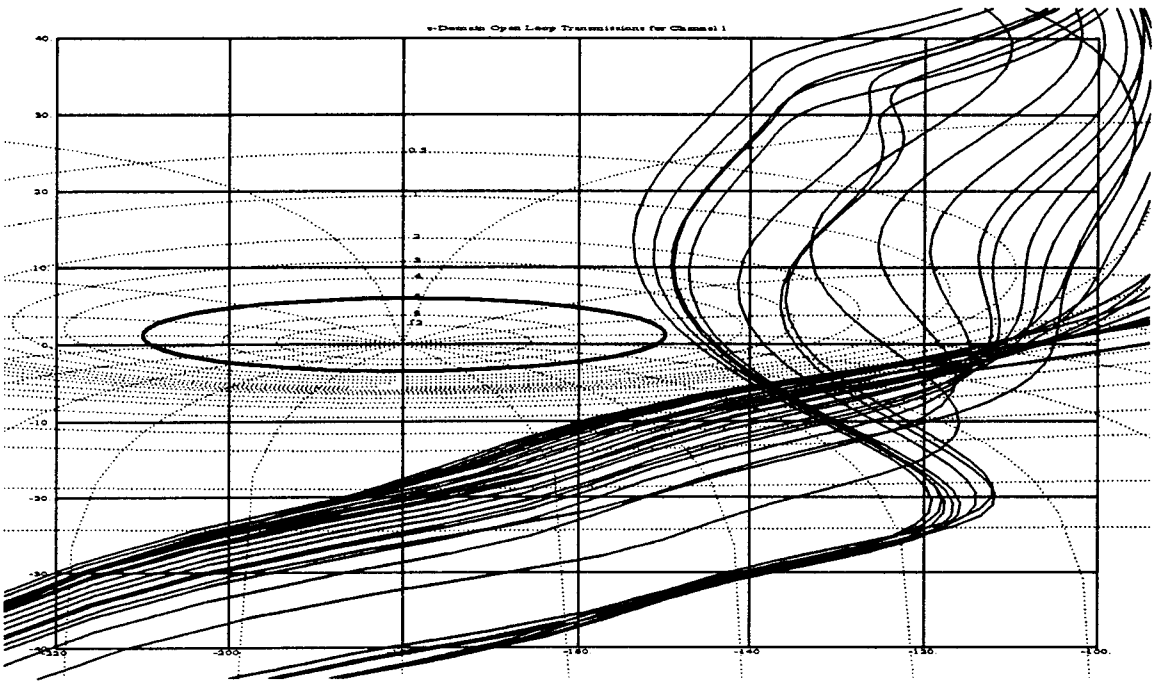

Figure 4.18 Stability Validation for p Channel - Design 1

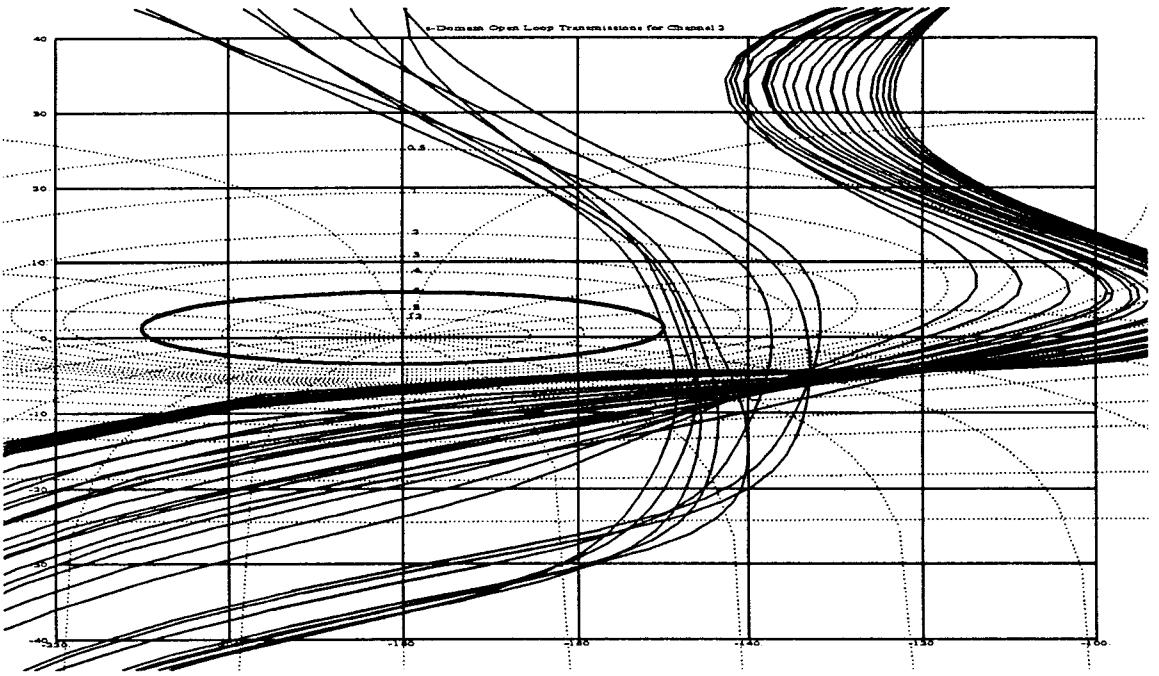

Figure 4.19 Stability Validation for β Channel - Design 1

The validation of tracking and cross-coupling effects rejection is shown in Fig. 4.20. This plot shows that the $\mathcal{J}$ plants lie within the tracking bounds over a frequency range for the 1,1 MISO loop. For the p channel (the (1,1) plot), this region is from $0.01 < \omega < 2.2$ (in radians/sec) for the low $\bar{q}$ plants and from $0.01 < \omega < 50$ for the rest of the plants. As mentioned before, a large amount of over-design exists in the QFT design method, so these values are determined to be acceptable since the design is also tested in the time domain. For the β channel (the (2,2) plot), the lower tracking bounds are not met for any frequency in the pilot's bandwidth. However, since these bounds are generated somewhat arbitrarily, and based on the results of the time domain simulations in Ch. V, the β channel tracking validation results are judged to be satisfactory. Looking at the off-diagonal plots, the cross-coupling effects are acceptable for the β response to a roll rate input (the (2,1) plot). While a couple of the bounds lie above the -23 dB line, the over-design should ensure that the actual time domain response meet specifications. Looking at the p channel response to a sideslip input(the (1,2) plot), the results obviously don't meet the given specifications. However, since there are no set specifications for this type of response in MIL-STD 1797A, and since the rest of the design is deemed acceptable, it is left to the time domain simulation to determine if the cross-coupling effects are indeed acceptable.

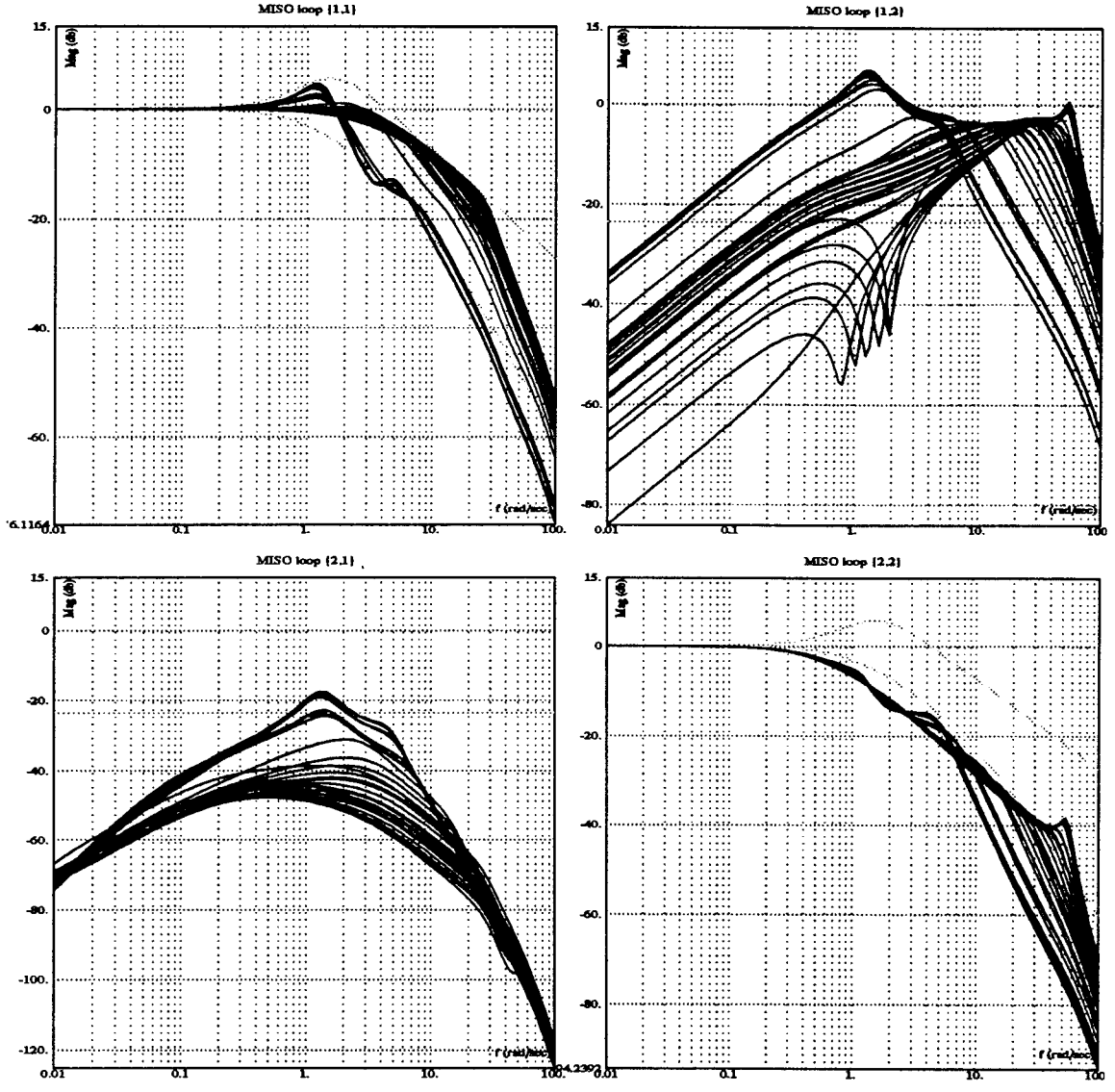

Figure 4.20 Tracking Validation for Design 1

4.4 Design 2

4.4.1 Weighting Matrix. For the second design, the weighting matrix is similar to that of the first design. The difference is that for the low $\bar{q}$ flight conditions ($\bar{q} < 200$) only the ailerons and rudders are used as control surfaces. This is a reasonable course of action since it is obvious from the **B** matrices (see Appendix A) that the other control surfaces (stabilators, trailing edge flaps, and leading edge flaps) have little control power in the low $\bar{q}$ regions. Thus for $\bar{q} < 200$ the weighting matrix is:

$$W_2 = \begin{bmatrix} 1 & 0 \\ 0 & 0 \\ 0 & 1 \\ 0 & 0 \\ 0 & 0 \end{bmatrix} \tag{4.12}$$

and for $\bar{q} > 200$ the weighting matrix is the same as in Design 1:

$$W_2 = \begin{bmatrix} 1 & 0 \\ 0.3333 & 0 \\ 0 & 1 \\ 0.7333 & 0 \\ 1 & 0 \end{bmatrix} \tag{4.13}$$

Again, these weighting matrices are pre-multiplied by the rudder-aileron interconnect weighting matrix (see Eq. (4.5)).

The aim of the second design is to reduce some of the cross-coupling effects on the β channel when a roll rate input is applied. The low $\bar{q}$ plants have a relatively high trim angle of attack. Under these conditions, more cross-coupling effects are to be expected. By using fewer control surfaces in the low $\bar{q}$ regions, there is less surface area capable of generating a side force and in turn sideslip.

4.4.2 QFT FCS Design. With the new weighting matrix, the effective plant is generated and new templates are determined. The templates are shown in Fig. 4.21 for the p channel and in Fig. 4.22 for the β channel. These templates show that the weighting matrix has the desired effects. There is little change in the p channel templates from Design 1 to Design 2 demonstrating that using only the rudder and ailerons at low $\bar{q}$ flight conditions has little effect on the plant uncertainty in the p channel. On the other hand, there is a dramatic effect on the β channel templates. The size of the templates is smaller especially at lower frequencies. This allows for greater freedom in designing the compensator for the β channel. The smaller β templates allow a lower gain to be used for the compensator while still meeting the tracking bounds. The lower gain also reduces the cross-coupling effects which is what this design hopes to accomplish. Although it is not shown here, since the plot looks similar to Fig. 4.4, the diagonal dominance condition is met with the incorporation of this weighting matrix.

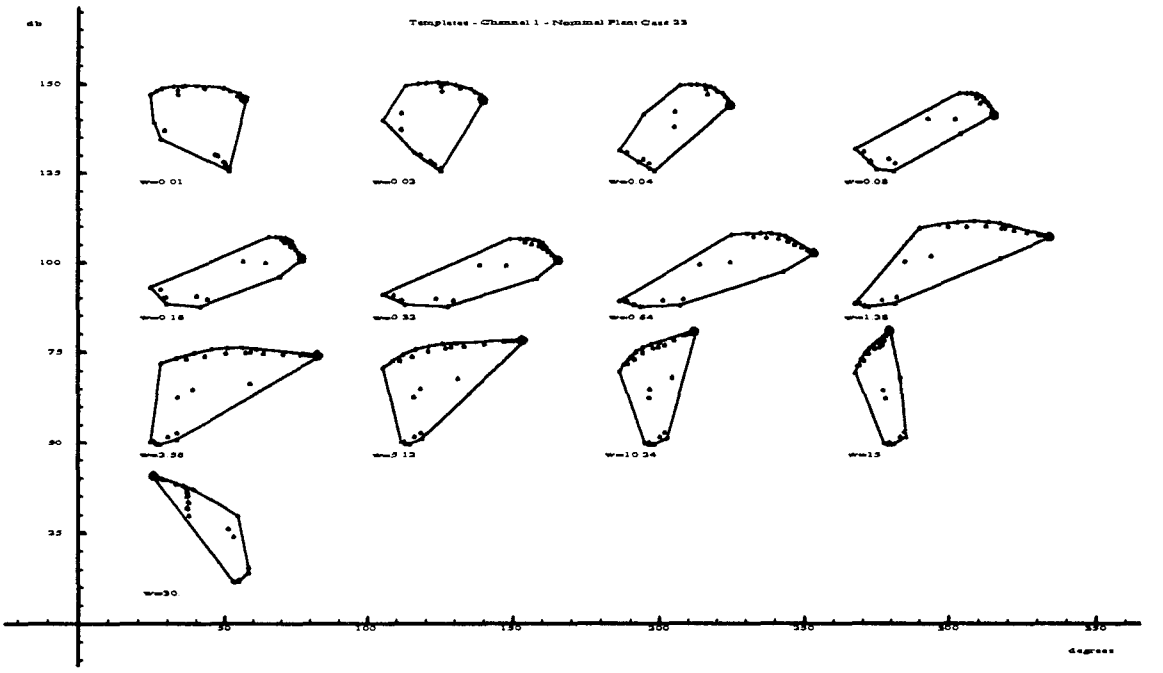

Figure 4.21 p Channel Templates - Design 2

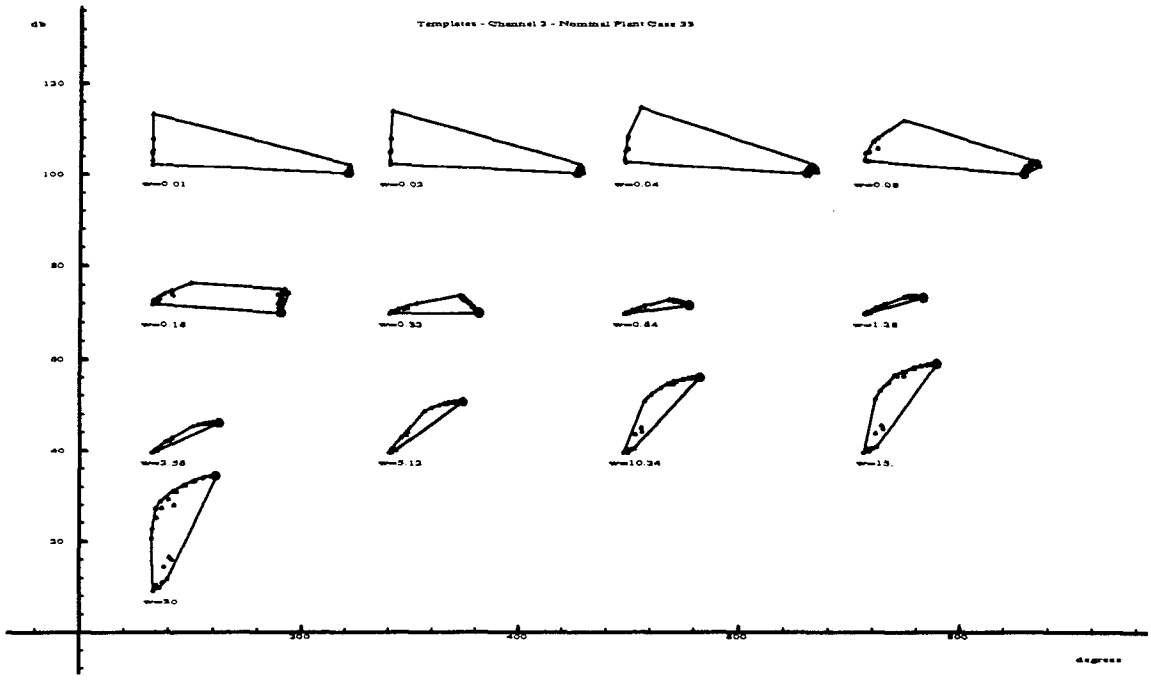

Figure 4.22 β Channel Templates - Design 2

To avoid repetition, only the composite bound are shown here (Fig. 4.23 and Fig. 4.24). Once again the cross-coupling effects bounds are not used in generating the composite bounds as they are similar to those seen in Fig. 4.12 and Fig. 4.13 and they mask the tracking bounds. The same dips are seen in the Design 2 bounds as in Design 1 enabling lower gains to be used and still achieve the desired tracking responses.

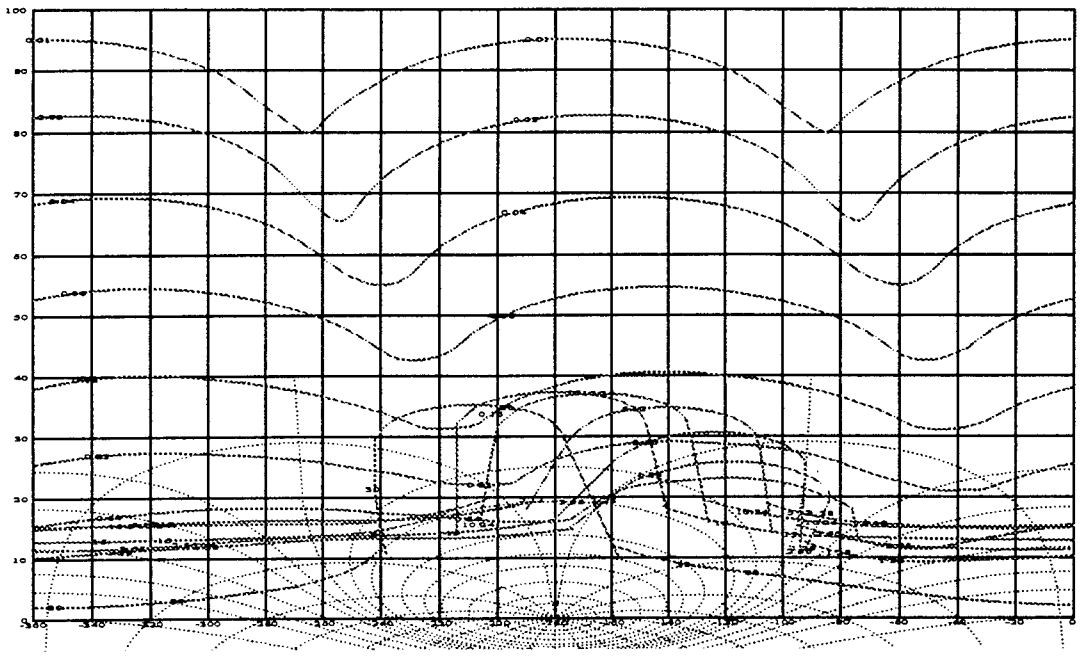

Figure 4.23 Composite Bounds for p Channel - Design 2

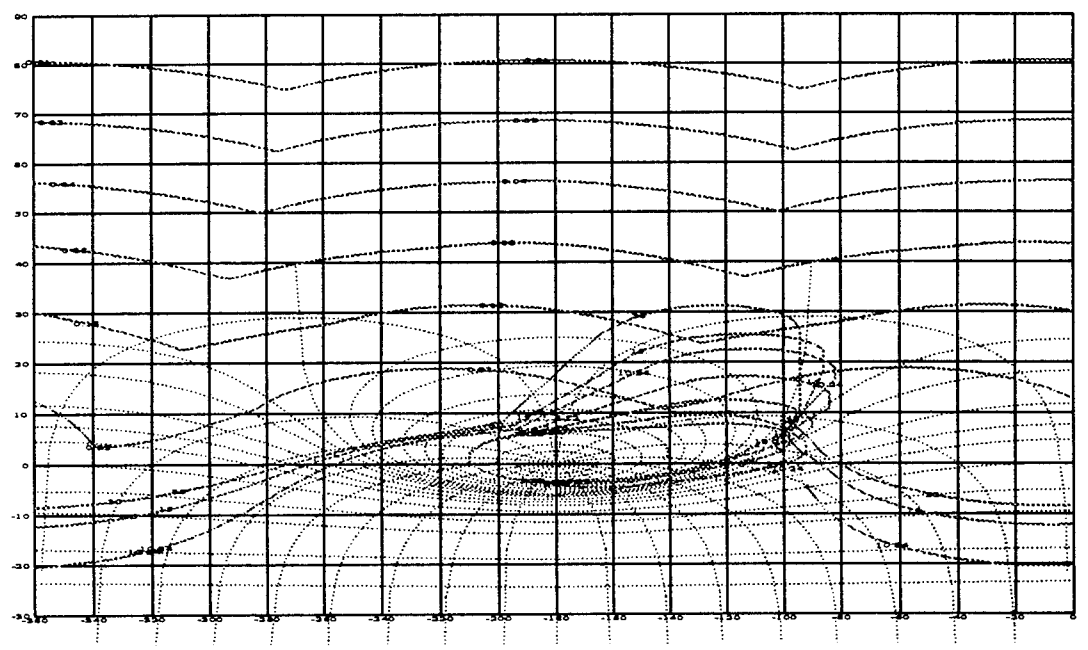

Figure 4.24 Composite Bounds for β Channel - Design 2

Plots of the loop transmission functions for the final Design 2 compensators are shown in Fig. 4.25 and Fig. 4.26. These figures show that the loop transmission functions go through the dips in the composite bounds where possible. For the p channel the dips in the composite bounds level out at higher frequencies, thus less effort is made in trying to pass through the dips. In addition, for both compensators, the stability bounds are met for all frequencies and the tracking bounds are met over the pilot's bandwidth. These plots also show that the phase margin frequency is indeed the specified value of 15rps for both channels.

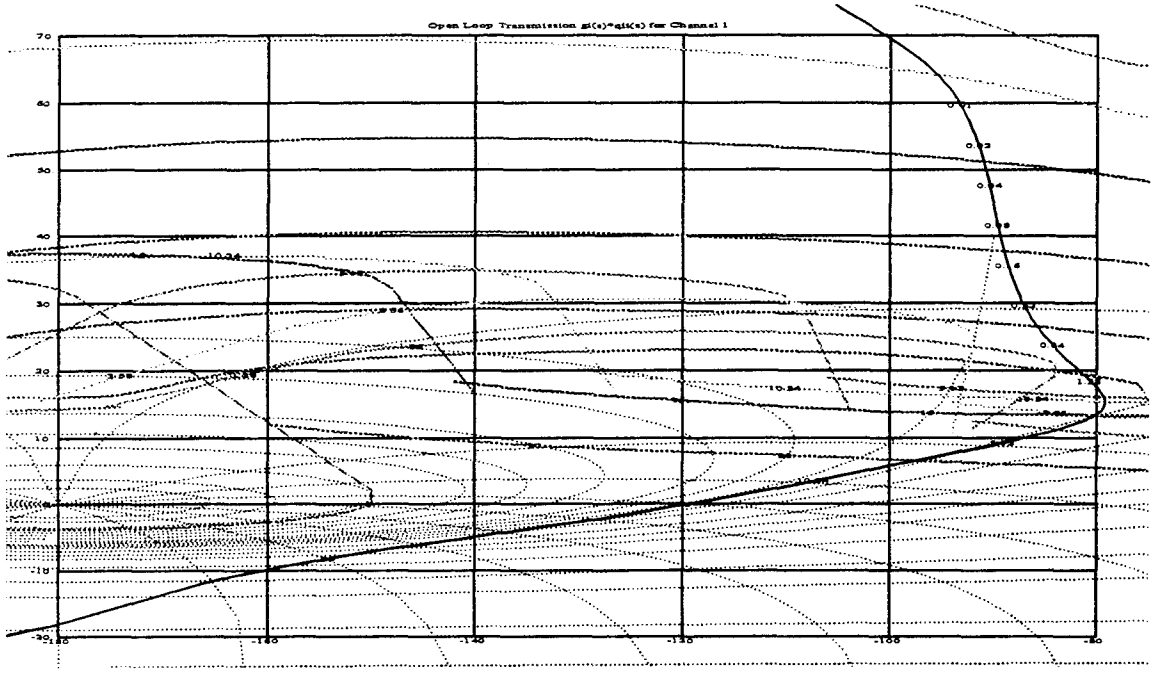

Figure 4.25 Nominal Loop Transmission for p Channel - Design 2

The final compensators generated for Design 2 are:

$$G_p = \frac{0.4(s+2)(s+10)}{s(s+5)} \tag{4.14}$$

$$G_\beta = \frac{135(s+0.9)(s+3)}{s(s+7)} \tag{4.15}$$

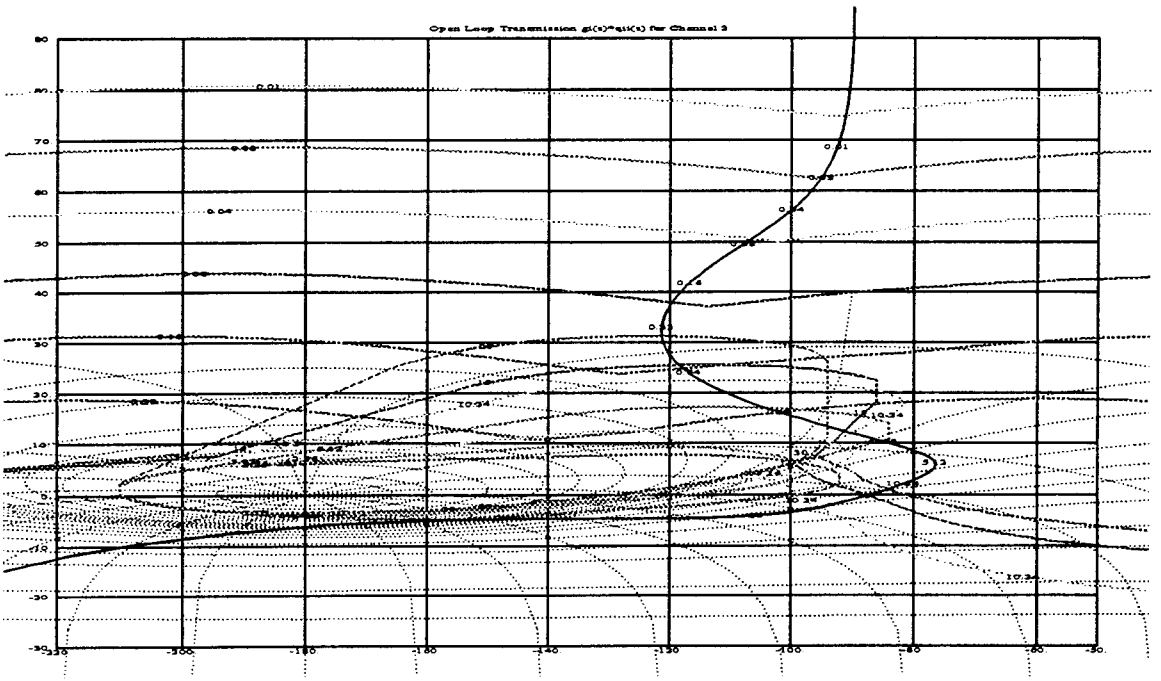

Figure 4.26 Nominal Loop Transmission for β Channel - Design 2

The pre-filters are designed based on the same criterion of not attenuating the pilot's tracking signal as described in Design 1. The final pre-filters for Design 2 are represented by:

$$F_p = \frac{4}{(s+4)} \tag{4.16}$$

$$F_\beta = \frac{0.5}{(s+0.5)} \tag{4.17}$$

4.4.3 Design Validation. The compensators and pre-filters generated in Design 2 are first checked to verify that the stability bounds have been met for both channels. The plots generated by the QFT CAD package for stability validation are shown in Fig. 4.27 for the p channel and in Fig. 4.28. Since none of the loop transmission functions for either channel pass through the stability contour, the stability specifications are met for both channels.

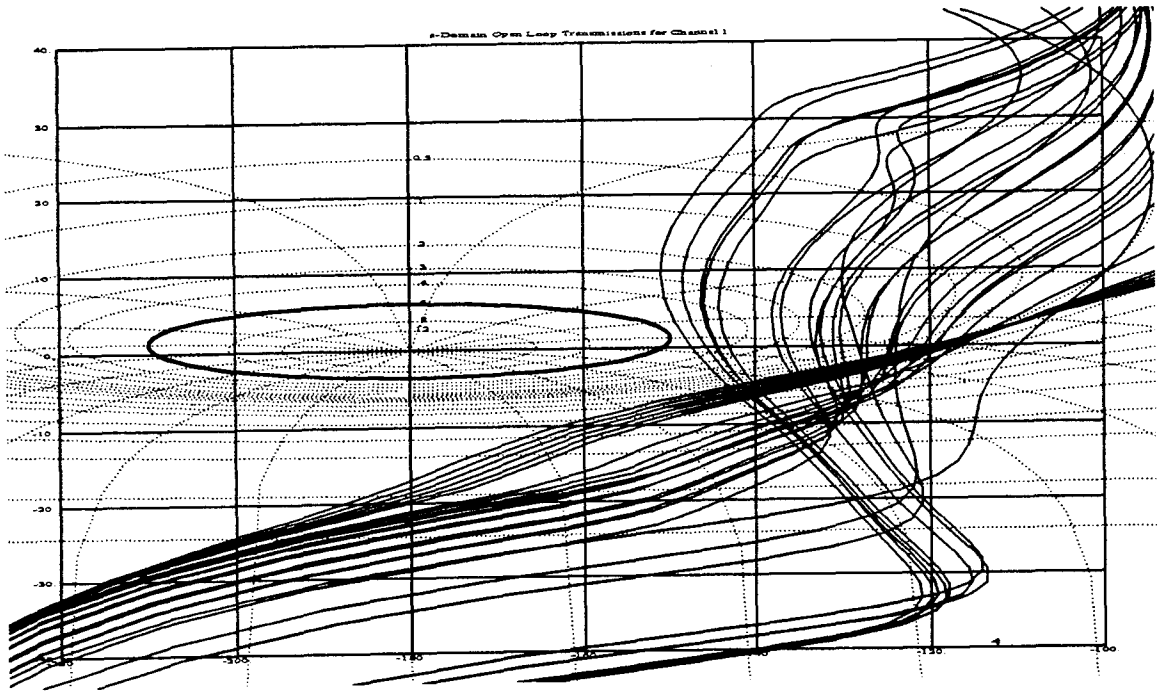

Figure 4.27 Stability Validation for p Channel - Design 2

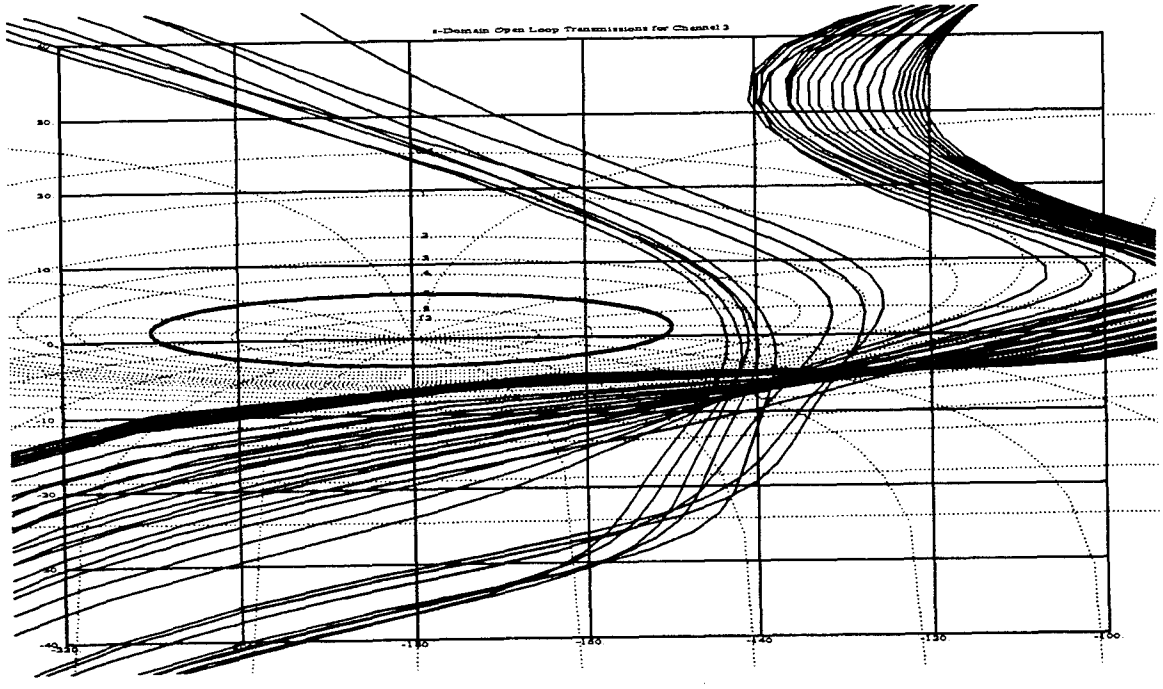

Figure 4.28 Stability Validation for β Channel - Design 2

The tracking validation plot of Fig. 4.29 is also generated via the QFT CAD package. Looking at the upper left hand graph, it is seen that the p channel tracking bounds are met over the pilot's bandwidth for the high $\bar{q}$ plants. The low $\bar{q}$ plants don't meet the tracking bounds very well, but based on QFT's inherent over-design the responses are accepted for now and are tested in the time domain to ensure tracking responses are acceptable. The poorer responses of the low $\bar{q}$ p channel tracking is expected since by not using all of the available control surfaces, some control power is lost and tracking becomes more difficult. However, in the low $\bar{q}$ range, degraded roll performance is expected and exists in current fighter aircraft. The lower right hand graph shows a similar response to that seen in Design 1 (Fig. 4.20) and is deemed acceptable based on the same reasons. Looking at the cross-coupling effects (upper right hand and lower left hand graphs), similar responses to those seen in Design 1. Taking a closer look, it is seen that Design 2 has slightly better attenuation of β response generated by a roll rate command (lower left hand graph.) Since this is the desired effect of the second design, the QFT portion of this design is complete and it is left to the time domain simulation to verify that military specifications are met.

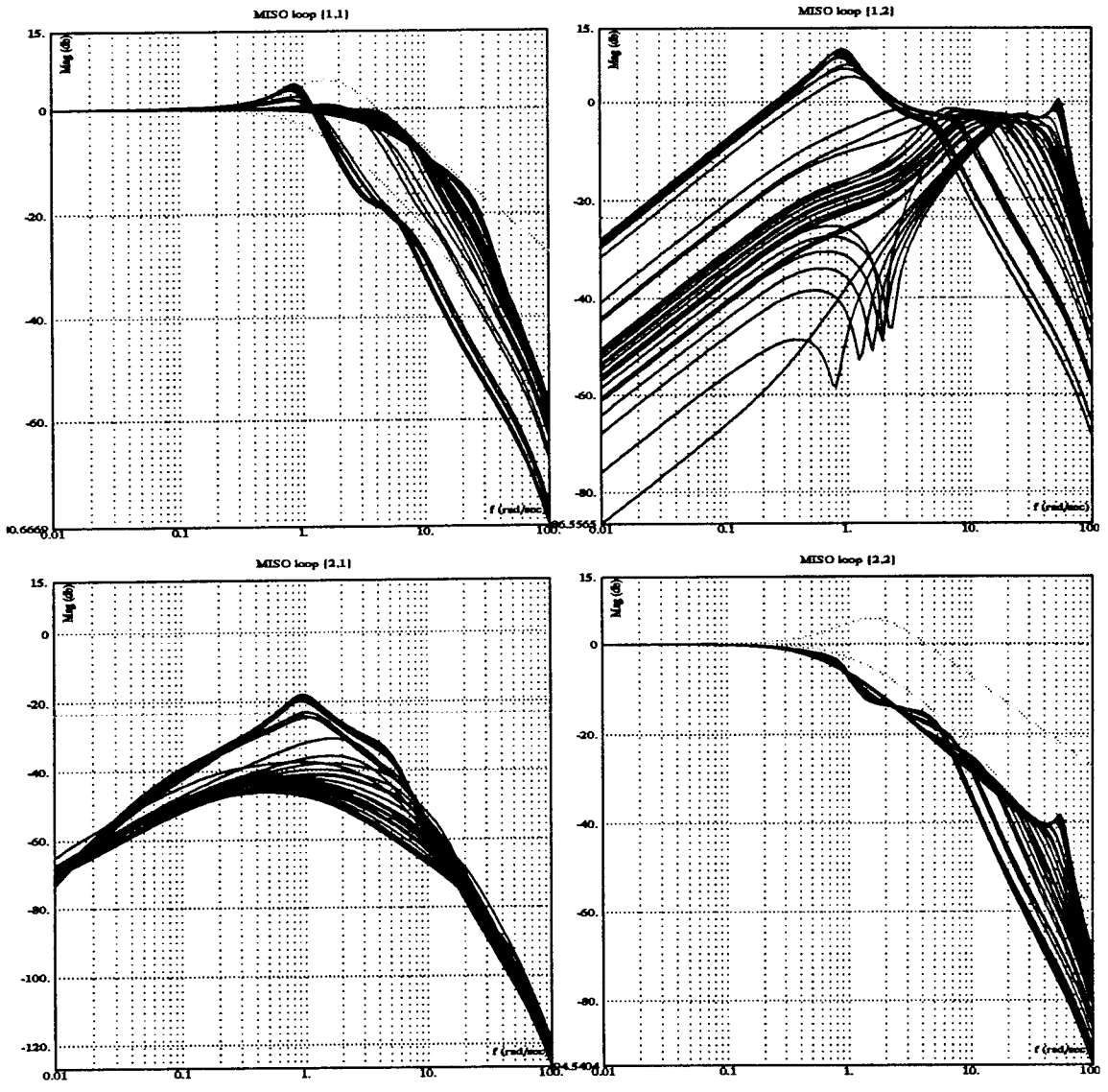

Figure 4.29 Tracking Validation for Design 2

4.5 Design 3

The third design goes beyond just trying to control the F-18. The objective of Design 3 is to reduce the loads on the wing, thus reducing the bending and twisting of the wing. This is accomplished using load alleviation techniques in conjunction with QFT.

4.5.1 Weighting Matrix. The weighting matrix of Design 3 is developed to maximize control power while at the same time reducing wing load. Data for the influence coefficients was obtained from the Structures Division of Wright Laboratory. Unfortunately, due to problems with the finite element model, data was only provided for the trailing edge flaps and the ailerons. The influence coefficients describe the load generated by a degree of deflection of a control surface. Based on this knowledge, it is possible to optimize the available control power while minimizing the load on the wings. The optimization problem is formulated in the following manner:

- Since no data is available for the leading edge flaps, it is decided to use the leading edge flaps with the ailerons to generate roll control power. This is accomplished by using the leading edge flaps so they reach their maximum deflection at the same time as the ailerons reach their maximum position. Mathematically this is expressed as:

$$\delta_{lef} = \delta_{ail} \frac{\delta_{lef}^{max}}{\delta_{ail}^{max}}$$

$$\delta_{lef} = \frac{33^\circ}{45^\circ} \delta_{ail} = 0.7333 \delta_{ail} \tag{4.18}$$

- Trailing edge flaps are used in the negative direction to alleviate load.

- The roll control power equation to be maximized is written as follows:

$$C_l = C_{l_{\delta_{ail}}}\delta_{ail} + C_{l_{\delta_{lef}}}\delta_{lef} + C_{l_{\delta_{tef}}}\delta_{tef} \tag{4.19}$$

$$C_l = \left(C_{l_{\delta_{ail}}} + (0.7333)C_{l_{\delta_{lef}}}\right)\delta_{ail} + C_{l_{\delta_{tef}}}\delta_{tef} \tag{4.20}$$

- Restrictions are placed on the maximum bending and torsion moments:

$$\left|C_{B_{\delta_{ail}}}\delta_{ail} + C_{B_{\delta_{tef}}}\delta_{tef}\right| \leq \frac{1}{2}C_{B_{\delta_{ail}}}\delta_{ail}^{max} \tag{4.21}$$

$$\left|C_{T_{\delta_{ail}}}\delta_{ail} + C_{T_{\delta_{tef}}}\delta_{tef}\right| \leq \frac{1}{2}C_{T_{\delta_{ail}}}\delta_{ail}^{max} \tag{4.22}$$

  where C_{B_δ} and C_{T_δ} are the influence coefficients provided by the Structures Division.

- Additional constraints are set by maximum control surface deflections.

$$-25 \leq \delta_{ail} \leq 45 \tag{4.23}$$

$$-8 \leq \delta_{tef} \leq 45 \tag{4.24}$$

Thus, there are four constraint equations: bending moment (Eq. (4.21)), torsion moment (Eq. (4.22)), and two position limits (Eq. (4.23) and Eq. (4.24)). The cost function for this optimization is the two degree of freedom roll control power equation (Eq. (4.18)). The optimization algorithm for this research is a two dimensional linear programming problem. If data had been available for the leading edge flap, the optimization would have involved three degrees of freedom. A graphical representation of the optimization problem is shown in Fig. 4.30. The weighting matrix element is then determined by the ratio of trailing edge flap deflection to aileron deflection at the point of maximum roll control power. From this graph, it is seen that for this design, the maximum roll control power is always obtained when

the line described by the bending or torsion moment equations intersects the maximum negative deflection of the trailing edge flaps. The slope between the origin and this point is negative showing that the control surfaces are working in the predicted directions.

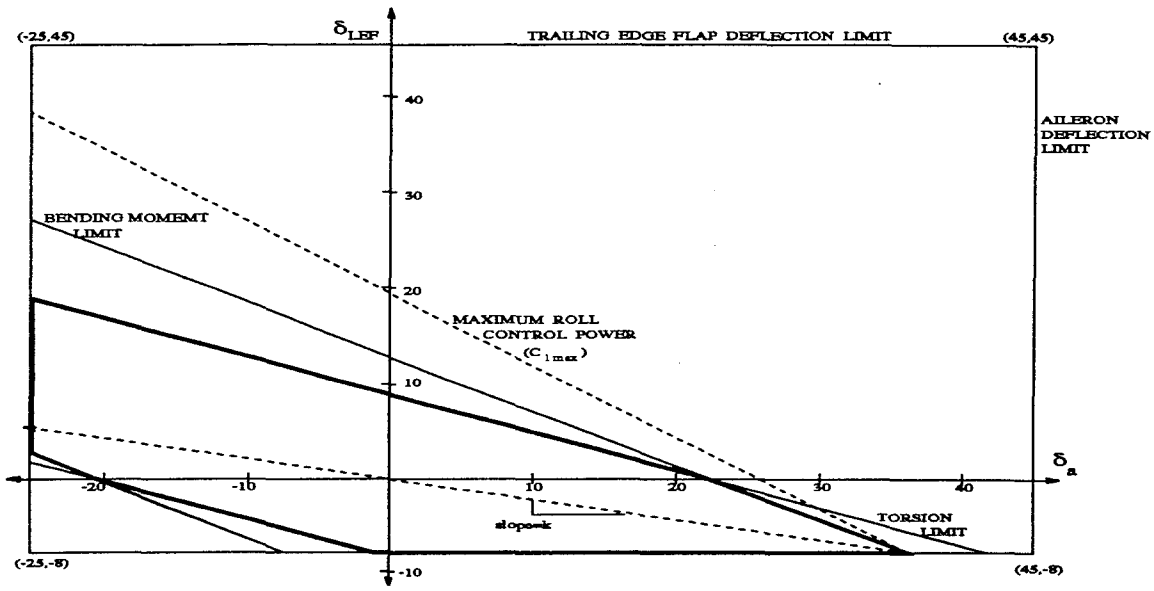

Figure 4.30 Example of Optimal Weighting Matrix Calculation

The weighting matrix developed by this optimization routine is:

$$W_2 = \begin{bmatrix} 1 & 0 \\ 0.3333 & 0 \\ 0 & 1 \\ 0.7333 & 0 \\ k & 0 \end{bmatrix} \tag{4.25}$$

where k is the optimal slope (average for all plants of -0.177). Notice that the weighting matrix element relating to the stabilators is once again chosen to be 0.3333. In addition, the optimal weighting matrices are dependent on flight condition.

4.5.2 QFT FCS Design. With the new weighting matrix, the effective plants and the MISO loops are generated. The templates for Design 3 are shown in Fig. 4.31 for the p channel and Fig. 4.32 for the β channel. The templates show that the plant uncertainty for the p channel has been reduced (the templates are smaller.) In addition, although the β channel templates are slightly larger than those in Design 2, they are still smaller that the first design's templates.

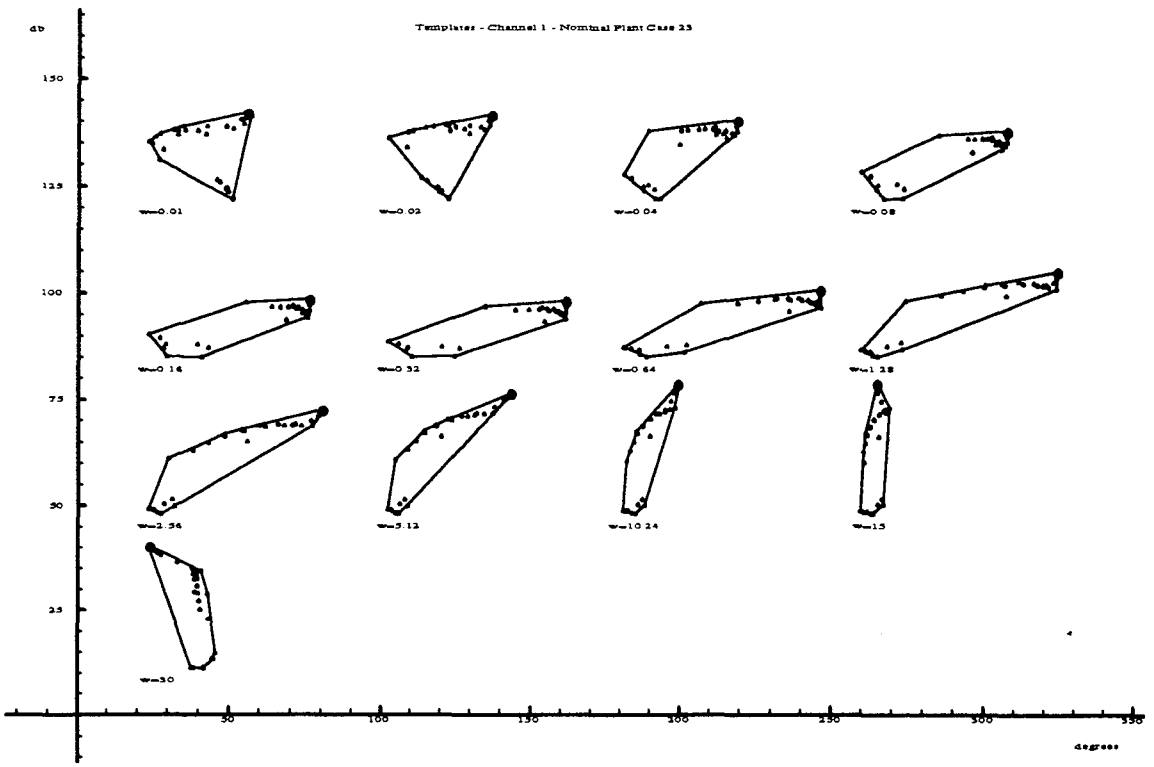

Figure 4.31 p Channel Templates - Design 3

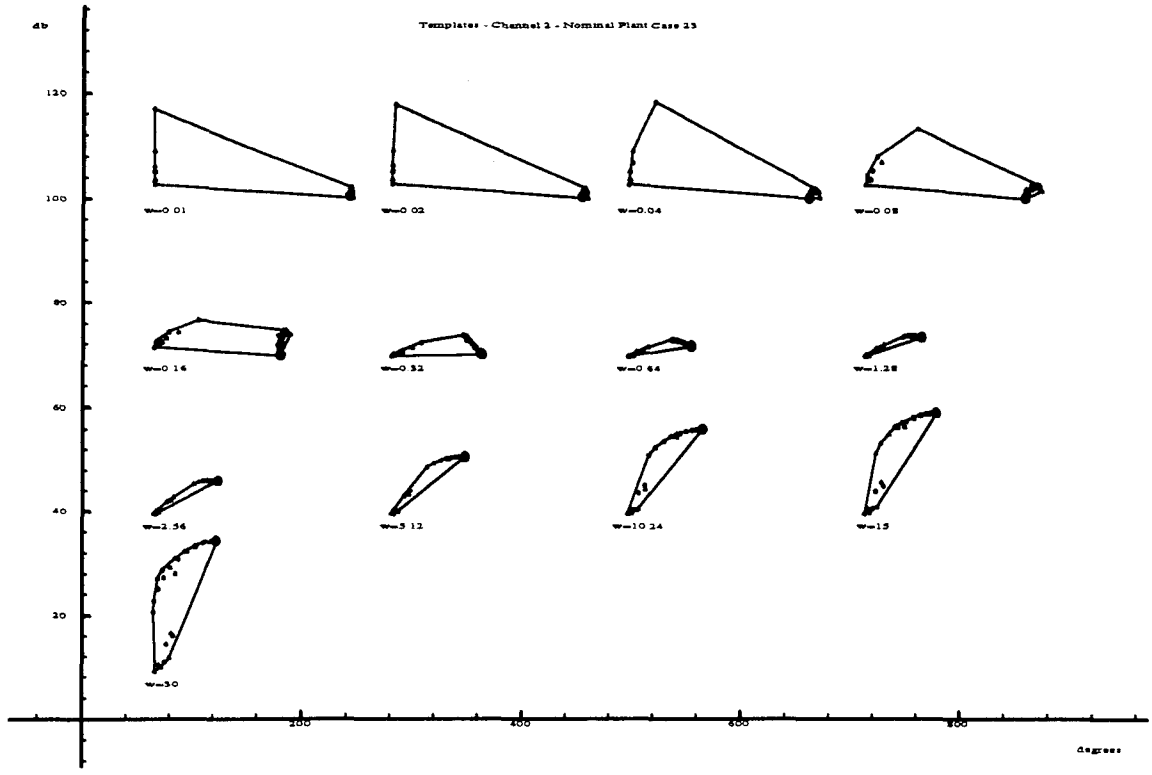

Figure 4.32 β Channel Templates - Design 3

Based on the templates, composite bounds are generated for Design 3 (Fig. 4.33 and Fig. 4.34). Comparing these composite bounds to those generated in Design 2 (Fig. 4.23 and Fig. 4.24) show that the magnitude of the p channel bounds is slightly reduced in Design 3 over Design 2. For the β channel bounds, there is no visible difference between Design 2 and Design 3.

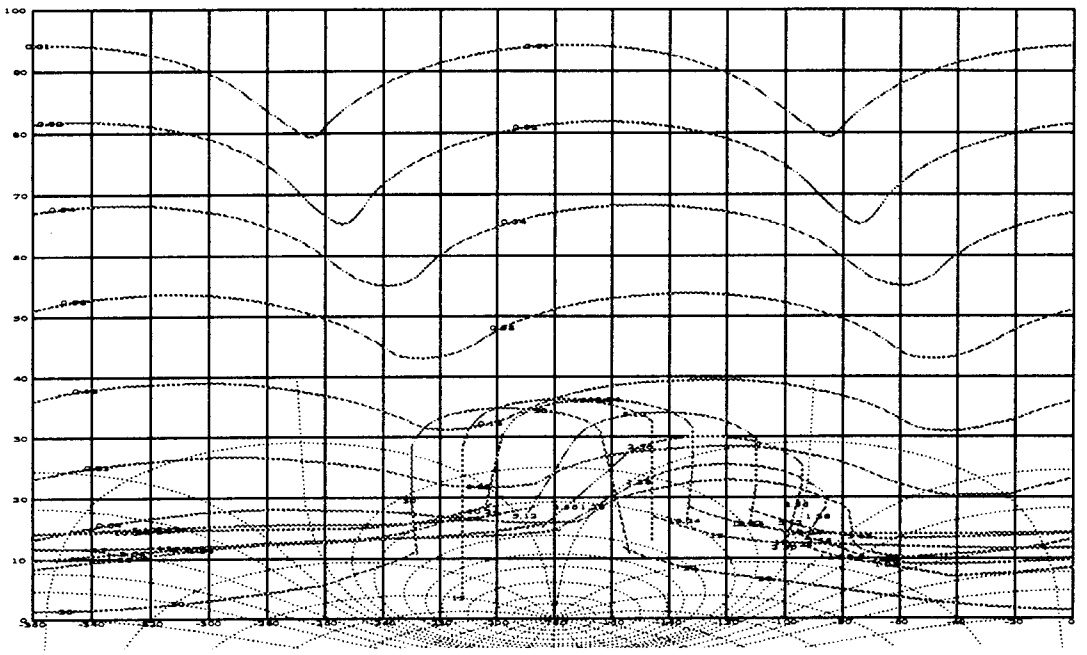

Figure 4.33 Composite Bounds for p Channel - Design 3

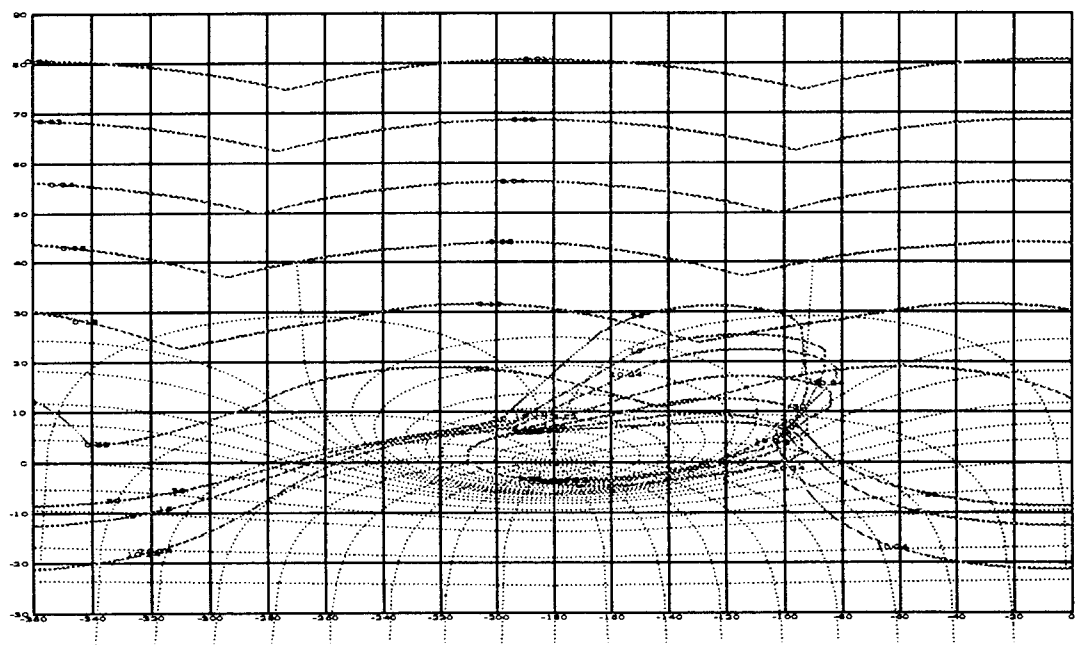

Figure 4.34 Composite Bounds for β Channel - Design 3

Using the composite bounds generated by the QFT CAD package, loop shaping is performed for both channels. The final loop transmission functions are shown in Fig. 4.35 and Fig. 4.36 for the p and β channels respectively. These plots show that the stability bounds are met for all frequencies for both channels. In addition, the tracking bounds are met over most frequencies for the β channel and over most of the pilot's bandwidth for the p channel. Even though the tracking bounds for the p channel are not satisfied for the pilot's entire bandwidth, based on QFT's inherent over-design, this design is acceptable and is further tested in the time domain simulations.

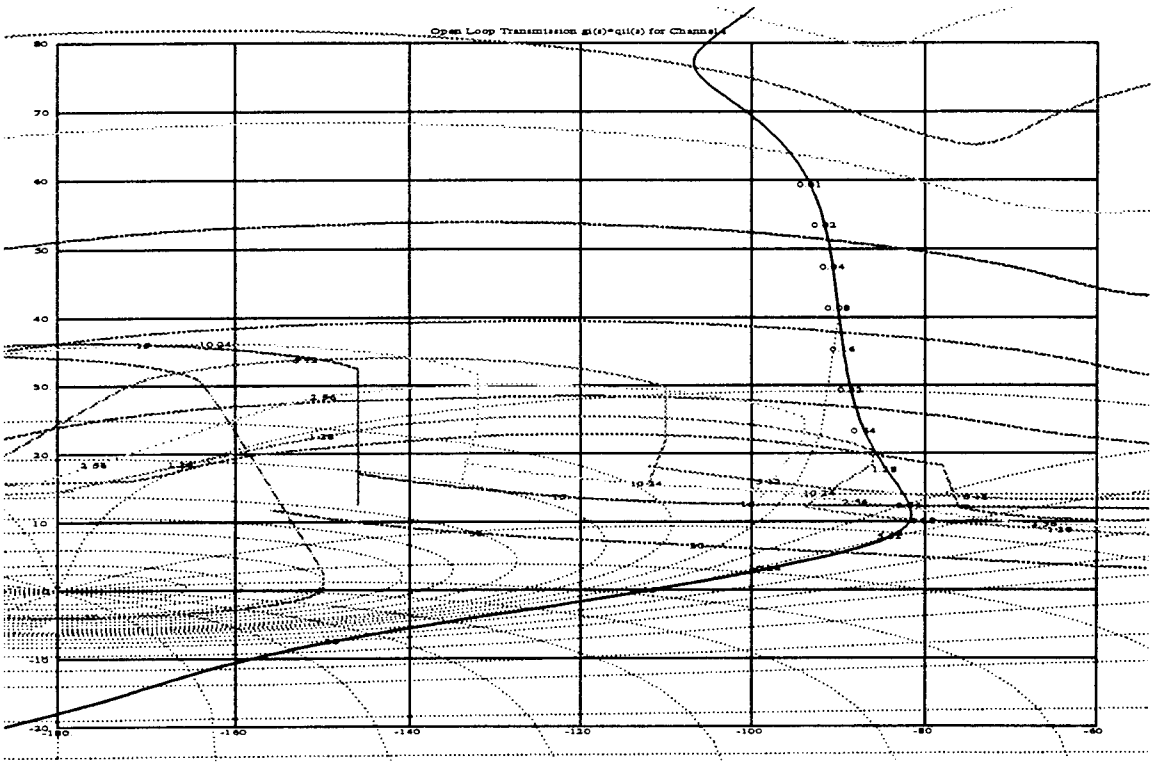

Figure 4.35 Nominal Loop Transmission for p Channel - Design 3

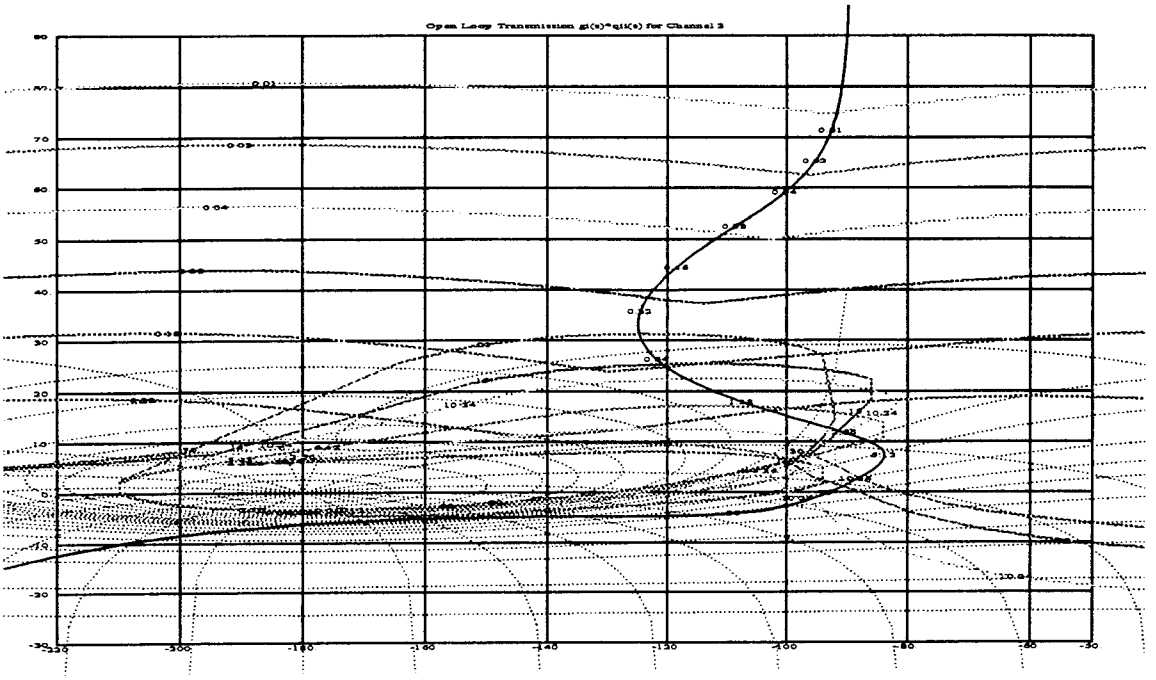

Figure 4.36 Nominal Loop Transmission for β Channel - Design 3

The final compensators describing the loop transmission functions for Design 3 are:

$$G_p = \frac{0.38(s+4.1)}{s} \tag{4.26}$$

$$G_\beta = \frac{130(s+1.1)(s+2.5)}{s(s+5)} \tag{4.27}$$

The final pre-filters developed for Design 3, determined using the same criteria as the previous designs, are:

$$F_p = \frac{4}{(s+4)} \tag{4.28}$$

$$F_\beta = \frac{0.5}{(s+0.5)} \tag{4.29}$$

4.5.3 Design Validation. After the completion of the compensator and pre-filter designs, both channels are checked to ensure that the stability specifications are satisfied. The plots for the stability validation performed by the QFT CAD package are shown in Fig. 4.37 for the p channel and in Fig. 4.38 for the β channel. Since

none of the $\mathcal{J}$ plants cross through the highlighted M_L contour, the Nichols chart stability criterion is satisfied.

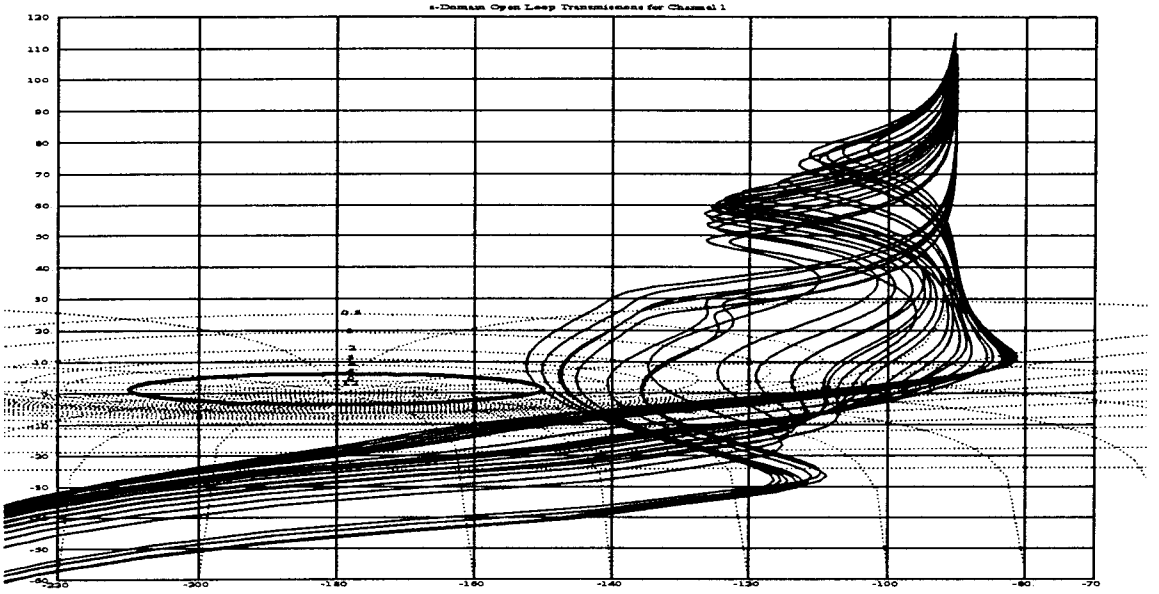

Figure 4.37 Stability Validation for p Channel - Design 3

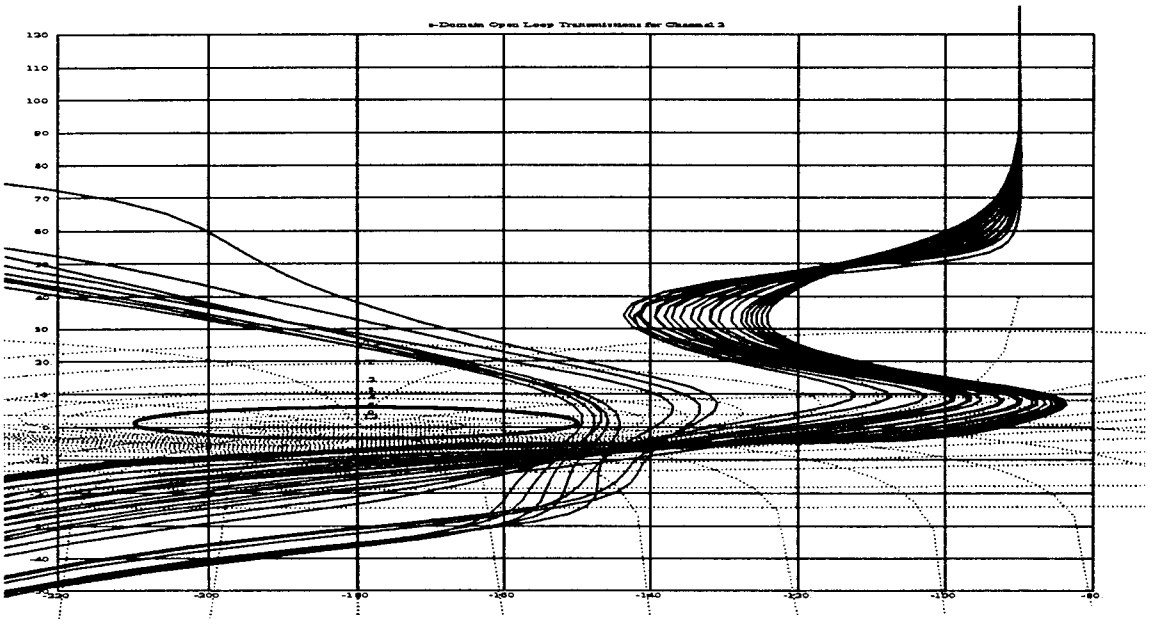

Figure 4.38 Stability Validation for β Channel - Design 3

The frequency domain tracking validation is also performed via the QFT CAD package and the results are shown in Fig. 4.39. These results are very similar to those seen in Fig. 4.29 and based on the same reasons, the third flight control system design is considered acceptable. Further testing is done in the time domain simulations found in Ch. V.

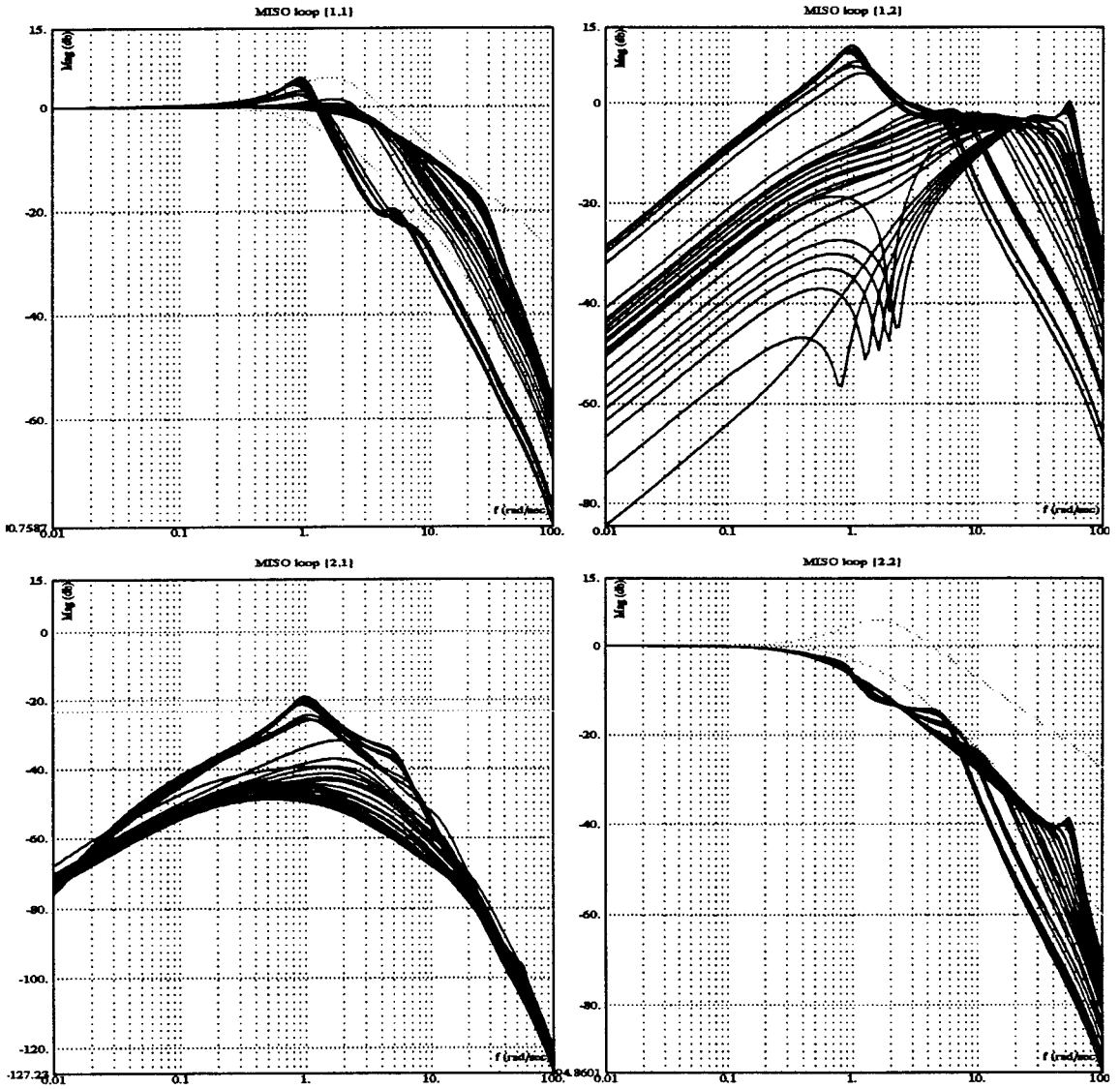

Figure 4.39 Tracking Validation for Design 3

4.6 Chapter Summary

Three flight control system designs are performed in this chapter. The only difference in the designs is in the selection of the weighting matrix. For Design 1, the weighting matrix is chosen so that all of the control surfaces on the wing reach their maximum position deflection at the same time. The second design uses the same weighting matrices for the high $\bar{q}$ plants ($\bar{q} > 200$) but for the low $\bar{q}$ plants only the ailerons and rudders are used. The more sophisticated third design employs optimization techniques to produce maximum roll control power while reducing the wing loads. Using these weighing matrices and the resultant effective plants, three sets of compensator and pre-filter matrices are generated using the QFT robust control design method. These designs are then checked to ensure that stability specifications are met and that tracking responses are reasonable. The next step in this research is to determine the time domain responses of these three designs. The time domain simulations are performed in Ch. V.

V. Time Domain Simulation

Having designed the flight control system in the frequency domain, it is then important to test the resultant design in the time domain. If the time domain responses meet the given specifications then the design process is completed. For this research the time domain responses are simulated using MATLAB's nonlinear Simulink program. This program is very effective since it allows the user to construct a block diagram to simulate both linear and non-linear systems. Three specifications are evaluated in this chapter: time response to a unit step roll rate command, time response to a unit step sideslip command, and time to bank to 90°. For all of these test conditions, time histories are shown for roll rate, sideslip, bank angle, as well as the position of all the control surfaces.

5.1 Setup

The top level of the simulation (Fig. 5.1) shows the block diagram of the lateral/directional flight control system where G_{ii} represents the compensator transfer functions and F_{ii} are the pre-filter transfer functions. The block labeled P_e represents the effective plant and is shown in Fig. 5.2.

The second level, the effective plant, takes in the commanded signals, passes them through the weighting matrix and then on to the actuators (represented by the blocks labeled Aileron, etc.) These signals are then finally passed on to the aircraft dynamics model. The dutch roll damper circuit is also incorporated at this level and is comprised of yaw rate feedback passed through a washout circuit. The signals coming out of this layer are then passed back to the top level.

The actuator block, Fig. 5.3, models the actuator dynamics in addition to position and rate limits. The position and rate limits make the overall system non-linear and are thus a truer representation of the F-18. All three of the flight control designs are evaluated using this same structure.

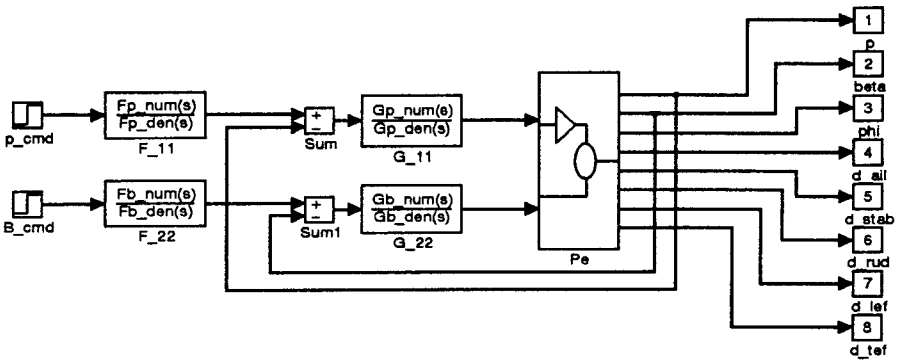

Figure 5.1 Block Diagram used for Time Domain Simulation

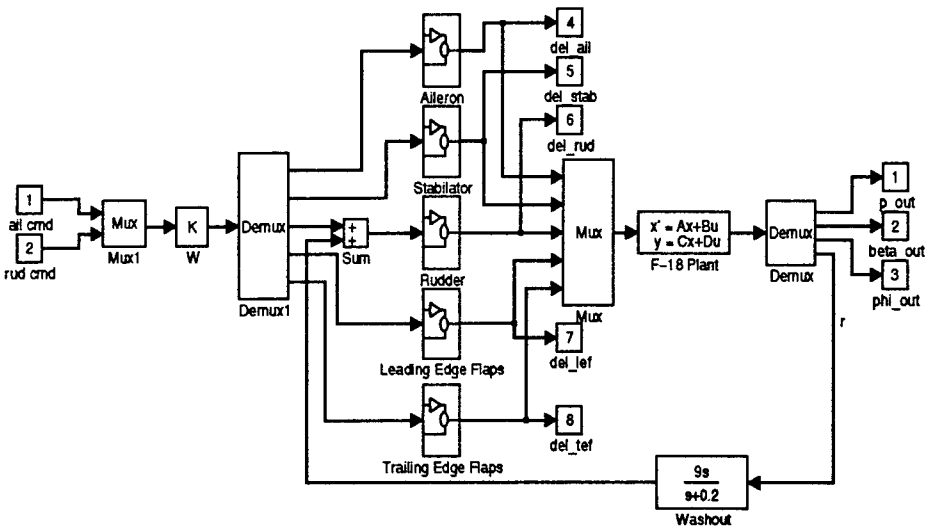

Figure 5.2 Block Diagram for the Effective Plant

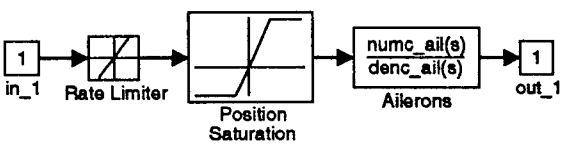

Figure 5.3 Example of Block Diagram for the Actuators

5.2 Design 1

As a reminder, the first design uses a weighing matrix developed to make all of the wing control surfaces reach their maximum deflection position simultaneously. The compensators and pre-filters generated based on this weighting matrix are re-stated here for convenience.

$$G_p = \frac{0.4(s+3)}{s} \qquad G_\beta = \frac{145(s+0.8)(s+5)}{s(s+10)}$$
$$F_p = \frac{5}{(s+5)} \qquad F_\beta = \frac{0.5}{(s+0.5)} \tag{5.1}$$

In general, the results of the time domain simulation for the first design are all good. The time responses to a unit step roll rate command are shown in Fig. 5.4 and Fig. 5.5. Looking at the roll rate time history plot, the high $\bar{q}$ plants (solid lines)

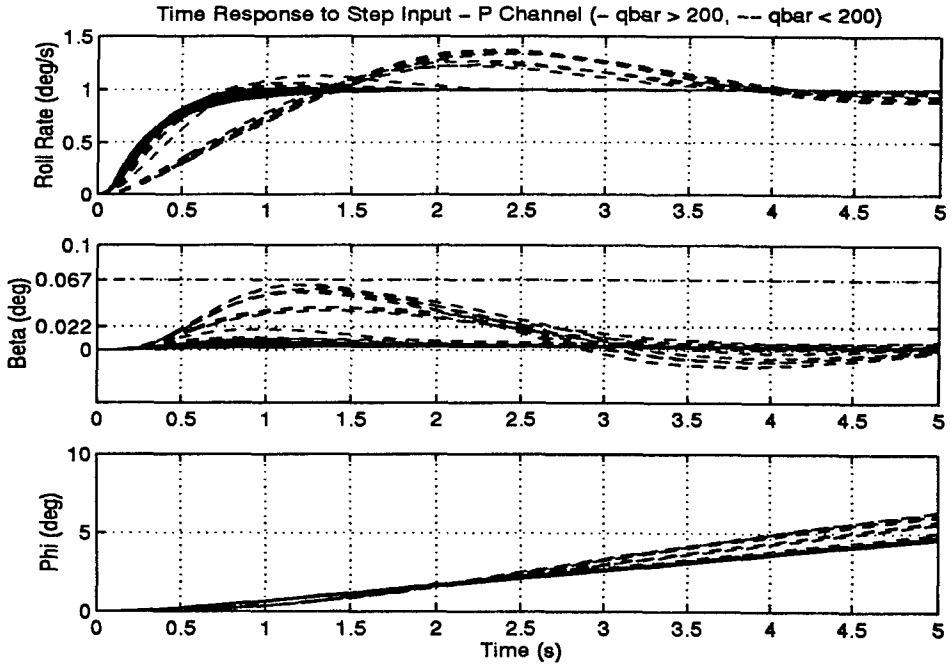

Figure 5.4 Time Response to Unit Step Input p Channel - Design 1 (1 of 2)

clearly exhibit the desired time response of a settling time of 4 seconds. For the low $\bar{q}$ conditions (dashed lines), not all of the plants meet the given tracking specifications

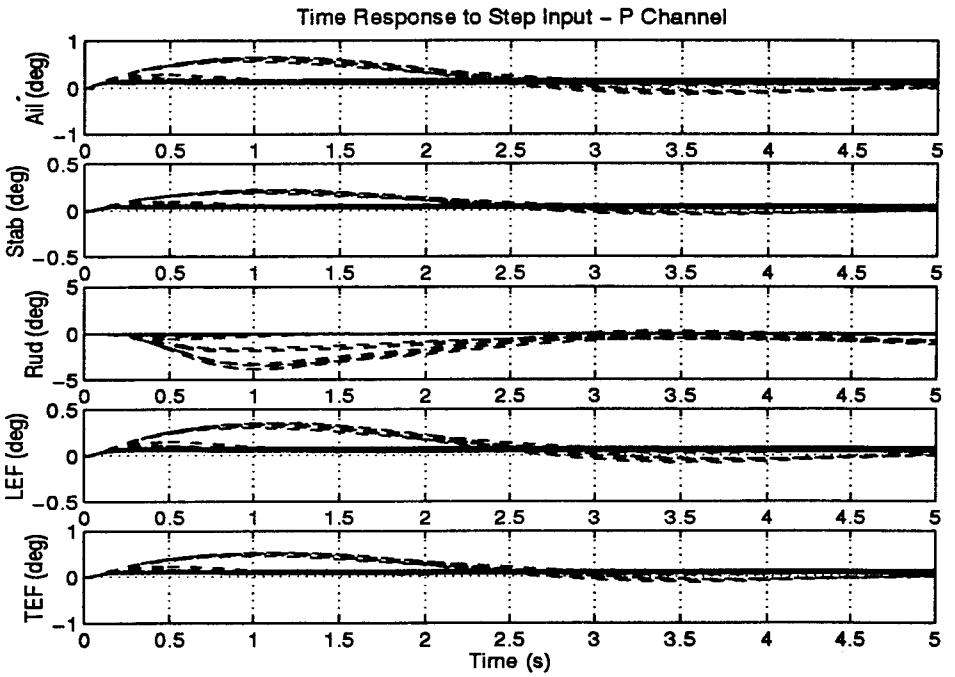

Figure 5.5 Time Response to Unit Step Input p Channel - Design 1 (2 of 2)

although the settling time is close. However, poorer tracking, i.e., "ballooning", is to be expected at higher trim angles of attack (low $\bar{q}$ regions.) In addition, the overshoot is larger than expected, but the damping of the signal is reasonably good. The β time response to a roll rate input shows excellent cross-coupling effect rejection. The low $\bar{q}$ plants do not exceed the maximum specified value of 0.067° of sideslip and the high $\bar{q}$ plants are well below the maximum value of 0.022° of sideslip. Figure 5.5 shows that all of the control surface deflections are within reasonable limits. This graph also clearly shows that a great deal of rudder is used to generate the desired roll rate for low $\bar{q}$ plants. This illustrates the effect of the stronger cross-coupling between the p and β channels which manifests itself as adverse yaw.

The time responses due to a unit step β command are shown in Fig. 5.6 and Fig. 5.7 for the variables of interest. The β response clearly shows the effects of the pre-filter which is designed to filter out high frequencies. This is done to reduce the cross-coupling effects, and is justifiable since the pilot rarely attempts to command β for lateral tracking tasks. The settling times for the β channel are greater than the specified value of 4 seconds, however, since this value was not based on military specifications, the time responses obtained from this design are deemed acceptable.

The roll rate response to a unit step β command show the results of the frequency domain cross-coupling effects plots (Fig. 4.20). For the low $\bar{q}$ plants, the cross-coupling effects are very evident, but since they are quickly damped out and these effects are inevitable at high angles of attack, the design is satisfactory for the β channel. Looking at the control surface time histories, Fig. 5.7, all of the surface deflections are within a reasonable range for a step input. Again, a large amount of rudder deflection is used to obtain the desired response for the low $\bar{q}$ plants, but this is expected for β tracking.

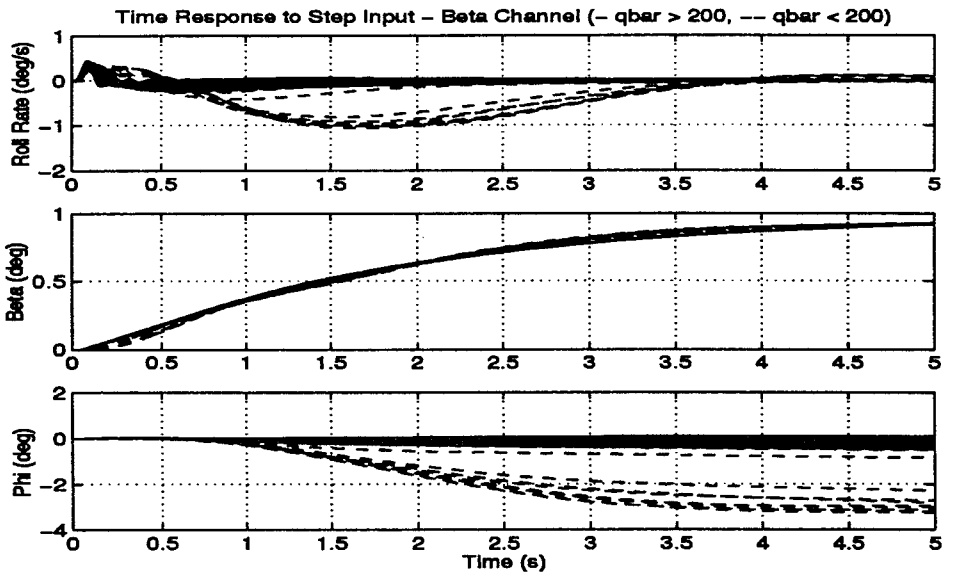

Figure 5.6 Time Response to Unit Step Input β Channel - Design 1 (1 of 2)

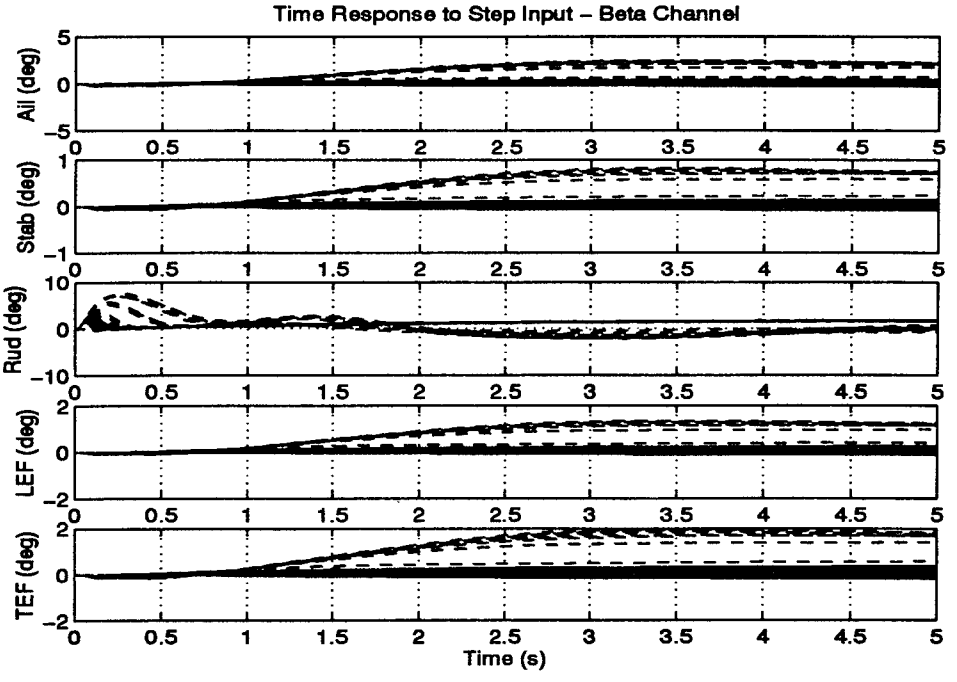

Figure 5.7 Time Response to Unit Step Input β Channel - Design 1 (2 of 2)

A final time domain simulation is performed to determine the time required to bank 90°. The results of this simulation are shown in Fig. 5.8 and Fig. 5.9. The roll rate command needed to obtain the desired results is $p_{cmd} = 155$ deg/sec. With this commanded signal, all of the high $\bar{q}$ plants are able to achieve a 90° bank angle within 1 second. In addition, the β cross-coupling for the high $\bar{q}$ plants is on the order of 1°, well below the maximum allowable of 6°. The low $\bar{q}$ plants are unable to meet specifications, but again, these specifications are not really meant for high angle of attack flight. The time histories of the control surfaces show the effect of both the rate and position limits. The low $\bar{q}$ plants stay in deflection saturation for the positions over the entire time range. This shows that the aircraft is unable to meet the desired time responses even with increased roll rate signals. All of the plants are in rate saturation for at least 0.3 seconds. Thus, the actuator rate limits are the limiting factor on the response of the F-18 aircraft. The high $\bar{q}$ plants do not reach position limits, indicating that greater bank angles than 90° are achievable in 1 second.

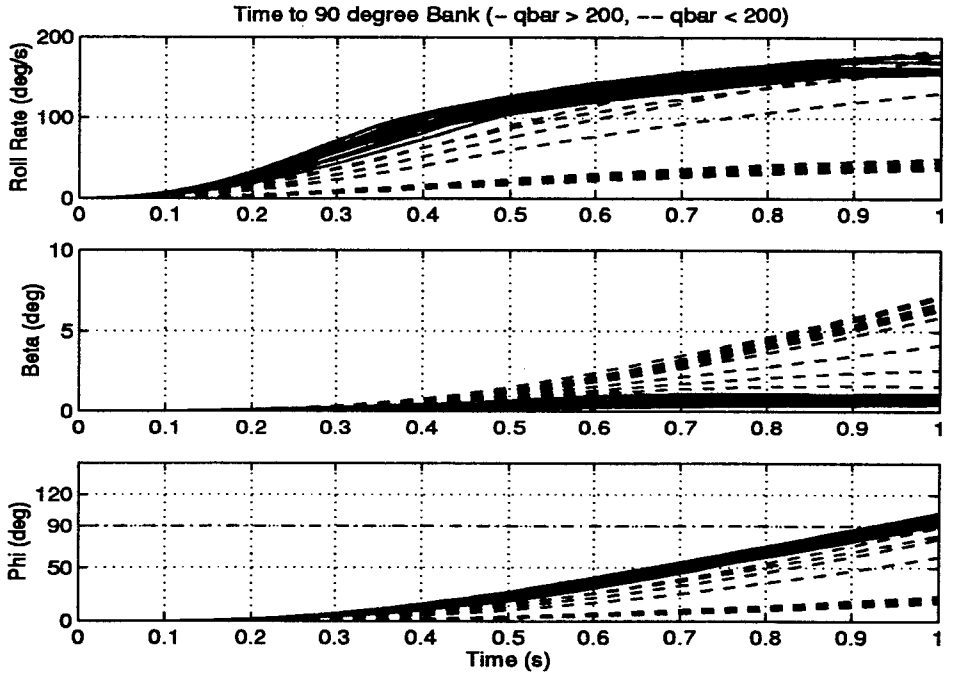

Figure 5.8 Time to Bank 90° - Design 1 (1 of 2)

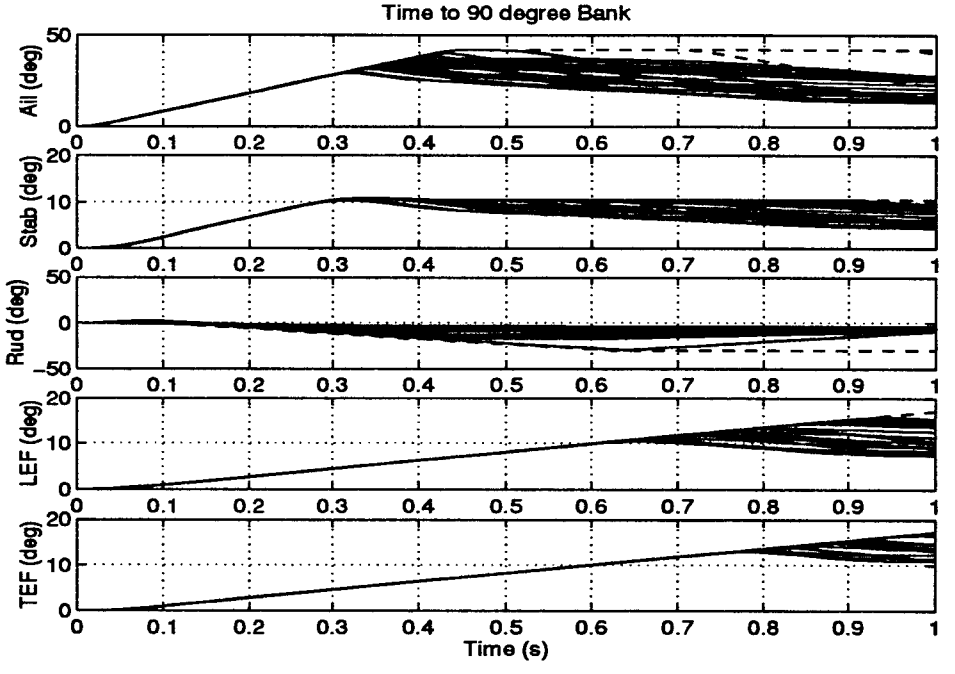

Figure 5.9 Time to Bank 90° - Design 1 (2 of 2)

Overall, based on the data from these three simulations, the first design is acceptable but there is definitely some room for improvement.

5.3 Design 2

The compensators and pre-filters determined in the second design are listed in Eq. (5.2). For the high $\bar{q}$ plants, the weighting matrix used in this design is identical to the first design. For the low $\bar{q}$ plants only the ailerons and rudders are used as control surfaces.

$$G_p = \frac{0.4(s+2)(s+10)}{s(s+5)} \qquad G_\beta = \frac{135(s+0.9)(s+3)}{s(s+7)}$$

$$F_p = \frac{4}{(s+4)} \qquad F_\beta = \frac{0.5}{(s+0.5)} \tag{5.2}$$

The time responses due to a unit step roll rate command (Fig. 5.10 and Fig. 5.11) are very similar to those seen in the first design. All of the high $\bar{q}$ plants meet the settling time specification generated from MIL-STD 1797A. In addition, some of the low $\bar{q}$ plants also display a satisfactory settling time. The settling time of the rest of the low $\bar{q}$ plants appear to have a slightly longer settling time than in the first design, and the overshoot is larger than specified, but since these plants represent the high angle of attack flight conditions, the responses are acceptable. The β channel cross-coupling is reduced over that seen in the first design, and is well within the specified limits. The control surface time histories of Fig. 5.11 show that in general the maximum deflection angle is reduced when compared to Design 1. The exception to this is the maximum aileron position for low $\bar{q}$ plants which is almost double the first design. This is an expected effect of only using ailerons for roll control at low $\bar{q}$. Since the maximum deflection is still relatively small, this design is acceptable. There appear to be some oscillatory problems in the simulation for the leading edge flaps, but the oscillations are so small (on the order of 0.01 degrees), that they are easily explainable as numerics problems.

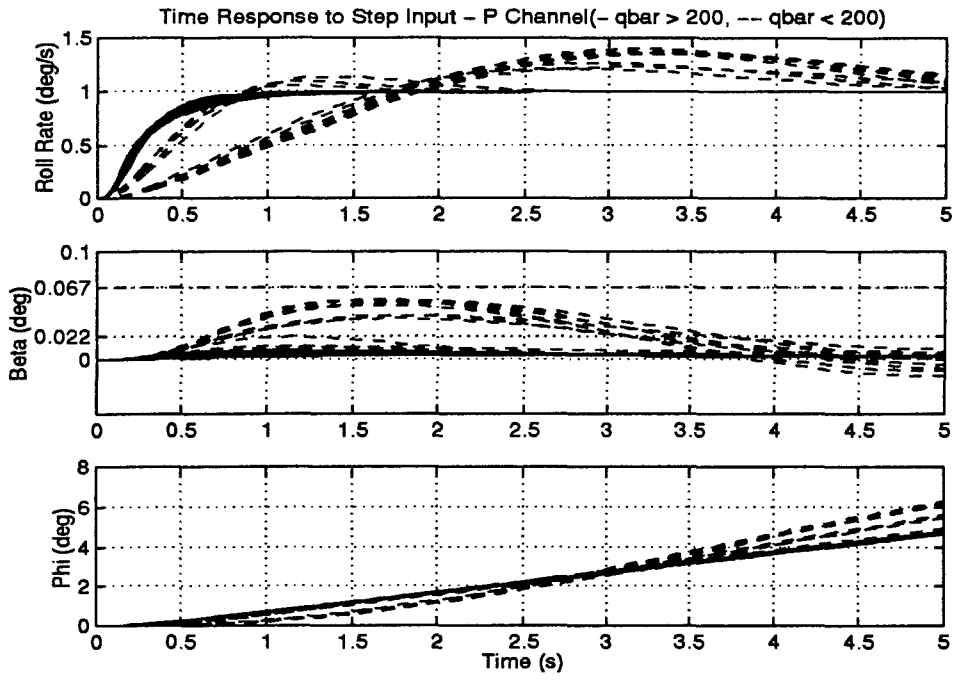

Figure 5.10 Time Response to Unit Step Input p Channel - Design 2 (1 of 2)

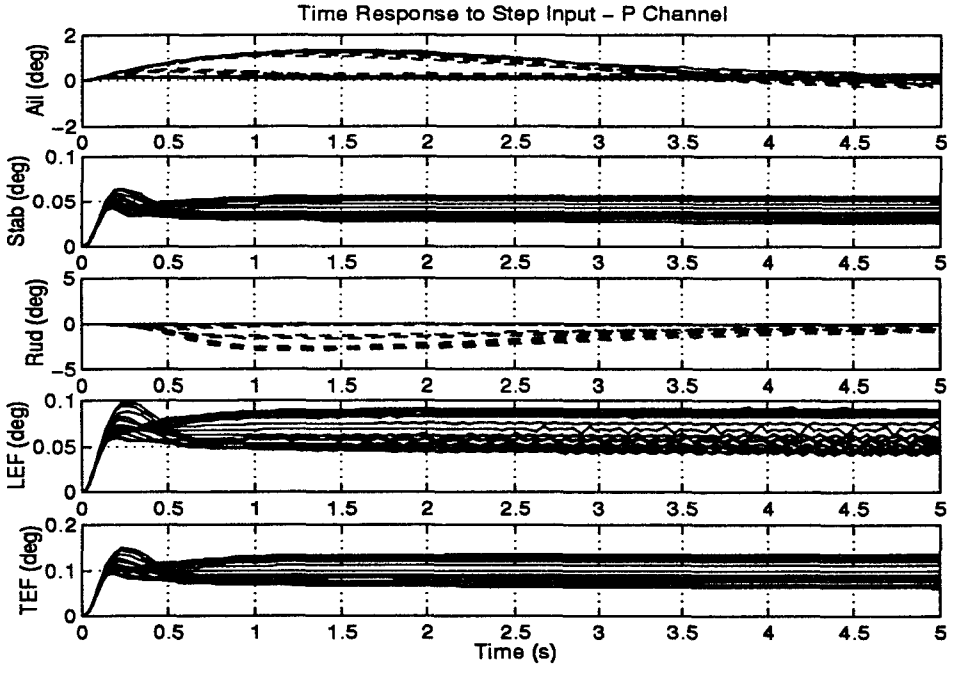

Figure 5.11 Time Response to Unit Step Input p Channel - Design 2 (2 of 2)

The time responses to a unit step β command for Design 2 are shown in Fig. 5.12 and Fig. 5.13. These plots are very similar to those of Design 1. One major difference is that Design 2 requires greater deflections of aileron to reach the tracking input. This is due to the fact that none of the other control surfaces are used and is a reasonable and expected consequence. In addition, a pilot would not typically attempt to track a β command when flying at high angles of attack. Since the β channel is not as important as the p channel in lateral/directional design, reduced performance in the β channel is an acceptable trade off to increased performance in the p channel.

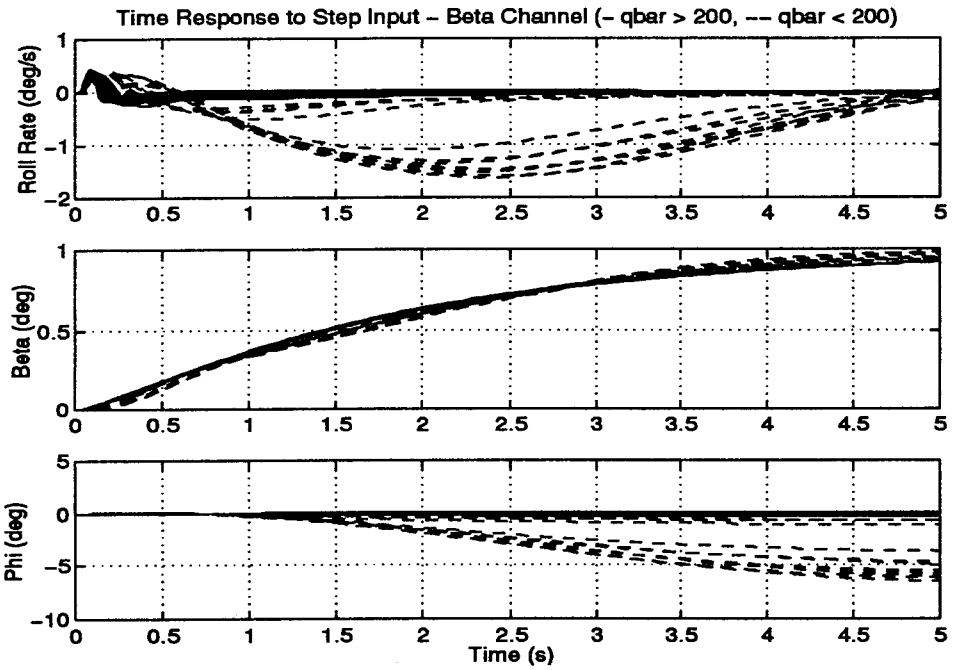

Figure 5.12 Time Response to Unit Step Input β Channel - Design 2 (1 of 2)

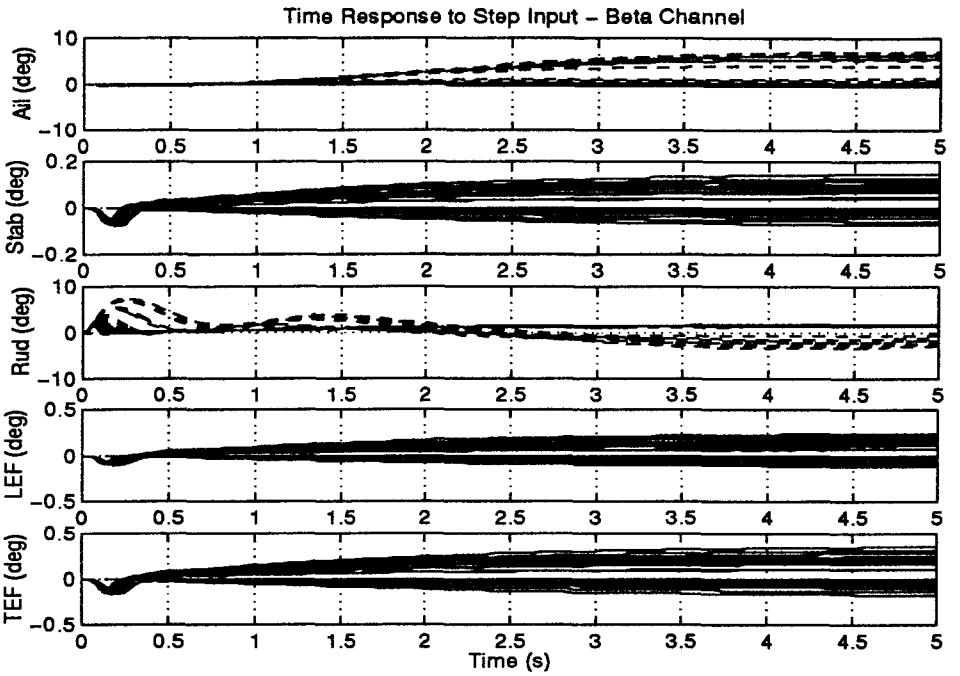

Figure 5.13 Time Response to Unit Step Input β Channel - Design 2 (2 of 2)

The time to bank 90° simulation results (Fig. 5.14 and Fig. 5.15) show that for the high $\bar{q}$ plants Level 1 military specifications are met. The low $\bar{q}$ plants reach a lower bank angle than in the first design, but again this is to be expected since only ailerons and rudders are used for roll control. The benefit of this design is that none of the plants obtain a sideslip angle greater than 6° as specified in MIL-STD 1797A. The commanded signal required to meet the given specifications is p_{cmd} = 145 deg/sec, which is 10 deg/sec lower than that required in Design 1. The benefit of this reduction is that the control surfaces come out of rate saturation earlier and this translates to a greater potential maximum bank angle obtainable in one second than in Design 1.

Due to the reduced β cross-coupling effects from roll rate commands and the shorter time spent in rate saturation, the second design is superior to the first design.

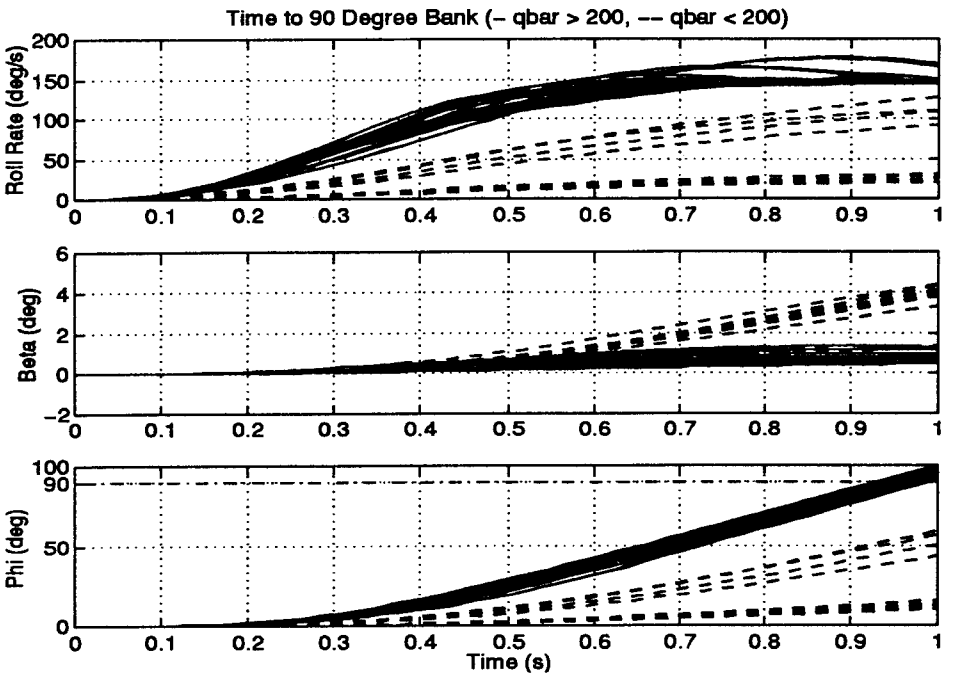

Figure 5.14 Time to Bank 90° - Design 2 (1 of 2)

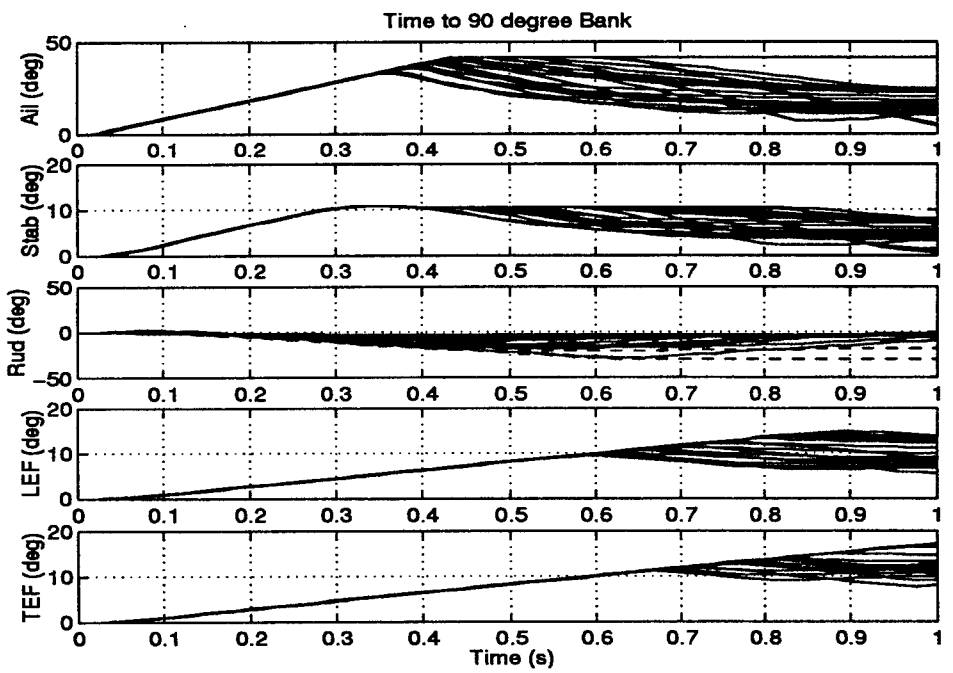

Figure 5.15 Time to Bank 90° - Design 2 (2 of 2)

5.4 Design 3

Both of the first two designs concentrate only on meeting military specifications. The third design attempts to reduce the wing loads experienced during rolling maneuvers in addition to meeting military specifications. This is done by designing a weighting matrix that uses the trailing edge flaps to reduce the wing loads while using the leading edge flaps and ailerons to generate roll control power. The compensators and pre-filters generated based on this concept are shown in Eq. (5.3).

$$G_p = \frac{0.38(s+4.1)}{s} \qquad G_\beta = \frac{130(s+1.1)(s+2.5)}{s(s+5)}$$
$$F_p = \frac{4}{(s+4)} \qquad F_\beta = \frac{0.5}{(s+0.5)} \tag{5.3}$$

The time responses to a unit step roll rate command for this design are shown in Fig. 5.16 and Fig. 5.17. These results are very similar to those seen in the first two designs. All of the high $\bar{q}$ plants and some of the low $\bar{q}$ plants demonstrate the desired settling time of 4 seconds. Like all of the previous designs, the flight conditions with high trim angles of attack have relatively large overshoots which are quickly damped out, but the settling times are longer than the desired time. One improvement in Design 3 over the other designs is that the sideslip cross-coupling is reduced even further than either of the previous designs. This is a direct result of using the trailing edge flaps in the opposite direction of the other wing control surfaces. The control surface time histories (Fig. 5.17) show that larger deflections than in the first two designs are needed to generate the same step response. This is again caused by the trailing edge flap's generation of a negative rolling moment which must be compensated for by slightly increasing the deflections of the remaining control surfaces. Overall, the time responses in this design to a unit step roll rate command are acceptable; also, one should not forget the load alleviation benefits of this design.

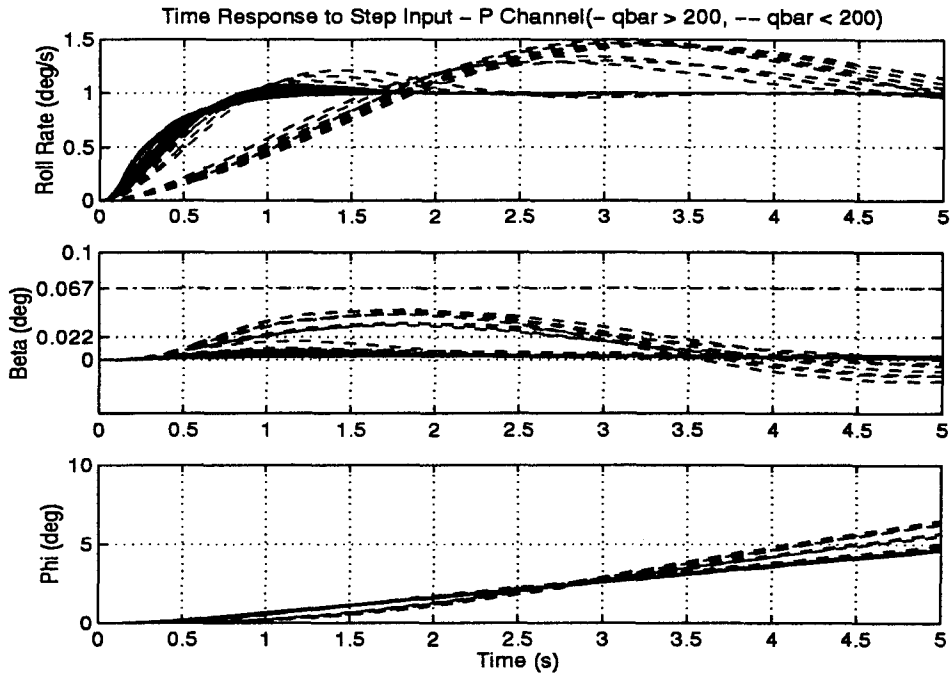

Figure 5.16 Time Response to Unit Step Input p Channel - Design 3 (1 of 2)

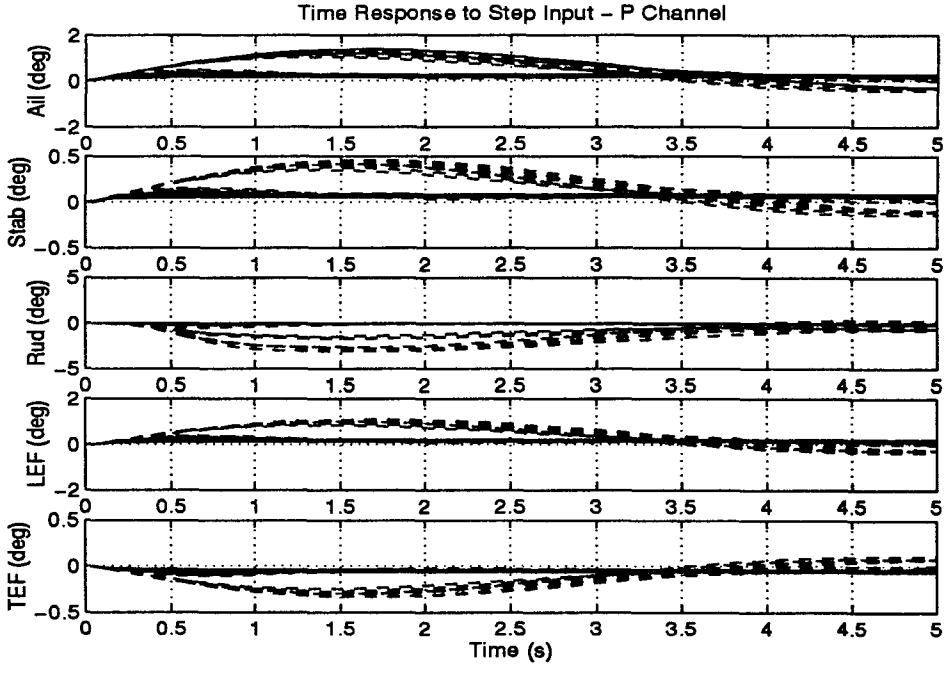

Figure 5.17 Time Response to Unit Step Input p Channel - Design 3 (2 of 2)

The time histories generated by a unit step β command are shown in Fig. 5.18 and Fig. 5.19. These results are again very similar to those seen in the first two designs. The only real difference is that larger surface deflections are needed to produce the desired results for the low $\bar{q}$ plants. However, as stated in the previous designs, since β tracking is not often attempted in high angle of attack flight, these time responses are acceptable.

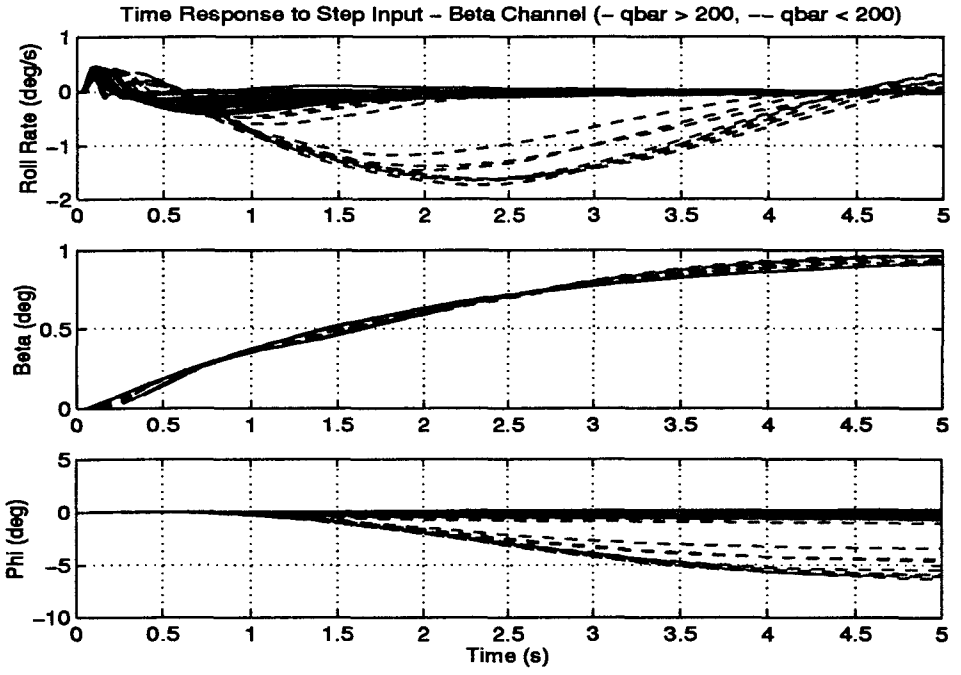

Figure 5.18 Time Response to Unit Step Input β Channel - Design 3 (1 of 2)

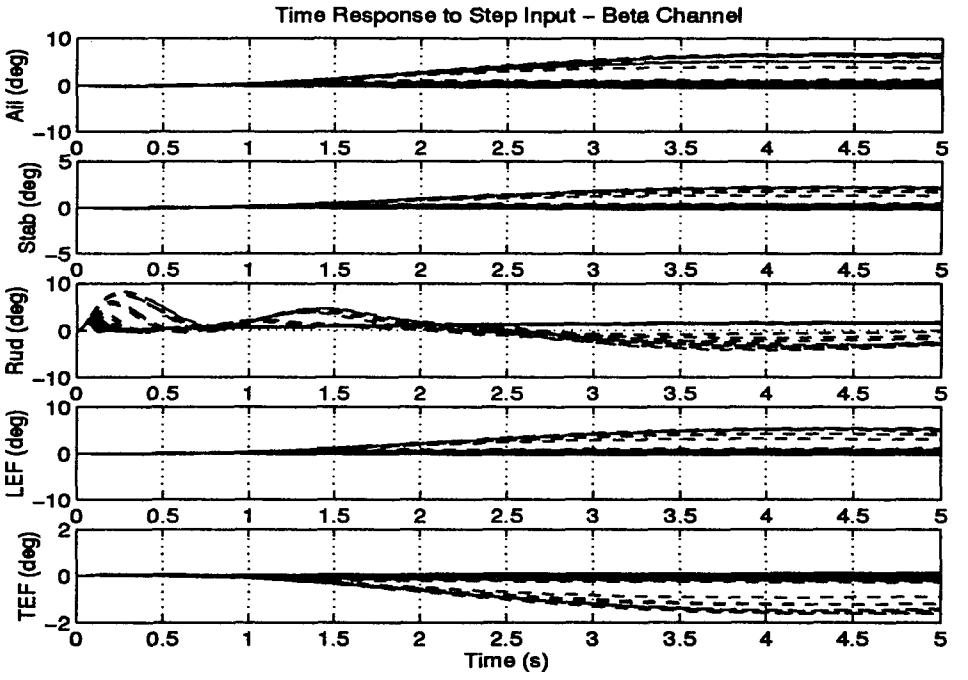

Figure 5.19 Time Response to Unit Step Input β Channel - Design 3 (2 of 2)

In determining the time to bank 90°, a roll rate step command of 150 deg/sec is initially given. The results of this operation are shown in Fig. 5.20 and Fig. 5.21. Using this command signal only a couple of the plants are able to reach a 90° bank angle in one second. Looking at the time histories of the control surfaces it is evident that increasing the roll rate command won't increase the number of plants that meet the military specification since all of the control surfaces except the rudders are saturated over the entire one second time range. These time responses demonstrate the severe restrictions that the actuator rate limits place on the F-18's roll performance.

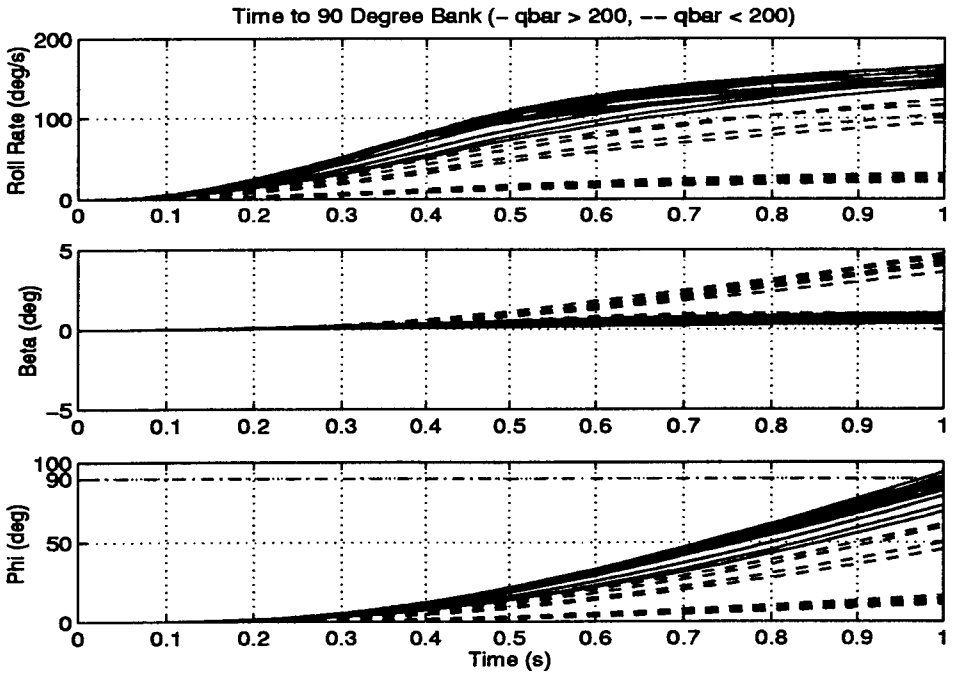

Figure 5.20 Time to Bank 90° - Design 3 (1 of 2)

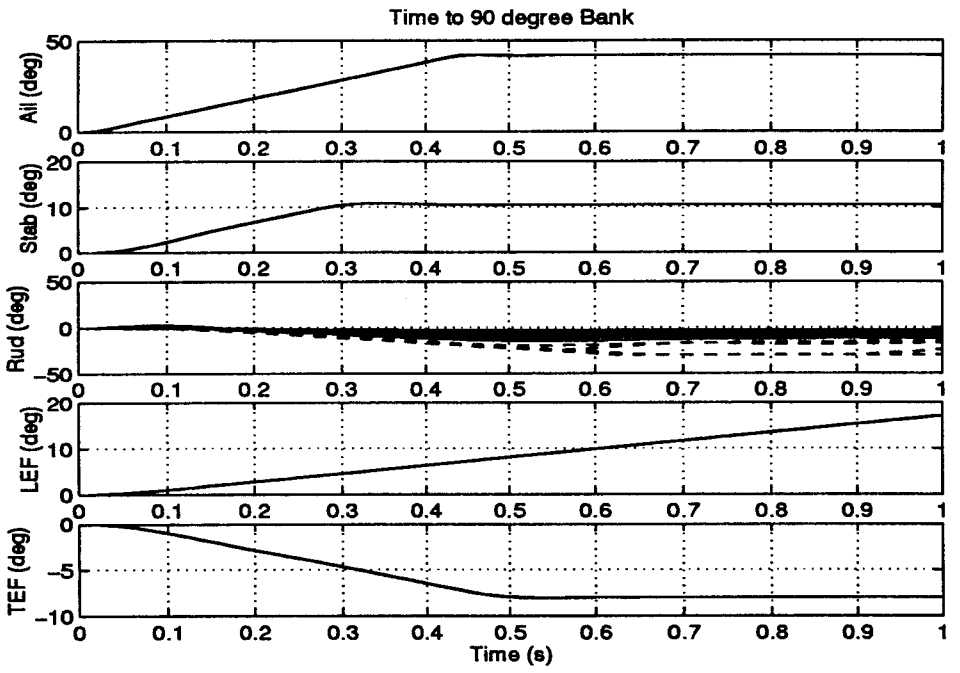

Figure 5.21 Time to Bank 90° - Design 3 (2 of 2)

One major problem with attempting to apply the load alleviation concept to the F-18 is that the actuator rate limits on the leading edge and trailing edge flaps are extremely low (18 and 15 deg/sec respectively.) Indeed, the flaps were not meant to be primary control surfaces. Thus, although the leading edge flaps are available to create roll control power, they deflect very slowly and do not provide enough roll control power fast enough to be of use in difficult tracking tasks. Based on the knowledge that faster actuators are available, the rate limits are removed from the simulation to determine the time responses as an academic problem. Without the rate limits, a roll rate command of 170 deg/sec is used to determine the bank angle reached in one second (Fig. 5.22 and Fig. 5.23). These time responses show that most of the high $\bar{q}$ plants are capable of reaching a 90° bank angle in one second. Although the performance in Design 3 is slightly degraded, there are great benefits achieved by reducing the wing bending and torsion moments. Since the maximum load limits used in determining the weighting matrix were not based on actual limits (this data was unavailable), with additional information, a more reasonable design could be developed.

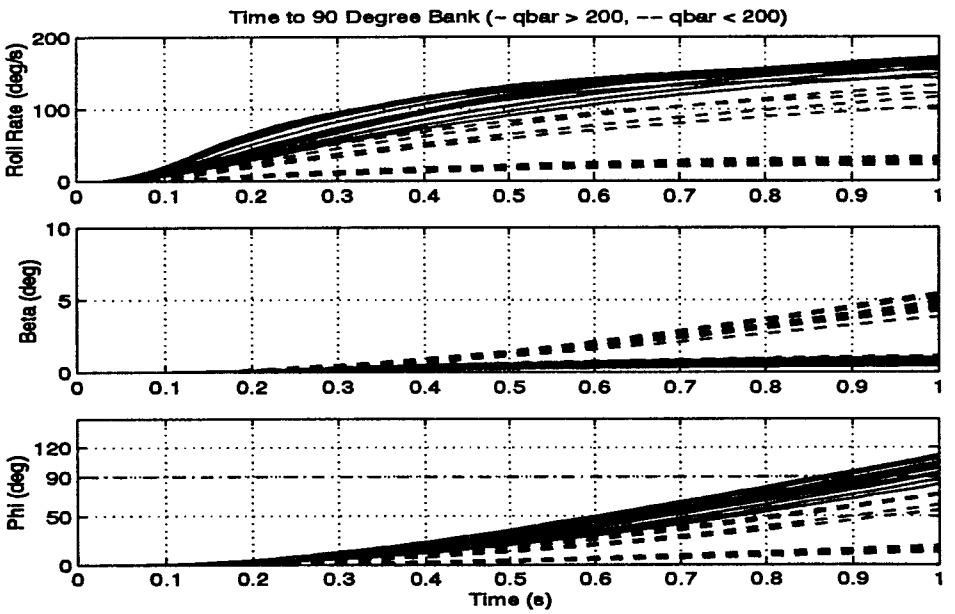

Figure 5.22 Time to Bank 90° - Design 3 with no Rate Limits (1 of 2)

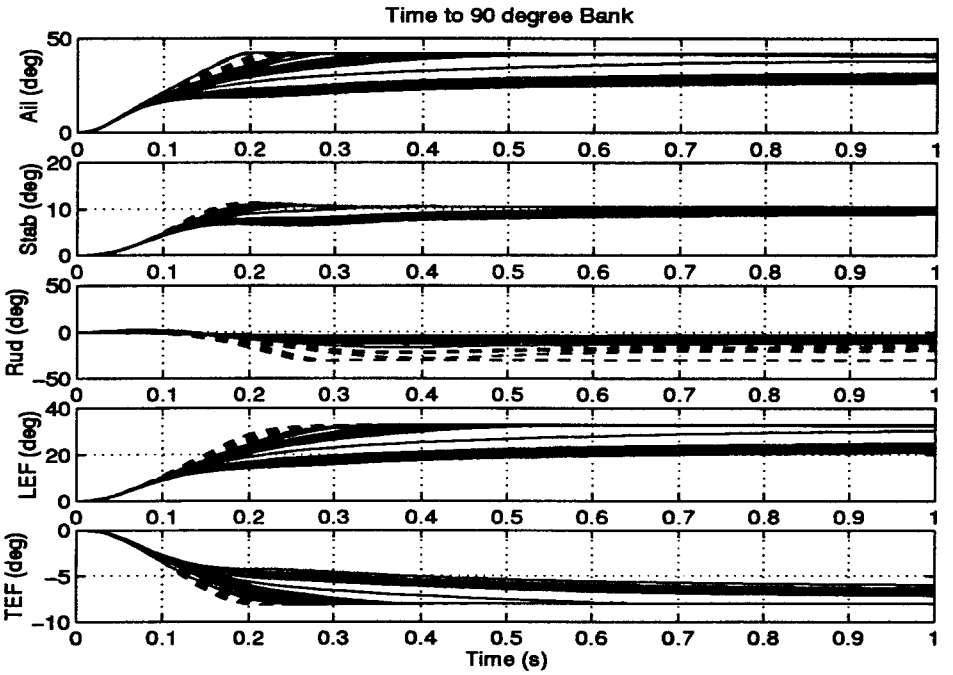

Figure 5.23 Time to Bank 90° - Design 3 with no Rate Limits (2 of 2)

5.5 Comparison of Designs

In order to compare the designs in a more systematic fashion, the maximum wing loads are examined for a unit step roll rate command. A unit step is used so that the position and rate limits are not a factor. This comparison is done for one flight condition in the middle of the flight envelope, altitude = 10,000 ft Mach = 0.7. The maximum control surface deflections reached for a unit step roll rate command are shown in Table 5.1.

Control Surface	Design 1	Design 2	Design 3
Aileron	0.1226°	0.1226°	0.2313°
Trailing Edge Flap	0.0970°	0.0970°	−0.0409°

Table 5.1 Maximum Surface Deflection Due to a Unit Step Roll Rate Command

From the data provided by the Structures Division, WL/FIB, for this flight condition the torsion influence coefficients (units are inch pounds per degree) are

	Torsion Load (rad lbs in)	Bending Moment Load (rad lbs in)
Design 1 & 2	29.6	-167.88
Design 3	12.86	-79.73
Percent Change	-56.5%	-52.5%

Table 5.2 Comparison of Wing Torsion and Bending Moment Loads

5134.7 for the ailerons and 10,998 for the trailing edge flap. Likewise, the bending moment influence coefficients are -30,486 for the ailerons and -60,638 for the trailing edge flaps. The values for the maximum wing load determined from these numbers are shown in Table 5.2. Note that the maximum surface positions for design 1 and 2 are the same so their results are combined.

The time histories for a unit step roll rate command, Fig. 5.24 and Fig. 5.25, show that the roll rate and sideslip time responses are nearly identical for all three designs. Thus based on the time response and the wing loading, Design 3 is a superior design.

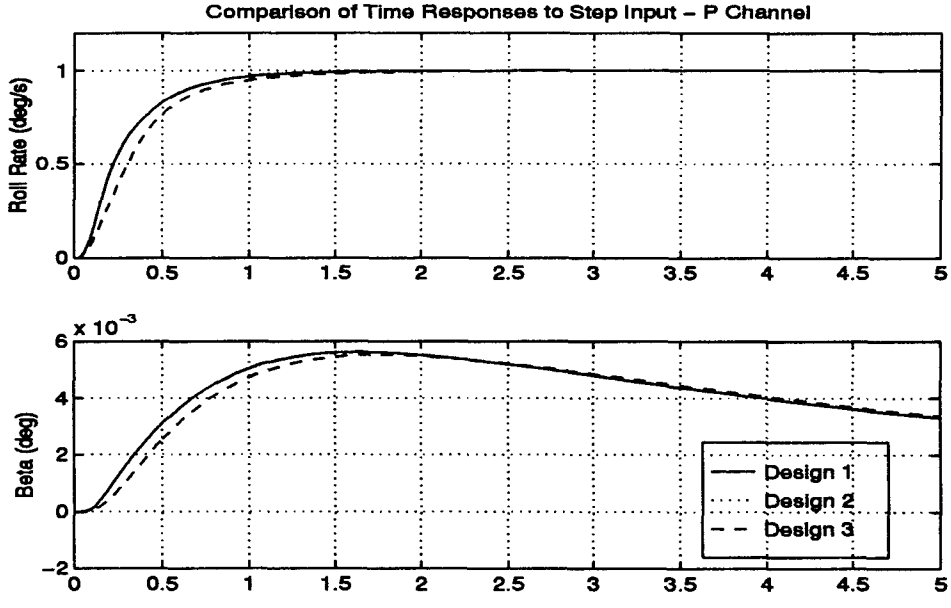

Figure 5.24 Comparison of the Three Designs (1 of 2)

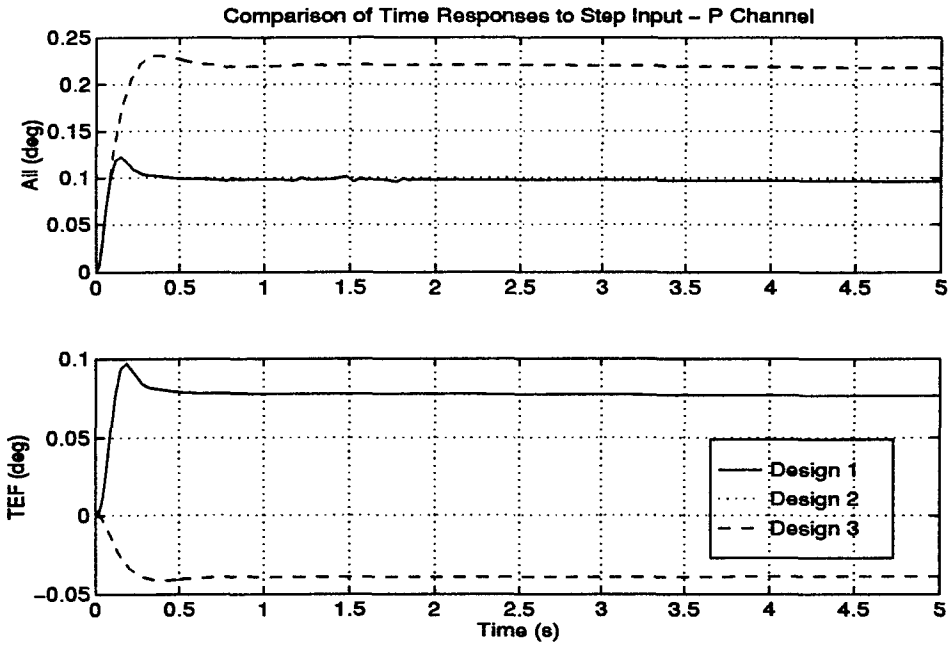

Figure 5.25 Comparison of the Three Designs (2 of 2)

Additional comparisons made between the three designs are shown in Table 5.3. Looking at the DC gains, Design 3 has the largest DC gain for the β channel compensator. The larger gain results in a lower cross-coupling effect from a roll rate command, a highly desirable attribute for flight control system designs. In addition, although the DC gain for the p channel is lower in Design 3 than in Design 2, Design 3 only uses a first-order compensator. Looking at all of these factors combined, Design 3 is judged to be the best flight control system.

	Design 1	Design 2	Design 3
G_p	$\frac{0.4(s+3)}{s}$	$\frac{0.4(s+2)(s+10)}{s(s+5)}$	$\frac{0.38(s+4.1)}{s}$
DC Gain (G_p)	1.20	1.98	1.56
G_β	$\frac{145(s+0.8)(s+5)}{s(s+10)}$	$\frac{135(s+0.9)(s+3)}{s(s+7)}$	$\frac{130(s+1.1)(s+2.5)}{s(s+5)}$
DC Gain (G_β)	58.0	52.1	71.5
F_p	$\frac{5}{s+5}$	$\frac{4}{s+4}$	$\frac{4}{s+4}$
F_β	$\frac{0.5}{s+0.5}$	$\frac{0.5}{s+0.5}$	$\frac{0.5}{s+0.5}$

Table 5.3 Comparison of Compensator Designs

5.6 Design Summary

The block diagram for the complete lateral/directional flight control system is shown in Fig. 5.26. Measurements of yaw rate, roll rate, sideslip and dynamic pressure are needed for this design. The values of the weighting matrix are dependent on flight condition and thus must be scheduled.

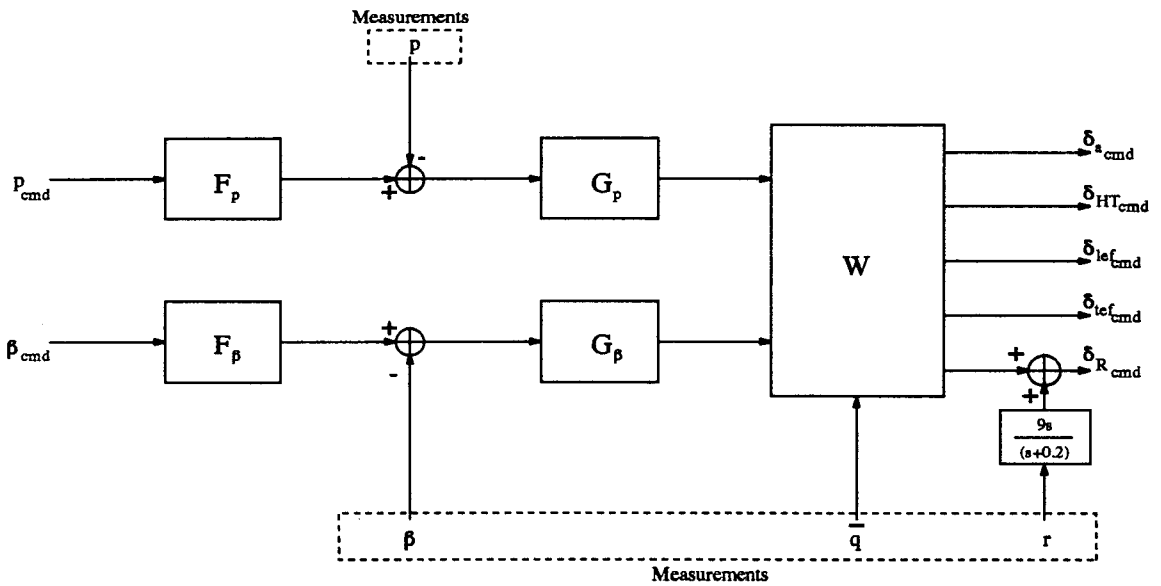

Figure 5.26 Final Lateral/Directional Flight Control System Block Diagram

VI. Conclusions and Recommendations

6.1 Summary

This thesis research successfully develops three lateral/directional flight control systems for the F-18. As a first step, performance baselines for roll rate and sideslip are established based on specifications found in MIL-STD 1797A. Following this, a set of linear time-invariant plants which encompasses the subsonic flight envelope are generated from the WL/FIG F-18 HARV simulation. These LTI plants are generated for thirty-one flight conditions covering the sub-sonic flight envelope of the F-18, including high angle of attack and high $\bar{q}$ regions.

Using the thirty-one plants, three separate QFT designs are performed to obtain viable lateral/directional flight control systems. The difference in the setup of the three designs lies in the selection of the weighting matrices. For the first design, the weighting matrix is chosen so that maximum deflections are reached simultaneously for all wing control surfaces. The weighting matrix for the second design is identical to the first design for high $\bar{q}$ plants. For the weighting matrix of the low $\bar{q}$ plants only the ailerons and rudders are used for lateral/directional control. In the third design, the weighting matrix is designed using optimization to alleviate wing loads. This is accomplished by commanding the trailing edge flaps in the opposite direction of all the other wing control surfaces. An optimal weighting matrix is then determined based on the structural influence coefficients of the wing surfaces, to reduce wing loads while maximizing roll control power.

Using these weighting matrices, the QFT method is employed and the effective plants and QFT Q matrices are generated. From the Q matrices, the MIMO plant is decomposed into four MISO equivalent plants and the compensators and pre-filters are designed. The final designs are validated in the frequency domain and then tested in time domain simulations. Both frequency and time domain validations show that all three designs meet military specifications for high $\bar{q}$ plants. In order

to determine a superior design, the three designs are evaluated for maximum wing loading at a single flight condition. From this analysis the third design is deemed the best since it provides the same roll control while alleviating the aerodynamically induced structural loads on the wing surfaces.

6.2 Conclusions

This thesis demonstrates the ability of the QFT robust control design technique to generate flight control systems for aircraft with flexible wings. The variability of the aircraft dynamics is easily incorporated into the design so the final control laws are indeed robust. The time responses for the high $\bar{q}$ plants easily meet the military specifications for roll rate settling time and time to bank to 90°. While some of the low $\bar{q}$ plants meet the roll rate settling time, none of the high angle of attack plants met the time to bank 90° specification. However, from practical experience, roll rates of 90 deg/sec are not to be expected of in high angle of attack flight.

The QFT design techniques yield compensators of second order or less. This is a valuable result since fewer poles translate directly to a shorter delay time in a digital controller. In addition, due to the graphical design techniques, trade-offs between compensator order and performance are easy to make. The low order compensators designed in this thesis research are shown to be capable of meeting the given specifications.

A more sophisticated design incorporating load alleviation concepts was successfully designed using QFT. It has been shown that QFT is capable of incorporating optimization-based control concepts and still provide all of the benefits of QFT's transparency using its graphical appeal. Overall, this thesis shows the versatility and effectiveness of QFT in designing robust MIMO flight control designs.

This thesis research showed that given multiple wing control surfaces it is possible to reduce the wing loads while maintaining adequate roll control power. Load alleviation is an important criterion to meet for flexible wings to be used success-

fully. An additional benefit of this research is that it showed that the performance of the F-18 is limited most severely by the actuator rate limits. Higher performance actuators could greatly improve the capabilities of the F-18.

6.3 Recommendations

The load alleviation methods attempted in this thesis are somewhat limited due to the lack of available data for the wing control surfaces. To better optimize the load alleviation, while still providing adequate roll control, data for the leading edge flaps structural influence coefficients as well as the maximum load limits for the wings need to be determined. With this data, an extra degree of freedom (leading edge flap deflection) is available for the optimization process. In addition, with better data for the maximum load limits, a more realistic design can be generated.

With the load alleviation control laws designed in this thesis, the major problem with performance is due to the rate limits of the wing control surface actuators. Dynamic load alleviation requires actuators that meet the same specifications as those used for the primary surfaces. Load alleviation control turns the otherwise secondary control surfaces, e.g., the leading edge flaps and trailing edge flaps, into primary control surfaces. To demonstrate QFT's effectiveness in the generation of control laws for the load alleviation concept a design should be attempted on an aircraft with faster actuators. As a suggestion, the Active Flexible Wing designed by NASA and Rockwell could be used as the test bed. Advantages of the AFW include: data being available for the system dynamics; four control surfaces per wing; and faster actuators. The Active Flexible Wing program was specifically designed to test load alleviation control laws and this would be a good chance to demonstrate all of the capabilities of QFT.

The designs generated in this thesis are tested on a mostly linear continuous time simulation. As a further validation of the designs, they should be tested on the full non-linear F-18 HARV simulation program. This would require that the

design be transformed into the $\mathcal{Z}$-domain to generate discrete control laws. Testing these designs on the HARV simulation would provide a better evaluation of the capabilities of the proposed designs. In addition, and perhaps prior to testing on the HARV simulation, a longitudinal channel should be designed using QFT so that the complete flight control system for the aircraft could be tested.

Another area for further research would be to generate a separate control law for the low $\bar{q}$ plants. In the high angle of attack flight regions, the assumptions used to make the linearizations are not as valid. This area could be treated as a separate region and a compensator designed to handle the specific problems of high angle of attack flight.

Appendix A. Plant Transfer Functions

This appendix lists the **A** and **B** matrices of all the plants (flight conditions) used in this research.

Plant #1

$$A = \begin{bmatrix} -0.767193 & 0.693031 & -7.482590 & -0.000030 \\ 0.008330 & -0.076456 & -0.003191 & 0.000785 \\ 0.328652 & -0.944591 & -0.092365 & 0.125834 \\ 1.000000 & 0.347772 & 0.000000 & 0.000000 \end{bmatrix}$$

$$B = \begin{bmatrix} 1.489423 & 1.539380 & 0.385794 & 0.000001 & 1.855690 \\ -0.062534 & 0.000899 & -0.282128 & -0.000012 & -0.020904 \\ 0.000043 & -0.001051 & 0.014396 & 0.000000 & 0.000000 \\ 0.000000 & 0.000000 & 0.000000 & 0.000000 & 0.000000 \end{bmatrix}$$

Plant #2

$$A = \begin{bmatrix} -0.504209 & 0.570566 & -6.401240 & -0.000045 \\ 0.011945 & -0.067203 & 0.193798 & 0.001179 \\ 0.401117 & -0.916899 & -0.060497 & 0.111324 \\ 1.000000 & 0.437775 & 0.000000 & 0.000000 \end{bmatrix}$$

$$B = \begin{bmatrix} 1.127680 & 1.124970 & 0.154353 & 0.000001 & 1.612860 \\ -0.060647 & -0.041704 & -0.189488 & -0.000009 & -0.018168 \\ 0.002030 & 0.000617 & 0.008911 & 0.000000 & 0.000000 \\ 0.000000 & 0.000000 & 0.000000 & 0.000000 & 0.000000 \end{bmatrix}$$

Plant #3

$$A = \begin{bmatrix} -0.466365 & 0.475063 & -6.904790 & 0.000000 \\ 0.009708 & -0.061089 & 0.307424 & 0.000000 \\ 0.418876 & -0.908583 & -0.041416 & 0.083661 \\ 1.000000 & 0.461280 & 0.000000 & 0.000000 \end{bmatrix}$$

$$B = \begin{bmatrix} 1.099182 & 1.372970 & 0.114612 & 0.000000 & 1.577030 \\ -0.071666 & -0.023515 & -0.180497 & 0.000000 & -0.017756 \\ 0.001855 & -0.000034 & 0.006586 & 0.000000 & 0.000000 \\ 0.000000 & 0.000000 & 0.000000 & 0.000000 & 0.000000 \end{bmatrix}$$

Plant #4

$$A = \begin{bmatrix} -0.346492 & 0.398999 & -6.918330 & 0.000000 \\ 0.006992 & -0.054560 & 0.254572 & 0.000000 \\ 0.411626 & -0.911653 & -0.021593 & 0.067048 \\ 1.000000 & 0.451683 & 0.000000 & 0.000000 \end{bmatrix}$$

$$B = \begin{bmatrix} 1.139407 & 1.284330 & 0.110959 & 0.000000 & 1.536420 \\ -0.074070 & -0.025443 & -0.183071 & 0.000000 & -0.017299 \\ 0.001253 & -0.000205 & 0.005452 & 0.000000 & 0.000000 \\ 0.000000 & 0.000000 & 0.000000 & 0.000000 & 0.000000 \end{bmatrix}$$

Plant #5

$$A = \begin{bmatrix} -0.770966 & 0.478858 & -8.635980 & -0.000009 \\ -0.003640 & -0.059293 & 1.444680 & 0.000228 \\ 0.182444 & -0.982677 & -0.077940 & 0.050078 \\ 1.000000 & 0.185526 & 0.000000 & 0.000000 \end{bmatrix}$$

$$B = \begin{bmatrix} 4.724071 & 3.139900 & 0.912888 & 0.000001 & 3.887220 \\ -0.087435 & 0.072643 & -0.680775 & -0.000003 & -0.043770 \\ -0.000984 & -0.002329 & 0.015093 & 0.000000 & 0.000000 \\ 0.000000 & 0.000000 & 0.000000 & 0.000000 & 0.000000 \end{bmatrix}$$

Plant #6

$$A = \begin{bmatrix} -1.657750 & 0.367758 & -12.485400 & 0.000001 \\ -0.007509 & -0.079799 & 2.419500 & -0.000025 \\ 0.061462 & -0.997704 & -0.101286 & 0.036715 \\ 1.000000 & 0.061667 & 0.000000 & 0.000000 \end{bmatrix}$$

$$B = \begin{bmatrix} 8.599120 & 7.455550 & 2.006260 & -0.000000 & 9.855070 \\ -0.012645 & 0.068786 & -1.412490 & 0.000000 & -0.110961 \\ -0.002206 & -0.004015 & 0.020763 & 0.000000 & -0.000000 \\ 0.000000 & 0.000000 & 0.000000 & 0.000000 & 0.000000 \end{bmatrix}$$

Plant #7

$$A = \begin{bmatrix} -2.679530 & 0.426341 & -16.104100 & -0.000017 \\ -0.009829 & -0.121269 & 3.746450 & 0.000460 \\ 0.041996 & -0.998550 & -0.154317 & 0.035796 \\ 1.000000 & 0.042165 & 0.000000 & 0.000000 \end{bmatrix}$$

$$B = \begin{bmatrix} 11.732200 & 12.079800 & 3.498760 & 0.000000 & 13.544600 \\ -0.017743 & 0.054389 & -2.191630 & -0.000004 & -0.152507 \\ -0.002942 & -0.005963 & 0.031243 & 0.000000 & 0.000000 \\ 0.000000 & 0.000000 & 0.000000 & 0.000000 & 0.000000 \end{bmatrix}$$

Plant #8

$$A = \begin{bmatrix} -5.191480 & 0.552692 & -17.257900 & 0.000034 \\ -0.015176 & -0.214070 & 6.755080 & -0.000900 \\ 0.026656 & -0.998759 & -0.270667 & 0.033750 \\ 1.000000 & 0.026869 & 0.000000 & 0.000000 \end{bmatrix}$$

$$B = \begin{bmatrix} 13.417100 & 23.419600 & 6.527620 & 8.333800 & 15.439200 \\ -0.085674 & -0.037453 & -3.769390 & -0.093822 & -0.173826 \\ -0.001591 & -0.009880 & 0.050427 & -0.000000 & -0.000000 \\ 0.000000 & 0.000000 & 0.000000 & 0.000000 & 0.000000 \end{bmatrix}$$

Plant #9

$$A = \begin{bmatrix} -6.412340 & 0.609874 & -14.451900 & -0.000027 \\ -0.013568 & -0.252544 & 8.061670 & 0.000699 \\ 0.023659 & -0.998708 & -0.321395 & 0.033136 \\ 1.000000 & 0.023904 & 0.000000 & 0.000000 \end{bmatrix}$$

$$B = \begin{bmatrix} 10.877100 & 28.740200 & 7.711370 & 21.804500 & 13.613500 \\ -0.122479 & -0.099846 & -4.387240 & -0.245509 & -0.153283 \\ 0.000000 & -0.011469 & 0.057570 & 0.000000 & 0.000000 \\ 0.000000 & 0.000000 & 0.000000 & 0.000000 & 0.000000 \end{bmatrix}$$

Plant #10

$$A = \begin{bmatrix} -7.937370 & 0.668865 & -8.051080 & -0.000042 \\ -0.012296 & -0.297995 & 9.533600 & 0.001115 \\ 0.020906 & -0.998633 & -0.381306 & 0.032558 \\ 1.000000 & 0.021185 & 0.000000 & 0.000000 \end{bmatrix}$$

$$B = \begin{bmatrix} 6.631840 & 35.099500 & 8.901820 & 43.066500 & 7.933980 \\ -0.074699 & -0.163004 & -4.997100 & -0.484918 & -0.089347 \\ 0.000000 & -0.013215 & 0.064367 & 0.000000 & 0.000000 \\ 0.000000 & 0.000000 & 0.000000 & 0.000000 & 0.000000 \end{bmatrix}$$

Plant #11

$$A = \begin{bmatrix} -3.547520 & 0.733331 & -14.599700 & -0.000019 \\ -0.014746 & -0.190622 & 4.532750 & 0.000490 \\ 0.043383 & -0.997810 & -0.280585 & 0.048805 \\ 1.000000 & 0.043427 & 0.000000 & 0.000000 \end{bmatrix}$$

$$B = \begin{bmatrix} 14.794500 & 15.275300 & 4.415400 & 0.000000 & 15.372300 \\ -0.210880 & 0.110922 & -2.709220 & -0.000004 & -0.173085 \\ -0.003891 & -0.010900 & 0.056915 & 0.000000 & 0.000000 \\ 0.000000 & 0.000000 & 0.000000 & 0.000000 & 0.000000 \end{bmatrix}$$

Plant #12

$$A = \begin{bmatrix} -2.321160 & 0.751135 & -11.232000 & 0.000006 \\ -0.017249 & -0.127734 & 2.116700 & -0.000149 \\ 0.090188 & -0.994456 & -0.177932 & 0.072982 \\ 1.000000 & 0.090421 & 0.000000 & 0.000000 \end{bmatrix}$$

$$B = \begin{bmatrix} 8.428221 & 6.810860 & 2.137730 & -0.000000 & 7.384790 \\ -0.154252 & 0.106494 & -1.281360 & 0.000001 & -0.083147 \\ -0.002313 & -0.006517 & 0.039779 & -0.000000 & -0.000000 \\ 0.000000 & 0.000000 & 0.000000 & 0.000000 & 0.000000 \end{bmatrix}$$

Plant #13

$$A = \begin{bmatrix} -0.772093 & 0.662469 & -7.238150 & 0.000027 \\ 0.004162 & -0.074547 & 0.139374 & -0.000697 \\ 0.310969 & -0.950237 & -0.083190 & 0.113428 \\ 1.000000 & 0.326987 & 0.000000 & 0.000000 \end{bmatrix}$$

$$B = \begin{bmatrix} 1.776601 & 1.646040 & 0.437061 & -0.000001 & 1.946310 \\ -0.066948 & 0.006905 & -0.313196 & 0.000009 & -0.021906 \\ -0.000239 & -0.001093 & 0.014634 & -0.000000 & -0.000000 \\ 0.000000 & 0.000000 & 0.000000 & 0.000000 & 0.000000 \end{bmatrix}$$

Plant #14

$$A = \begin{bmatrix} -6.698930 & 0.623709 & -13.561800 & -0.000005 \\ -0.014270 & -0.262007 & 8.347630 & 0.000129 \\ 0.023206 & -0.998690 & -0.332608 & 0.033020 \\ 1.000000 & 0.023455 & 0.000000 & 0.000000 \end{bmatrix}$$

$$B = \begin{bmatrix} 10.189500 & 29.887500 & 7.942120 & 25.393800 & 12.689300 \\ -0.114728 & -0.106857 & -4.508450 & -0.285919 & -0.142875 \\ 0.000000 & -0.011877 & 0.058940 & 0.000000 & 0.000000 \\ 0.000000 & 0.000000 & 0.000000 & 0.000000 & 0.000000 \end{bmatrix}$$

Plant #15

$$A = \begin{bmatrix} -0.602130 & 0.559692 & -7.607640 & 0.000013 \\ 0.005309 & -0.063895 & -0.090715 & -0.000330 \\ 0.333557 & -0.942832 & -0.065161 & 0.097321 \\ 1.000000 & 0.353687 & 0.000000 & 0.000000 \end{bmatrix}$$

$$B = \begin{bmatrix} 1.556402 & 1.506170 & 0.355953 & -0.000000 & 1.828420 \\ -0.065371 & -0.000662 & -0.275692 & 0.000003 & -0.020585 \\ 0.000160 & -0.000971 & 0.011047 & -0.000000 & -0.000000 \\ 0.000000 & 0.000000 & 0.000000 & 0.000000 & 0.000000 \end{bmatrix}$$

Plant #16

$$A = \begin{bmatrix} -0.435486 & 0.492586 & -6.312270 & -0.000051 \\ 0.009854 & -0.059443 & 0.145268 & 0.001339 \\ 0.395051 & -0.919203 & -0.047570 & 0.093597 \\ 1.000000 & 0.429979 & 0.000000 & 0.000000 \end{bmatrix}$$

$$B = \begin{bmatrix} 1.150995 & 1.163410 & 0.160559 & -0.000001 & 1.580600 \\ -0.065911 & -0.032268 & -0.192323 & -0.000010 & -0.017805 \\ 0.001622 & 0.000171 & 0.007668 & 0.000000 & 0.000000 \\ 0.000000 & 0.000000 & 0.000000 & 0.000000 & 0.000000 \end{bmatrix}$$

Plant #17

$$A = \begin{bmatrix} -0.377513 & 0.431523 & -6.751030 & 0.000009 \\ 0.006366 & -0.055757 & 0.108739 & -0.000225 \\ 0.390079 & -0.921092 & -0.032976 & 0.075867 \\ 1.000000 & 0.423614 & 0.000000 & 0.000000 \end{bmatrix}$$

$$B = \begin{bmatrix} 1.228928 & 1.216340 & 0.163463 & -0.000000 & 1.584310 \\ -0.069474 & -0.026706 & -0.200568 & 0.000002 & -0.017837 \\ 0.001126 & -0.000148 & 0.006590 & -0.000000 & -0.000000 \\ 0.000000 & 0.000000 & 0.000000 & 0.000000 & 0.000000 \end{bmatrix}$$

Plant #18

$$A = \begin{bmatrix} -2.133280 & 0.479560 & 1.229700 & -0.000017 \\ -0.008255 & -0.100359 & 2.951160 & 0.000458 \\ 0.064131 & -0.997432 & -0.134429 & 0.036542 \\ 1.000000 & 0.064377 & 0.000000 & 0.000000 \end{bmatrix}$$

$$B = \begin{bmatrix} 10.072300 & 8.611120 & 2.445080 & 0.000001 & 11.625300 \\ -0.020420 & 0.189181 & -1.752000 & -0.000005 & -0.130898 \\ -0.002422 & -0.006190 & 0.025638 & 0.000000 & 0.000000 \\ 0.000000 & 0.000000 & 0.000000 & 0.000000 & 0.000000 \end{bmatrix}$$

Plant #19

$$A = \begin{bmatrix} -3.356480 & 0.456339 & -17.275900 & 0.000016 \\ -0.012417 & -0.148149 & 4.600940 & -0.000417 \\ 0.034922 & -0.998729 & -0.187455 & 0.035076 \\ 1.000000 & 0.035095 & 0.000000 & 0.000000 \end{bmatrix}$$

$$B = \begin{bmatrix} 13.223900 & 15.229200 & 4.423020 & -0.000000 & 14.943300 \\ -0.033540 & 0.031897 & -2.665650 & 0.000003 & -0.168249 \\ -0.002913 & -0.007074 & 0.037161 & -0.000000 & -0.000000 \\ 0.000000 & 0.000000 & 0.000000 & 0.000000 & 0.000000 \end{bmatrix}$$

Plant #20

$$A = \begin{bmatrix} -4.162900 & 0.501764 & -17.933300 & 0.000009 \\ -0.013486 & -0.178128 & 5.599170 & -0.000232 \\ 0.030378 & -0.998774 & -0.225973 & 0.034393 \\ 1.000000 & 0.030571 & 0.000000 & 0.000000 \end{bmatrix}$$

$$B = \begin{bmatrix} 14.559800 & 18.947000 & 5.439060 & 0.108689 & 16.032400 \\ -0.059306 & 0.005898 & -3.200940 & -0.001222 & -0.180513 \\ -0.002593 & -0.008388 & 0.043693 & -0.000000 & -0.000000 \\ 0.000000 & 0.000000 & 0.000000 & 0.000000 & 0.000000 \end{bmatrix}$$

Plant #21

$$A = \begin{bmatrix} -6.993410 & 0.632661 & -12.384400 & 0.000040 \\ -0.015491 & -0.272210 & 8.633030 & -0.001063 \\ 0.022475 & -0.998677 & -0.344471 & 0.032907 \\ 1.000000 & 0.022727 & 0.000000 & 0.000000 \end{bmatrix}$$

$$B = \begin{bmatrix} 9.423680 & 31.212400 & 8.185770 & 29.279200 & 11.661900 \\ -0.106076 & -0.126463 & -4.630050 & -0.329647 & -0.131290 \\ -0.000000 & -0.012106 & 0.060303 & -0.000000 & -0.000000 \\ 0.000000 & 0.000000 & 0.000000 & 0.000000 & 0.000000 \end{bmatrix}$$

Plant #22

$$A = \begin{bmatrix} -7.293460 & 0.649836 & -11.338700 & -0.000006 \\ -0.013786 & -0.279965 & 8.928130 & 0.000162 \\ 0.022257 & -0.998657 & -0.355629 & 0.032788 \\ 1.000000 & 0.022520 & 0.000000 & 0.000000 \end{bmatrix}$$

$$B = \begin{bmatrix} 8.571790 & 32.308700 & 8.403030 & 33.435900 & 10.523800 \\ -0.096516 & -0.126665 & -4.748090 & -0.376466 & -0.118493 \\ 0.000000 & -0.012634 & 0.061614 & 0.000000 & 0.000000 \\ 0.000000 & 0.000000 & 0.000000 & 0.000000 & 0.000000 \end{bmatrix}$$

Plant #23

$$A = \begin{bmatrix} -7.608660 & 0.663813 & -9.999990 & 0.000008 \\ -0.014163 & -0.289793 & 9.229860 & -0.000201 \\ 0.021826 & -0.998637 & -0.367673 & 0.032674 \\ 1.000000 & 0.022094 & 0.000000 & 0.000000 \end{bmatrix}$$

$$B = \begin{bmatrix} 7.643750 & 33.581700 & 8.638010 & 38.031700 & 9.284630 \\ -0.086061 & -0.136927 & -4.870640 & -0.428210 & -0.104536 \\ -0.000000 & -0.013036 & 0.062973 & -0.000000 & -0.000000 \\ 0.000000 & 0.000000 & 0.000000 & 0.000000 & 0.000000 \end{bmatrix}$$

Plant #24

$$A = \begin{bmatrix} -0.995121 & 0.400329 & -7.651290 & 0.000009 \\ -0.005358 & -0.062181 & 1.552800 & -0.000248 \\ 0.111456 & -0.993306 & -0.086868 & 0.047001 \\ 1.000000 & 0.112148 & 0.000000 & 0.000000 \end{bmatrix}$$

$$B = \begin{bmatrix} 5.630787 & 4.282090 & 1.128890 & -0.000000 & 7.468840 \\ -0.052309 & 0.085606 & -0.851678 & 0.000004 & -0.084092 \\ -0.001715 & -0.002789 & 0.017486 & -0.000000 & -0.000000 \\ 0.000000 & 0.000000 & 0.000000 & 0.000000 & 0.000000 \end{bmatrix}$$

Plant #25

$$A = \begin{bmatrix} -1.268920 & 0.450016 & -9.939560 & -0.000012 \\ -0.005910 & -0.076412 & 1.893380 & 0.000304 \\ 0.091665 & -0.995242 & -0.103574 & 0.046882 \\ 1.000000 & 0.092053 & 0.000000 & 0.000000 \end{bmatrix}$$

$$B = \begin{bmatrix} 6.946037 & 5.646620 & 1.513300 & 0.000000 & 9.391930 \\ -0.060705 & 0.090803 & -1.082180 & -0.000004 & -0.105751 \\ -0.002273 & -0.003633 & 0.021997 & 0.000000 & 0.000000 \\ 0.000000 & 0.000000 & 0.000000 & 0.000000 & 0.000000 \end{bmatrix}$$

Plant #26

$$A = \begin{bmatrix} -1.579670 & 0.496914 & -11.792500 & 0.000015 \\ -0.008259 & -0.093529 & 2.332530 & -0.000391 \\ 0.074897 & -0.996560 & -0.126712 & 0.045938 \\ 1.000000 & 0.075109 & 0.000000 & 0.000000 \end{bmatrix}$$

$$B = \begin{bmatrix} 8.462715 & 7.302210 & 1.987610 & -0.000000 & 11.553100 \\ -0.070368 & 0.103484 & -1.362720 & 0.000003 & -0.130078 \\ -0.002854 & -0.004737 & 0.026978 & -0.000000 & -0.000000 \\ 0.000000 & 0.000000 & 0.000000 & 0.000000 & 0.000000 \end{bmatrix}$$

Plant #27

$$A = \begin{bmatrix} -1.955720 & 0.533686 & -13.571600 & -0.000008 \\ -0.009014 & -0.112248 & 2.863420 & 0.000201 \\ 0.061694 & -0.997377 & -0.154567 & 0.045038 \\ 1.000000 & 0.061833 & 0.000000 & 0.000000 \end{bmatrix}$$

$$B = \begin{bmatrix} 10.234204 & 9.256380 & 2.532590 & 0.000000 & 13.871900 \\ -0.082607 & 0.105115 & -1.684430 & -0.000002 & -0.156189 \\ -0.003391 & -0.005909 & 0.032614 & 0.000000 & 0.000000 \\ 0.000000 & 0.000000 & 0.000000 & 0.000000 & 0.000000 \end{bmatrix}$$

Plant #28

$$A = \begin{bmatrix} -2.398220 & 0.566125 & -15.106500 & 0.000001 \\ -0.011005 & -0.134987 & 3.487130 & -0.000026 \\ 0.051480 & -0.997854 & -0.187117 & 0.044181 \\ 1.000000 & 0.051594 & 0.000000 & 0.000000 \end{bmatrix}$$

$$B = \begin{bmatrix} 12.173729 & 11.542000 & 3.158940 & -0.000000 & 16.459700 \\ -0.096871 & 0.099694 & -2.054940 & 0.000000 & -0.185325 \\ -0.003882 & -0.007196 & 0.038996 & -0.000000 & -0.000000 \\ 0.000000 & 0.000000 & 0.000000 & 0.000000 & 0.000000 \end{bmatrix}$$

Plant #29

$$A = \begin{bmatrix} -2.936820 & 0.604717 & -16.176200 & -0.000002 \\ -0.012501 & -0.161132 & 4.220780 & 0.000042 \\ 0.043422 & -0.998122 & -0.225147 & 0.043365 \\ 1.000000 & 0.043536 & 0.000000 & 0.000000 \end{bmatrix}$$

$$B = \begin{bmatrix} 13.516949 & 14.270300 & 3.868000 & -0.000000 & 19.052800 \\ -0.108263 & 0.090024 & -2.473780 & -0.000000 & -0.214523 \\ -0.004027 & -0.008711 & 0.046046 & 0.000000 & 0.000000 \\ 0.000000 & 0.000000 & 0.000000 & 0.000000 & 0.000000 \end{bmatrix}$$

Plant #30

$$A = \begin{bmatrix} -3.565210 & 0.648104 & -16.395600 & 0.000003 \\ -0.014535 & -0.191195 & 5.059590 & -0.000073 \\ 0.036965 & -0.998254 & -0.268634 & 0.042589 \\ 1.000000 & 0.037093 & 0.000000 & 0.000000 \end{bmatrix}$$

$$B = \begin{bmatrix} 14.699708 & 17.483400 & 4.670160 & 0.000000 & 21.771500 \\ -0.121263 & 0.070985 & -2.947270 & 0.000000 & -0.245132 \\ -0.003903 & -0.010419 & 0.053844 & -0.000000 & -0.000000 \\ 0.000000 & 0.000000 & 0.000000 & 0.000000 & 0.000000 \end{bmatrix}$$

Plant #31

$$A = \begin{bmatrix} -4.336140 & 0.700107 & -15.276200 & -0.000015 \\ -0.015502 & -0.225314 & 6.024250 & 0.000397 \\ 0.031883 & -0.998290 & -0.319015 & 0.041851 \\ 1.000000 & 0.032037 & 0.000000 & 0.000000 \end{bmatrix}$$

$$B = \begin{bmatrix} 14.978950 & 21.282000 & 5.540370 & -0.000000 & 24.092900 \\ -0.127586 & 0.060602 & -3.460670 & -0.000003 & -0.271273 \\ -0.003513 & -0.012392 & 0.062096 & 0.000000 & 0.000000 \\ 0.000000 & 0.000000 & 0.000000 & 0.000000 & 0.000000 \end{bmatrix}$$

Bibliography

1. Buffington, James M., Andrew G. Sparks and Siva S. Banda. "Robust Longitudinal Axis Flight Control for an Aircraft with Thrust Vectoring," *Automatica*, *30*(10):1527–1540 (October 1994).
2. Copeland, W., L. Grubbs and B. Kneeland and C. Senn. *Navy evaluation of the F/A-18A Airplane with Roll Rate Improvements Incorporated.* Technical Report, Naval Air Test Center, 1981 (AD-B056292).
3. D'Azzo, John J. and Constantine H. Houpis. *Linear Control System Analysis and Design, Conventional and Modern* (Fourth Edition). New York: McGraw-Hill, 1995.
4. Enns, Dale, Dan Bugajski, Russ Hendrick and Gunter Stein. "Dynamic Inversion: an Evolving Methodology for Flight Control Design," *International Journal of Control*, *59*(1):71–91 (January 1994).
5. "Flying Qualities of Piloted Aircraft (Mil-Std 1797A),". ASD/ENES, Wright-Patterson AFB,OH 45433-6503, January 1990.
6. Hartley, Gerald A. *F-18 Robust Control Design Using H_2 and H_∞ Methods.* MS thesis, Naval Postgraduate School, Monterey, CA 93943, 1990 (AD-A242562).
7. Horowitz, Isaac. "Survey of Quantitative Feedback Theory," *International Journal of Control*, *53*(2):255–291 (February 1991).
8. Houpis, Constantine H. *Quantitative Feedback Theory (QFT) for the Engineer A Paradigm for the Design of Control Systems for Uncertain Nonlinear Plants.* Technical Report WL-TR-95-3601, Wright-Patterson AFB,OH 45433-7521: Wright Laboratory Flight Dynamics Directorate, June 1995.
9. "MIMO/QFT CAD program,". Air Force Institute of Technology, Department of Electrical and Computer Engineering, Wright-Patterson AFB, OH 45433-6503, May 1993.
10. Moore, Doug. "Maneuver Load Control Using Optimized Feedforward Commands," *Journal of Aircraft*, *32*(1):206–207 (January-February 1995).
11. Perry III, Boyd, Stanley R. Cole and Gerald D. Miller. "Summary of an Active Flexible Wing Program," *Journal of Aircraft*, *32*(1):10–15 (January-February 1995).
12. Reynolds, Odell R. *Design of a Subsonic Envelope Flight Control System for the VISTA F-16 using Quantitative Feedback Theory.* MS thesis, Air Force Institute of Technology, 1993 (AD-A274057).
13. Sating, Richard R. *Development of an Analog MIMO Quantitative Feedback Theory (QFT) CAD Package.* MS thesis, Air Force Institute of Technology, 1992.

14. Sparks, A. G., J. M. Buffington and S. S. Banda. "Fighter Aircraft Lateral Axis Full Envelope Control Law Design." *Secong IEEE Conference on Control Applications*. 21–26. 1993 (Cat. No. 93CH3243-3).

15. Wheaton, David G. *Automatic Flight Control System Design for an Unmanned Research Vehicle using Discrete Quantitative Feedback Theory*. MS thesis, Air Force Institute of Technology, 1990 (AD-A230364).

16. Woods-Vedeler, Jessica A., Anthony S. Pototzky and Sherwood T. Hoadley. "Rolling Maneuver Load Alleviation Using Active Controls," *Journal of Aircraft*, *32*(1):68–76 (January-February 1995).

17. Yurkovich, Rudy. "Flutter of Wings with Leading Edge Control Surfaces," *AAIA-86-0897*, 693–700 (1991).

Vita

Christina L. Osmon [redacted]. She grew up in Colorado and graduated from Green Mountain High School in May 1989. She then attended The University of Arizona and completed a Bachelor of Science in Electrical Engineering degree and was commissioned through ROTC in May 1994. Her first assignment was to the Air Force Institute of Technology beginning in May 1994. Following the completion of her Master's degree in Electrical Engineering she will be assigned to Wright Laboratories Flight Dynamics Directorate at Wright-Patterson AFB, OH.

[redacted]

ADA309939

REPORT DOCUMENTATION PAGE

Form Approved
OMB No. 0704-0188

Public reporting burden for this collection of information is estimated to average 1 hour per response, including the time for reviewing instructions, searching existing data sources, gathering and maintaining the data needed, and completing and reviewing the collection of information. Send comments regarding this burden estimate or any other aspect of this collection of information, including suggestions for reducing this burden, to Washington Headquarters Services, Directorate for Information Operations and Reports, 1215 Jefferson Davis Highway, Suite 1204, Arlington, VA 22202-4302, and to the Office of Management and Budget, Paperwork Reduction Project (0704-0188), Washington, DC 20503.

1. AGENCY USE ONLY *(Leave blank)*	2. REPORT DATE	3. REPORT TYPE AND DATES COVERED
	December 1995	Master's Thesis

4. TITLE AND SUBTITLE

DESIGN OF FLIGHT CONTROL LAWS FOR AIRCRAFT WITH FLEXIBLE WINGS USING QUANTITATIVE FEEDBACK THEORY

5. FUNDING NUMBERS

6. AUTHOR(S)

Christina L. Osmon
Second Lieutenant, USAF

7. PERFORMING ORGANIZATION NAME(S) AND ADDRESS(ES)

Air Force Institute of Technology
WPAFB OH 45433-6583

8. PERFORMING ORGANIZATION REPORT NUMBER

AFIT/GE/ENG/95D-20

9. SPONSORING / MONITORING AGENCY NAME(S) AND ADDRESS(ES)

Captain Peter Eide
WL/FIGS
2210 Eighth St STE 11
Wright-Patterson AFB, OH 45433-7521

10. SPONSORING / MONITORING AGENCY REPORT NUMBER

11. SUPPLEMENTARY NOTES

12a. DISTRIBUTION / AVAILABILITY STATEMENT

Approved for public release, Distribution Unlimited

12b. DISTRIBUTION CODE

13. ABSTRACT *(Maximum 200 words)*

Aircraft composed of lightweight composite materials are extremely enticing since their structural weight is greatly reduced. However, the control of these aircraft is complicated by the resultant flexibility of the wings. Two avenues of approach are possible; stiffen the wings thus losing some of the weight reduction benefits, or design the lateral/directional flight control system cognizant of the wing's flexibility. In this thesis the second approach is taken. The design of three lateral/directional flight control systems for the sub-sonic flight envelope of the F-18 is presented. The Quantitative Feedback Theory (QFT) robust control design technique is used. These designs incorporate weighting matrices to distribute generalized aileron and rudder commands to the five control surfaces available on the F-18. The degree of freedom afforded by the use of all control surfaces allows for the reduction of the load on the wings, while at the same time meeting military specifications for roll maneuvers. A baseline flight control system is designed and then improved upon; the final design incorporates load alleviation concepts to reduce the load on the wings thus avoiding wing twisting. All flight control systems designed in this thesis are shown to meet military specifications, as verified with nonlinear time simulations.

14. SUBJECT TERMS

Quantitative Feedback Theory, QFT, Flexible Wing, F-18, Load Alleviation, Flight Control

15. NUMBER OF PAGES

130

16. PRICE CODE

17. SECURITY CLASSIFICATION OF REPORT	18. SECURITY CLASSIFICATION OF THIS PAGE	19. SECURITY CLASSIFICATION OF ABSTRACT	20. LIMITATION OF ABSTRACT
Unclassified	Unclassified	Unclassified	UL

GENERAL INSTRUCTIONS FOR COMPLETING SF 298

The Report Documentation Page (RDP) is used in announcing and cataloging reports. It is important that this information be consistent with the rest of the report, particularly the cover and title page. Instructions for filling in each block of the form follow. It is important to ***stay within the lines*** to meet ***optical scanning requirements***.

Block 1. Agency Use Only *(Leave blank)*.

Block 2. Report Date. Full publication date including day, month, and year, if available (e.g. 1 Jan 88). Must cite at least the year.

Block 3. Type of Report and Dates Covered. State whether report is interim, final, etc. If applicable, enter inclusive report dates (e.g. 10 Jun 87 - 30 Jun 88).

Block 4. Title and Subtitle. A title is taken from the part of the report that provides the most meaningful and complete information. When a report is prepared in more than one volume, repeat the primary title, add volume number, and include subtitle for the specific volume. On classified documents enter the title classification in parentheses.

Block 5. Funding Numbers. To include contract and grant numbers; may include program element number(s), project number(s), task number(s), and work unit number(s). Use the following labels:

C	- Contract	**PR**	- Project
G	- Grant	**TA**	- Task
PE	- Program Element	**WU**	- Work Unit Accession No.

Block 6. Author(s). Name(s) of person(s) responsible for writing the report, performing the research, or credited with the content of the report. If editor or compiler, this should follow the name(s).

Block 7. Performing Organization Name(s) and Address(es). Self-explanatory.

Block 8. Performing Organization Report Number. Enter the unique alphanumeric report number(s) assigned by the organization performing the report.

Block 9. Sponsoring/Monitoring Agency Name(s) and Address(es). Self-explanatory.

Block 10. Sponsoring/Monitoring Agency Report Number. *(If known)*

Block 11. Supplementary Notes. Enter information not included elsewhere such as: Prepared in cooperation with...; Trans. of...; To be published in.... When a report is revised, include a statement whether the new report supersedes or supplements the older report.

Block 12a. Distribution/Availability Statement. Denotes public availability or limitations. Cite any availability to the public. Enter additional limitations or special markings in all capitals (e.g. NOFORN, REL, ITAR).

- **DOD** - See DoDD 5230.24, "Distribution Statements on Technical Documents."
- **DOE** - See authorities.
- **NASA** - See Handbook NHB 2200.2.
- **NTIS** - Leave blank.

Block 12b. Distribution Code.

- **DOD** - Leave blank.
- **DOE** - Enter DOE distribution categories from the Standard Distribution for Unclassified Scientific and Technical Reports.
- **NASA** - Leave blank.
- **NTIS** - Leave blank.

Block 13. Abstract. Include a brief *(Maximum 200 words)* factual summary of the most significant information contained in the report.

Block 14. Subject Terms. Keywords or phrases identifying major subjects in the report.

Block 15. Number of Pages. Enter the total number of pages.

Block 16. Price Code. Enter appropriate price code *(NTIS only)*.

Blocks 17. - 19. Security Classifications. Self-explanatory. Enter U.S. Security Classification in accordance with U.S. Security Regulations (i.e., UNCLASSIFIED). If form contains classified information, stamp classification on the top and bottom of the page.

Block 20. Limitation of Abstract. This block must be completed to assign a limitation to the abstract. Enter either UL (unlimited) or SAR (same as report). An entry in this block is necessary if the abstract is to be limited. If blank, the abstract is assumed to be unlimited.